Abstract of "Aspects of High Energy Scattering and AdS/CFT" by Marko Djurić, Ph.D., Brown University, May 2011.

We study several aspects of high energy scattering using the AdS/CFT correspondence. We begin with concise theoretical overviews of a few relevant topics. First is a general introduction to scattering theory, where we define most of the relevant concepts and terms which we will use later, and introduce the physical motivation for studying them. We follow that by introducing Regge theory, which has had a storied history since its' beginnings. We discuss Regge trajectories and the Pomeron and Odderon, which we will return to later. Next we turn to a short introduction to quantum chromodynamics. We discuss asymptotic freedom and confinement in quantum chromodynamics, which allows us to examine the main ideas from DIS processes and Pomeron exchange at weak coupling. We then turn to introducing relevant concepts from string theory. In particular, we study the massless spectrum of states, consisting of the graviton, Kalb-Ramond field and the dilaton, and then introduce string vertex operators and study how we can use them to calculate string scattering amplitudes. After these introductory chapters we introduce the formalism developed by Brower, Polchinski, Strassler and Tan [1], and Brower, Strassler and Tan [2, 3] to study high energy scattering in the Regge limit using string theory and the AdS/CFT correspondence. This involves developing a Pomeron vertex operator in AdS space string theory, and using it to find the eikonal approximation to the scattering amplitude. The Pomeron is found to correspond to the Regge trajectory of the graviton. Finally, we then apply these techniques to study at strong coupling some of the relevant concepts we introduced initially at weak coupling. We begin by keeping the next order term in the expansion that BPST used to define the Pomeron vertex operator, and find that doing so will correspond to defining the Odderon in AdS space. We note that due to symmetry arguments the Odderon can sometimes be the leading order exchange, and find that in AdS space it corresponds to the Regge trajectory of the Kalb-Ramond field. We next turn to the study of DIS at strong coupling. We find that indeed, using Pomeron exchange string theory in AdS background can provide a very good agreement with experiment, giving a renormalized $\chi^2_{d.o.f.} = 1.04$ for the best model we consider. A crucial step in this analysis is using the hard-wall model to approximate confinement, and the eikonal approximation to satisfy the unitarity bounds. Finally, we comment on some ongoing research and possible future research areas.

Aspects of High Energy Scattering and AdS/CFT

by
Marko Djurić
B. Sc., University of Belgrade, Serbia, 2004

Submitted in partial fulfillment of the requirements
for the Degree of Doctor of Philosophy in the
Department of Physics at Brown University

Providence, Rhode Island
May 2011

This dissertation by Marko Djurić is accepted in its present form by the Department of Physics as satisfying the dissertation requirement for the degree of Doctor of Philosophy.

Date ______________ ____________________________________

Chung-I Tan, Director

Recommended to the Graduate Council

Date ______________ ____________________________________

Antal Jevicki, Reader

Date ______________ ____________________________________

Marcus Spradlin, Reader

Approved by the Graduate Council

Date ______________ ____________________________________

Peter M. Weber
Dean of the Graduate School

Curriculum Vitæ

Author
Marko Djurić, born on August 16th 1982 in Belgrade, Serbia.

Education
University of Belgrade, Belgrade, Serbia, B.S. in Physics (2004)
Brown University, Providence, RI, Ph.D. in Physics (2010)

Publications

• R. C. Brower, M. Djuric, and C.-I. Tan, "Odderon in gauge/string duality," JHEP **0907** (2009) 063, arXiv:0812.0354.
• R. C. Brower, M. Djuric, and C.-I. Tan, "Saturation and Confinement: Analyticity, Unitarity and AdS/CFT Correspondence," arXiv:0812.1299.
• R. Brower, M. Djuric, and C.-I. Tan, "Elastic and Diffractive Scattering after AdS / CFT," arXiv:0911.3463.
• R. C. Brower, M. Djuric, I. Sarcevic, and C.-I. Tan, "String-Gauge Dual Description of Deep Inelastic Scattering at Small-x," arXiv:1007.2259.

Acknowledgments

Many people have helped me during the years working on my PhD. I would like to sincerely thank them.

First and foremost, my advisor Chung-I Tan for his tireless guidance, patience, teaching me many things about physics and how to build a deep understanding of nature, answering my many questions, and too many other things he has helped me with throughout the years, for which this space is too small to list them all.

I would like to thank my collaborators, Richard Brower and Ina Sarčević, both for collaborating on papers with me, and for also teaching me a lot of things, and for helping me out both in physics related and non-physics related matters.

I would like to thank the readers, Antal Jevicki and Marcus Spradlin, for taking the time to read my thesis, and all the other professors of the High Energy Theory group together with Antal and Marcus for many fruitful and interesting physics discussions.

I would like to thank Michael Abbott, Ines Aniceto, Daniel Ferrante, Shubho Roy and Cristian Vergu for many useful physics discussions.

All my colleagues from room 540, throughout the years, for creating a great atmosphere and providing with their knowledge and thinking a great place to do physics, also deserve a big thanks. We have also had a great time outside the office.

Mary Ann Rotondo and Barbara Dailey have been a great help throughout my time at Brown in providing a lot of administrative help and advice, and I thank them.

I would like to thank the US Department of Energy, Brown, and everyone else who has provided financial support for my work.

Last but not least, I am very grateful to my family and all my friends for their invaluable support!

This thesis is dedicated to my parents and brother.

Contents

List of Tables

List of Figures

Chapter 1

Introduction

Strong interactions at strong coupling can be strongly difficult to study. Nevertheless, in this work we present some recent advances which allows us to study this. The main results will be presented in chapters 7 and 8, which are based on the work done in [7, 8, 9, 10]. Before we get to those chapters we need to develop quite a lot of intuition and knowledge of high energy scattering processes and the strong interactions, and therefore chapters 2-6 can be thought of as an introduction to the later chapters.

We begin in chapter 2 by giving a general overview of scattering theory. We define the relevant quantities, cross section and amplitude, which we will encounter again and again, and relate them to quantities that can be physically measured. We also give a proof of the optical theorem, a very useful tool in calculating the total cross section, and point out that the unitarity will give a strong bound on the total cross section for the strong interaction, $\sigma_{tot} \leq \log(s/s_0)^2$. We also meet the eikonal approximation for the first time, showing that it will lead to the unitarity bound being satisfied manifestly.

We next turn to Regge theory, chapter 3. This theory views scattering as being mediated by an infinite tower of particles, rather than just a single particle. This leads to the amplitude going as

$$A(s,t) \sim (\frac{s}{s_0})^{\alpha(t)}\,,$$

where $\alpha(t)$ represents the trajectory of these infinite particles. Such a trajectory is called a Regge trajectory, and we give special care to two of these, the Pomeron and the Odderon. Both of these correspond to states with the quantum numbers of the vacuum, but the Pomeron has $C = +1$ and the Odderon $C = -1$. The Pomeron has been well established experimentally, and appears to be the dominant contribution to all scattering cross sections that do not vanish as $s \to \infty$. The Odderon's trajectory lies below that of the Pomeron, and is usually overshadowed, but could be the dominant process when the Pomeron is not exchanged. We also show that one representation of the eikonal approximation involves an infinite number of Pomerons being exchanged.

Quantum chromodynamics is the subject of the following chapter, 4. This theory gained prominence in the 1970's, when it was shown that its coupling constant vanishes [11, 12, 13, 14],

$$\alpha(\mu) \to 0$$

as $\mu \to \infty$, a property known as asymptotic freedom, which we discuss in section 4.2. This was a very important discovery in the history of physics, since up to then most people expected all interaction to be more like QED, where the coupling is stronger as $\mu \to \infty$. However, we also see that the coupling will get very large when $\mu \to \Lambda_{QCD}$, a scale where perturbative QCD will break down. This shows us the need to develop methods that allow us to work at strong coupling. We next study deep inelastic scattering (DIS) which will illustrate many of the important features of QCD, and which we will return to from the point of view of strong coupling in chapter 8. Finally we briefly look at the BFKL equation, which gives the Pomeron propagator at weak coupling.

As we begin the transition to strong coupling, we first introduce a string theory, chapter 5. This theory first arose as an explanation of the Regge trajectories of chapter 3. We study the spectrum of states of the theory, and how we can study string scattering.

We then make use of this in the very next chapter, 6. We begin by giving a very quick introduction to a great tool in studying QCD at strong coupling, known as the AdS/CFT correspondence. Then we see how we can use it to describe Pomeron exchange using string theory in AdS background, using an approach developed by Brower, Polchinski, Strassler and Tan. This will give rise to a Pomeron with intercept

$$j = 2 - \frac{2}{\sqrt{\lambda}}\,.$$

Due to the general nature of Pomeron exchange, this can be applied to many processes. We then see how using techniques in the spirit of chapter 3 an eikonal approximation to Pomeron exchange can be formed in AdS space.

This section ends our introduction. We feel it is potentially useful to have the important results from a wide range of areas summarized in a consistent way in one place. We then turn to applying all the tools we have thus developed.

First in chapter 7 we generalize the methods of chapter 6 to Odderon exchange. At weak coupling, there are two possible solutions for Odderon exchange, one with an intercept at exactly 1 and one with an intercept slightly below 1. Remarkably, we find the same feature at strong coupling

$$j = 1 - \frac{m^2}{2\sqrt{\lambda}}$$

with m^2 taking the values of 0 or 16. This is summarized in table 7.1. We also study how the hard-wall model will modify our results. Using this model we are also able to calculate the masses of glueball states lying on the Regge trajectories, and are able to reproduce a feature calculated in lattice QCD,

$$m_0^2\left(0^{++}\right) < m_0^2\left(2^{++}\right) \simeq m_0^2\left(0^{-+}\right) < m_0^2\left(1^{+-}\right) < m_0^2\left(1^{--}\right) .$$

In chapter 8 we turn our attention to DIS, first encountered in chapter 4. We see how we can use the Pomeron exchange to study it, and look at several models - a conformal single Pomeron exchange, a conformal eikonalized Pomeron exchange, a hard-wall single Pomeron exchange, and finally an approximation for the hard-wall eikonalized Pomeron exchange. We compare these results to the most recent set of data, and find that the hard-wall eikonalized Pomeron exchange has the best agreement, with a renormalized $\chi^2_{d.o.f.} = 1.04$. It is gratifying that using a string theory calculation gives results with such a good agreement with experiment. The hard-wall single Pomeron exchange is not far behind, and it seems that a conclusion can be drawn that a model with confinement is truly necessary if we want to get a realistic theory of the strong interaction.

Finally, we will present some closing comments, and directions for future research. Without any further ado, let us begin our journey.

Chapter 2

Introduction to Scattering Theory

2.1 Cross Section and Amplitude

High energy physics is concerned with how elementary particles interact with each other, and in fact most of the information we have about the fundamental building blocks of nature comes from observing the scattering of elementary particles. Therefore it is important to understand what scattering is, and how we can extract information from it. The way experiments are usually set up involves starting with one set of states, which we can label with a multi particle state function $|in\rangle$. We imagine that in the 'infinite past', $t \to -\infty$, which is our starting point, the particles are sufficiently far from each other. This allows us to assume that $|in\rangle$ represents a collection of free particles. The particles then approach each other, or equivalently we turn on the interaction, the particles scatter, and we end up with a state of free particles $|out\rangle$ in the infinite future, $t \to \infty$. Note that for long range interactions such as gravity or electromagnetism, where the potential falls of as r^{-1} or slower, this approximation is not always viable. For short range interactions, such as the strong interaction, this is generally a very good assumption. Since the strong interaction is much stronger than gravity and electromagnetism, in many processes between elementary particles we can imagine that the other two are switched off, and just study the strong interaction. It can be shown that states $|in\rangle$ and $|out\rangle$ form complete sets of orthonormal states.

Once we have set up our initial and final states, we are interested in calculating the probability that starting from an initial state $|in\rangle$ we end up with a final state $|out\rangle$. We can define a matrix, called the scattering or S matrix, whose elements give us the probability amplitude for this transition to happen. Then clearly

$$P_{fi} = |\langle in| S |out\rangle|^2 \tag{2.1.1}$$

is the probability for this process to occur. Equation (2.1.1) can be taken as the definition of the S matrix. Starting from an arbitrary initial state, the probability of ending up in some final state has to be unity, and hence

$$1 = \sum_{out} |\langle in| S |out\rangle|^2 = \sum_{out} \langle in| S |out\rangle \langle out| S^\dagger |in\rangle = \langle in| SS^\dagger |in\rangle \tag{2.1.2}$$

Since $|in\rangle$ and $|out\rangle$ are complete sets of orthonormal states, the last equation implies that

$$SS^\dagger = 1. \tag{2.1.3}$$

Similarly, by examining the probability that any final state must be obtained from some initial state, we can show that $S^\dagger S = 1$, and therefore S is a unitary matrix.

Calling the $|in\rangle$ state a and the $|out\rangle$ state b, the ab component of the S matrix is given by

$$S_{ab} = \langle b|a\rangle \,. \tag{2.1.4}$$

Quantum mechanically, particles have a probability of going through each other without scattering. Hence we can write the S matrix element (2.1.4) as

$$S_{ab} = \delta_{ab} + i(2\pi)^4\delta^4(\sum_a p_a + \sum_b p_b)A_{ab}, \tag{2.1.5}$$

where the first term on the left hand side corresponds to the aforementioned probability of no scattering and ending up with the same state, and the second term defines A_{ab} the scattering amplitude for this process. The Kronecker delta in the first term is a symbolic representation of the conservation of all the quantum numbers and momenta for states a and b. The delta function in the second term enforces energy momentum conservation and is there to make the scattering amplitude Lorentz invariant. Note that throughout this work we will use an all incoming convention, which is why there is a plus sign between the sums of momenta. Some authors refer to the factor $(2\pi)^4\delta^4(\sum_a p_a + \sum_b p_b)A_{ab}$ as the T matrix element, so we can also write schematically $S = \mathbb{1} + iT$.

Now that we have defined the S matrix and the scattering amplitude, we can ask the question how they relate to quantities we get from experiments. For simplicity, let us now focus on scattering with two initial and two final particles

$$1 + 2 \to 3 + 4. \tag{2.1.6}$$

It is convenient to introduce the so called Mandelstam variables to study this process

$$s = -(p_1 + p_2)^2 \tag{2.1.7}$$

$$t = -(p_1 + p_3)^2 \tag{2.1.8}$$

$$u = -(p_1 + p_4)^2. \tag{2.1.9}$$

It is trivial to show that they are not all independent, in fact

$$s + t + u = \sum m_i^2. \tag{2.1.10}$$

It is conventional to take s, t to be independent variables, and u can then be expressed using (2.1.10). The Mandelstam variables thus defined are Lorentz invariant, and we can express the scattering amplitude just as a function of s and t, $A(s, t)$ (it will also depend on the masses of the external particles m_i, but these are fixed). In general for $2 \to n$ particle scattering it can be shown that we would need $3n - 4$ independent invariant variables.

We will come back to these below. But first, let us see what experimentalist generally measure in scattering experiments. Imagine we are looking at a particle which approaches

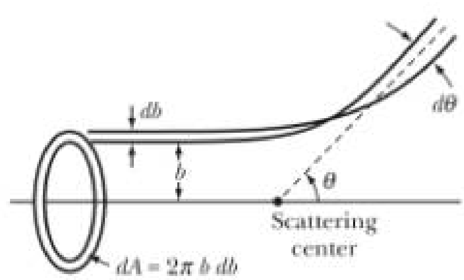

Figure 2.1: A particle passing between b and $b + db$ will scatter through $d\theta$ around θ.

some other particle at rest, and scatters. As a result of the scattering the direction in which the incoming particle is traveling is changed by an angle, θ, which we shall refer to as the scattering angle. In case that the interaction between these particles depends only on the distance between them, it is convenient to introduce another quantity, the impact parameter b, and express the scattering angle as a function of the impact parameter. The impact parameter is defined as the perpendicular distance between the two particles when they are far away, before the interaction. See figure 2.1. The functional form $\theta(b)$ will depend on the nature of the interaction.

If the incoming particle is passing through an infinitesimal area $d\sigma$ between b and $b + db$ after scattering it will emerge into a solid angle $d\Omega$. Looking at the figure we see that

$$d\sigma = |bdbd\phi| \quad d\Omega = |\sin\theta d\theta d\phi|, \tag{2.1.11}$$

and hence

$$\frac{d\sigma}{d\Omega} = |\frac{b}{\sin\theta}\frac{db}{d\theta}|. \tag{2.1.12}$$

The quantity $\frac{d\sigma}{d\Omega}$ is referred to as the differential cross section.

Now consider a beam of particles passing through the area $d\sigma$ with uniform number per unit time per unit area, or luminosity $\mathcal{L}$. The number of particles passing through $d\sigma$ per unit time (and scattering through solid angle $d\Omega$) is then

$$dN = \mathcal{L}d\sigma = \mathcal{L}\frac{d\sigma}{d\Omega}d\Omega. \tag{2.1.13}$$

Experimentally, we can set up a detector that counts the number of particles per unit time coming out of the solid angle $d\Omega$. This is dN in the above equation (also referred to as the event rate). The experimentalist can also control the luminosity of the incoming particles, and the position of the detector. Hence the only unknown in (2.1.13) is the differential cross section, and we can determine it experimentally using the equation

$$\frac{d\sigma}{d\Omega} = \frac{dN}{\mathcal{L}d\Omega}. \tag{2.1.14}$$

Adding up the contribution for each solid angle, we can then obtain the total cross section

$$\sigma = \int \frac{d\sigma}{d\Omega} d\Omega. \tag{2.1.15}$$

The above discussion was classical, but the relevant definitions carry over into the quantum case, and it is a useful intuitive picture to have. In quantum mechanics we can only talk about the probability of a particle being scattered through $d\Omega$. Also, the above discussion involves the same incoming and outgoing particles, or elastic scattering. We can also have processes where the outgoing particles are different (both in type and number) than the incoming particles, or inelastic scattering. In that case, the total cross section is the sum

$$\sigma = \sigma_{elastic} + \sigma_{inelastic}. \tag{2.1.16}$$

Besides the differential cross section with respect to the solid angle, (2.1.12), we can consider differential cross section with respect to other variables, for example $\frac{d\sigma}{dt}$, where t is the Mandelstam variable defined earlier, corresponding to the momentum transfer between the incoming and outgoing particle.

Intuitively, the cross section is related to the probability of scattering - in a process with a larger cross section the incoming particle sees a larger area of the target, and is therefore more likely to scatter.

Now that we have seen what is measured experimentally, we need to connect the scattering amplitude introduced earlier in (2.1.5) to the cross section. We will derive this relation in the case of $2 \to 2$ scattering. Let us represent the initial state by a wavepacket with momenta peaked around $k_1 \approx p_1$ and $k_2 \approx p_2$:

$$|in\rangle = \int \frac{d^4k_1}{(2\pi)^3} \frac{d^4k_2}{(2\pi)^3} \, \delta(-k_1^2 + m_1^2)\delta(-k_2^2 + m_2^2) \, \theta(E_1) \, \theta(E_2) \, f(\mathbf{k_1}) \, g(\mathbf{k_2}) \, |k_1, k_2\rangle. \quad (2.1.17)$$

The integration measure is Lorentz invariant, and often written after integrating out E_1 and E_2

$$\int \frac{d^4k}{(2\pi)^3} \delta(-k^2 + m^2)\theta(E) = \int d\tilde{k} \, , \quad (2.1.18)$$

where we have defined for notational simplicity $d\tilde{k} \stackrel{\text{def}}{=} d^3k/(2\pi)^3 2E$. From (2.1.5) the transition amplitude is

$$i(2\pi)^4 \int d\tilde{k}_1 d\tilde{k}_2 f(\mathbf{k_1}) g(\mathbf{k_2}) \delta(p_3 + p_4 + k_1 + k_2) A(k_1, k_2, p_3, p_4) \quad (2.1.19)$$

where $p_{3,4}$ are the momenta of final state particles. Since k_1 and k_2 are peaked around p_1 and p_2 we can approximate A by $A(p_1, p_2, p_3, p_4)$. The transition probability is the square of the amplitude

$$\begin{aligned} W =& (2\pi)^8 \int d\tilde{k}_1 d\tilde{k}_2 d\tilde{q}_1 d\tilde{q}_2 f(\mathbf{k_1}) g(\mathbf{k_2}) f^*(\mathbf{q_1}) g^*(\mathbf{q_2}) \\ & \times \delta(p_3 + p_4 + k_1 + k_2) \delta(p_3 + p_4 + q_1 + q_2) \\ & \times A(p_1, p_2, p_3, p_4) A(q_1, q_2, p_3, p_4) \, . \end{aligned} \quad (2.1.20)$$

If we then write f and g in terms of their Fourier transforms $\tilde{f}$ and $\tilde{g}$ we have

$$W = \int d^4x\, \frac{|\tilde{f}(x)|^2}{2E_1} \frac{|\tilde{g}(x)|^2}{2E_2}\, (2\pi)^4\, \delta(\sum p_i)|A(p_i)|^2\,. \tag{2.1.21}$$

We have approximated $\delta(k_1 + k_2 + p_3 + p_4) \approx \delta(p_1 + p_2 + p_3 + p_4)$, which we can do due to the fact that the detector always has a finite resolution and cannot differentiate between $k_1 + k_2$ and $p_1 + p_2$ [15]. From this expression we can read off the transition rate per unit volume

$$\frac{dW}{d^3x\, dt} = \frac{(2\pi)^4\delta(\sum p_i)}{4E_1E_2}\, |A|^2\, |\tilde{f}(x)|^2\, |\tilde{g}(x)|^2\,. \tag{2.1.22}$$

But ${}^{dW}/{}_{d^3x\,dt}$ is just the dN we defined earlier, (2.1.13). Hence

$$d\sigma = \frac{1}{\mathcal{L}} \frac{dW}{d^3x\, dt} = \frac{(2\pi)^4\delta(\sum p_i)}{4|\mathbf{p_1}|\sqrt{s}}\, |A(p_i)|^2\,. \tag{2.1.23}$$

From here we get the total cross section by integrating over the final state momenta

$$\sigma = \frac{1}{4|\mathbf{p_1}|\sqrt{s}} \int \frac{d^3p_3}{2E_3(2\pi)^3} \frac{d^3p_4}{2E_4(2\pi)^3} \delta^4(\sum p_i)|A(p_i)|^2 \tag{2.1.24}$$

More generally, for $2 \to n$ scattering we would integrate over all the n outgoing momenta and have the delta function respect energy momentum conservation appropriately. The factor $|\mathbf{p_1}|\sqrt{s}$ can be expressed in a manifestly Lorentz invariant way, equation (A.1.9).

Equation (2.1.24) expresses the total cross section, but as said before, in experiments only the differential cross section, $d\sigma/d\omega$ is measured. Here ω is usually a scattering angle, energy, or momentum transfer between an initial and final particle. To calculate the differential cross section, we would first express ω in terms of the momenta,

$$\omega = \omega(p_i), \tag{2.1.25}$$

and then add a delta function $\delta(\omega - \omega(p_i))$ in equation (2.1.17). For example, if we are interested in $d\sigma/dt$ we will have

$$\frac{d\sigma}{dt} = \frac{1}{64|p_1|^2 s}|A(p_i)|^2\delta(t + (p_1 + p_3)^2). \tag{2.1.26}$$

The strategy is complete. If we calculate the scattering amplitude from the S matrix, we can then express the cross section, and relate it to experimental results.

2.2 Optical Theorem

From the unitarity of the S matrix, (2.1.3), we can derive a very important and interesting result, known as the optical theorem.

Using (2.1.3) we can write

$$(SS^\dagger)_{fi} = \delta_{fi} = \sum_n S_{fn}S^\dagger_{ni}. \tag{2.2.1}$$

Plugging in equation (2.1.5) the above expression is

$$\sum_n(\delta_{fn} + i(2\pi)^4\delta(\sum p_f + \sum p_n)A_{fn})(\delta_{ni} - i(2\pi)^4\delta(-\sum p_n + \sum p_i)A^\dagger_{ni}). \tag{2.2.2}$$

Expanding and summing over n we have

$$\begin{aligned}\delta_{fi} = \delta_{fi} \quad &+ \quad i(2\pi)^4\delta(\sum p_f + \sum p_i)(A_{fi} - A^{\dagger}_{fi}) \\ &+ \quad (2\pi)^8 \sum_n \delta(\sum p_f + \sum p_n)\delta(-\sum p_n + \sum p_i)A_{fn}A^{\dagger}_{ni}.\end{aligned} \tag{2.2.3}$$

The two delta functions in the last term on the right hand side can be rewritten

$$\delta(\sum p_f + \sum p_n)\delta(-\sum p_n + \sum p_i) = \delta(\sum p_f + \sum p_n)\delta(\sum p_f + \sum p_i), \tag{2.2.4}$$

and therefore we can cancel $(2\pi)^4\delta(\sum p_f + \sum p_i)$ leading to

$$-\, i(A_{fi} - A^{\dagger}_{fi}) = (2\pi)^4 \sum_n \delta(\sum p_f + \sum p_n)A_{fn}A^{\dagger}_{ni}, \tag{2.2.5}$$

which gives

$$2\Im A_{fi} = (2\pi)^4 \sum_n \delta(\sum p_f + \sum p_n)A_{fn}A^{\dagger}_{ni}. \tag{2.2.6}$$

In case the final state is the same as initial, $f = i$, equation (2.2.6) is

$$2\Im A_{ii} = (2\pi)^4 \sum_n \delta(\sum p_i + \sum p_n)|A_{in}|^2. \tag{2.2.7}$$

We recognize the right hand side as the total transition rate for $2 \to n$ particle scattering. Using our earlier derivation, we can write

$$2\Im A_{ii} = 4|\mathbf{p_i}|\sqrt{s}\sigma_{tot}. \tag{2.2.8}$$

The factor A_{ii} on the left hand side is the elastic scattering amplitude for forward scattering, since the final state is unchanged with respect to the initial. This corresponds to the scattering angle $\theta = 0$, or the momentum transfer $t = 0$. So finally we have the optical theorem

$$\sigma_{tot} = \frac{1}{2|\mathbf{p_i}|\sqrt{s}} \Im A_{el}(s, t = 0). \tag{2.2.9}$$

In this thesis we are interested in scattering at high energy. In that case the factor $|\mathbf{p_i}|\sqrt{s} \approx \frac{s}{2}$ (see (A.1.9)) and the above equation becomes

$$\sigma_{tot} = \frac{1}{s} \Im A_{el}(s, t = 0), \tag{2.2.10}$$

which is the expression we will refer to in the rest of this work.

An important thing to note is that the left hand side of (2.2.10), σ_{tot} represents the total cross section for $2 \to n$ scattering, while the right hand side is the amplitude for $2 \to 2$ elastic scattering.

At first sight, the optical theorem might seem strange. Why is the total cross section determined just by the imaginary part of the forward scattering amplitude? The following intuitive picture might help. First note that if the particles were non-interacting, the outgoing particle would emerge with scattering angle $\theta = 0$ with probability 1. But as we said before, quantum mechanically for every scattering process there is a chance that the particles do not interact, and just pass through, as reflected by the δ_{ab} term in the expression for S_{ab}. This would also lead to the particle emerging with $\theta = 0$. However, the particle will also have a probability to scatter at angle $\theta = 0$. So in order for probability to be conserved (and unitarity is just an expression of this), the scattering amplitude at $\theta = 0$ has to contribute negatively, since clearly there is a probability to scatter at non-zero angles as well. Hence the amplitude at $\theta = 0$ has to account for all the particles scattered at all other angles, and intuitively it contains enough information to determine the total cross section.

2.3 Analyticity and Crossing Symmetry

Let us look at the scattering amplitude $A(s,t,u)$, where we explicitly put in the u dependence. For a process where particles 1 and 2 are the initial particles and s is the center of mass energy, or in other words in the s channel, there will be some bounds on the values s can take. Since $s=-(p_1+p_2)^2$, clearly $s \geq m_1^2+m_2^2$. Similarly t will depend on the scattering angle, and hence the condition $-1 \leq \cos\theta \leq 1$ will restrict the values of t, and therefore by (2.1.10) u as well. See Appendix A for more details. Hence there are specific ranges of values that the Mandelstam variables can take in the s channel.

Similarly, if we consider a process where 1 and 3 are the initial particles, t will be the center of mass energy (we can call it the t channel process) and we can again derive the bounds for the values of s, t and u. The same process can be repeated for the u channel.

The principle of analyticity then states that if we start from the s channel process, we can get the t and u channel processes by promoting s, t and u to complex variables and analytically continuing the function A to the t and u channel regions. To do this, we must assume that all the singularities of A have a dynamical origin, poles will correspond to bound states or resonances, and cuts will correspond to multiparticle thresholds.

Analyticity can be shown to be a consequence of causality, and can be shown true order by order for Feynman diagrams. It therefore seems to be a reasonable assumption. As a consequence, we can state more generally our opening discussion of viewing the amplitude in different channels. For any process

$$1 + 2 \to 3 + 4 \tag{2.3.1}$$

the processes related to it by crossing,

$$1 + \bar{3} \to \bar{2} + 4 \tag{2.3.2}$$

and

$$1 + \bar{4} \to \bar{2} + 3 \tag{2.3.3}$$

are all given by the same amplitude:

$$A_{1+2\to 3+4}(s,t,u) = A_{1+\bar{3}\to\bar{2}+4}(t,s,u) = A_{1+\bar{4}\to\bar{2}+3}(u,t,s)\,. \tag{2.3.4}$$

The particles with bars, e.g. $\bar{3}$, correspond to the antiparticles of the unbarred particles, e.g. 3. This property of the scattering amplitude is called crossing symmetry.

Because of the analyticity of the amplitude we can expand it into partial waves. In the s channel this reads

$$A(s,t) = 16\pi \sum_{j=0}^{\infty} (2j+1)\, A_j(s)\, P_j(z_s)\,, \tag{2.3.5}$$

with $P_j(z_s)$ the Legendre polynomials, and $z_s = \cos\theta_s$, with θ_s the scattering angle (Appendix A).

It can be shown [16], that $A_j(s)$ can be written

$$A_j(s) = -\frac{i}{2}\frac{e^{2i\delta_j} - 1}{\rho(s)}\,, \tag{2.3.6}$$

where δ_j is a complex variable called the phase shift, and

$$\rho(s) = 2\frac{|\mathbf{p_1}|}{\sqrt{s}}\,. \tag{2.3.7}$$

2.4 Unitarity Bound

As it turns out, unitarity (or in other words conservation of probability) puts a bound on the asymptotic growth of the cross section with increasing energy. A full proof would require developing some more machinery, but the basic idea would be to expand the amplitude into partial waves assuming it is bounded by some finite power of s, and then study the large s behavior of the partial waves. The proof can be found for example in [16]. Instead we will provide an intuitive argument originally due to Feynman and reported at a conference (although Froissart had a similar argument in his paper [17]).

If B is the effective range of the interaction, then for probability to be conserved the cross sectional area has to be less than the area of a circle with radius B^2:

$$\sigma_{tot} \leq 2\pi B^2\,. \tag{2.4.1}$$

To find the effective range we can view the interaction to be created by a potential

$$V = g_{12}(\frac{s}{s_0})^N \exp(-\frac{b}{B_0}) \tag{2.4.2}$$

where B_0 is the intrinsic range of the interaction, and g_{12} is some coupling constant. The term s^N appears because we assume the amplitude is bounded by some finite power. Then the effective range can be found from requiring $V \approx O(1)$

$$\begin{aligned} g_{12}(\frac{s}{s_0})^N \exp(-\frac{B}{B_0}) &= 1 \\ \implies B^2 &\sim c \log^2(\frac{s}{s_0}) \end{aligned} \tag{2.4.3}$$

as $s \to \infty$, with c a constant. Applying this to (2.4.1) gives

$$\sigma_{tot} \leq 2\pi c \log^2(\frac{s}{s_0}) \,. \tag{2.4.4}$$

This is the statement of the well known Froissart, or Froissart-Martin unitarity bound. It limits the asymptotic growth of the total cross section. Note that the bound depends crucially on the fact that the interaction is short range, and the potential is exponentially cut off (2.4.2). If, for example, the potential was long range like $1/r$, the above derivation would give us the maximal cross section growing as a power s^N, and unitarity would still be satisfied. Therefore scale invariant theories will not give us a $\log^2$ unitarity bound.

2.5 First Contact with the Eikonal Approximation

We saw in the previous section that unitarity puts bounds on the total cross section. That makes us wonder, how can we write an amplitude that will manifestly satisfy unitarity?

Let us write the T matrix symbolically

$$T = -i(e^{i\chi} - 1) \,. \tag{2.5.1}$$

Then $S = 1 + e^{i\chi} - 1 = e^{i\chi}$, and unitarity gives

$$\begin{aligned} e^{i\chi}e^{-i\chi^*} &= \mathbb{1} \\ \implies e^{-2\Im\chi} &= \mathbb{1}\,. \end{aligned} \tag{2.5.2}$$

Hence we see that unitarity would be automatically satisfied as long as $\Im\chi \geq 1$ (with equality saturating the bound).

Of course, we need a physical meaning for χ, and a physical derivation of the above form (2.5.1). We will defer such discussions to sections 3.3 and 6.3. For now, note that expressing an amplitude as (2.5.1) is called the eikonal approximation, and χ is often called the eikonal. This approximation has a long history, and uses in many areas of physics, such as optics and quantum mechanics. We recommend [18] as a great resource on the many forms eikonal models can take.

Chapter 3

Regge Theory

In this section we will introduce some of the basic ideas from Regge Theory, such as Regge trajectories, poles, Pomeron and Odderon. In this part, we will explain how these concepts first came about, in the pre-QCD days. We will revisit these in later chapters, first from the point of view of QCD, and then string theory. In this chapter, and most of this work, we will be chiefly interested in the so-called Regge limit, where the center of mass energy

$$s \gg |t|. \tag{3.0.1}$$

3.1 Regge Trajectories

Let us consider a $2 \to 2$ scattering process in the s channel. This process occurs by exchanging a particle or resonance with m^2 equal to the momentum transfer t. But also the quantum numbers, such as charge and isospin, of the process must be conserved, so the exchanged particle must have the correct quantum numbers. If there are no particles or resonances with the exchanged quantum numbers, then the cross section for the process will be small.

On the other hand, we could have multiple particles or resonances with the right quantum numbers, but with different masses t and spins. These would then correspond to poles in the t plane of the scattering amplitude $A(s,t)$.

We saw in section (2.3) that the scattering amplitude $A(s,t)$ can be expanded into partial waves. To study these poles, it is useful to do a partial wave expansion in the t channel

$$A(s,t) = 16\pi \sum_{j=0}^{\infty} (2j+1) A_j(t) P_j(z_t), \tag{3.1.1}$$

where

$$z_t = \cos\theta_t = 1 + \frac{2s}{t-4m^2}. \tag{3.1.2}$$

If only one resonance was exchanged in the process, then in equation (3.1.1) for some t and j corresponding to the mass and spin of that resonance, only one term would contribute to the sum, and we would have

$$A(s,t) = 16\pi(2j+1) A_j(t) P_j(z_t). \tag{3.1.3}$$

In the limit (3.0.1) the Legendre polynomial can be approximated

$$P_j(1 + \frac{2s}{t-4m^2}) \to \frac{\Gamma(2j+1)}{\Gamma^2(j+1)} (\frac{s}{2t})^j \sim f(t) s^j. \tag{3.1.4}$$

Hence we see that an exchange of particle with spin j leads to the asymptotic form for the amplitude $A(s,t) \sim s^j$. Applying the optical theorem, this would lead to the cross section having the form

$$\sigma_{tot} \sim s^{j-1}. \tag{3.1.5}$$

Experimentally, in hadron-hadron scattering in the Regge limit, the cross section does not fit with this form, for any integer j. The resolution of this is logical - we must sum all the possible particle and resonance exchanges. To do this, we must first study the poles of the scattering amplitude. Regge showed that we can continue the factors $A_j(t)$ from equation (3.1.1) to the complex angular momentum plane

$$A_j(t) \rightarrow A(j,t), \tag{3.1.6}$$

and $A(j,t)$ will have as singularities poles at integer j for some t. As we change t, the position of the pole will change, leading to a trajectory

$$j = \alpha(t). \tag{3.1.7}$$

These poles are known as Regge poles. In general it is possible for $A(j,t)$ to also have cuts. The theory of Regge cuts has not yet been fully developed or understood.

However, going from $A_j(t) \rightarrow A(j,t)$ is not unique. We need to introduce two amplitudes

$$A^{\pm}(j,t) = \begin{cases} A_j(t) & j\, even \\ A_j(t) & j\, odd \end{cases} \tag{3.1.8}$$

We can then write

$$A(s,t) = A^{+}(s,t) + A^{-}(s,t), \tag{3.1.9}$$

with

$$A^{\pm}(s,t) = 8\pi \sum_{j=0}^{\infty} (2j+1)\, A_j^{\pm}(t)(P_j(z_t) \pm P_j(-z_t)). \tag{3.1.10}$$

If we impose asymptotic behavior for $A_j^{\pm}(t)$ as $j \to \infty$ then there is a theorem due to Carlson we can use to affirm the continuation to the complex plane will be unique. The Legendre polynomials have a natural continuation to the complex plane in terms of hypergeometric function, and we can write equation (3.1.9)

$$A^{\pm}(s,t) = 8\pi \int_C dj(2j+1)A^{\pm}(j,t)\frac{P(j,-z_t) \pm P(j,z_t)}{\sin(\pi j)}, \tag{3.1.11}$$

and the contour C is chosen so it surrounds the positive real axis. Then picking up the residues at the zeros of $\sin(\pi j)$ reduces to our previous sum. Rewriting our initial partial wave sum as a contour integral in the complex plane is known as the Sommerfeld-Watson transform.

The next step is to deform the contour C to a contour C' which is parallel to the imaginary axis with real part equal to $-1/2$. The contour at infinity will not contribute, but we must be careful in doing this to include the contribution from the residues of the poles we pick up. This will lead to the result

$$\begin{aligned} A^{\pm}(s,t) = & - 16\pi^2 \sum_i \frac{(2\alpha_i^{\pm}(t)+1)\beta_i^{\pm}(t)}{\sin(\pi\alpha_i^{\pm}(t))}(P(\alpha_i^{\pm}(t),-z_t) \pm P(\alpha_i^{\pm}(t),z_t)) && (3.1.12) \\ & + 8\pi i \int_{-\frac{1}{2}-i\infty}^{-\frac{1}{2}+i\infty} dj \frac{(2j+1)A^{\pm}(j,t)(P(j,-z_t) \pm P(j,z_t))}{\sin(\pi j)}, && (3.1.13) \end{aligned}$$

with the position and the residues of the poles in the j plane labeled as $\alpha_i^{\pm}(t)$ and $\beta_i^{\pm}(t)$ respectively. Note that for a fixed t we could have multiple poles lying on different trajectories $\alpha_i^{\pm}(t)$. These would correspond to resonances with the same mass but a different spin. The sum above goes over all these poles.

Mandelstam showed that the integral in (3.1.13) goes to zero as $s \to \infty$, and we are left with just the first term on the left hand side. We can take advantage of the asymptotic form of the Legendre polynomials to further simplify this expression

$$\sqrt{\pi}P(j,z) \sim \begin{cases} \frac{\Gamma(j+1/2)}{\Gamma(j+1)}(2z)^j & \Re j \geq 1/2 \\ \frac{\Gamma(-j-1/2)}{\Gamma(-j)}(2z)^{-j-1} & \Re j \leq 1/2 \end{cases} \tag{3.1.14}$$

Plugging these in, we can show that equation (3.1.13) reduces to

$$A^{\pm}(s,t) \sim \sum_i \beta_i^{\pm}\Gamma(-\alpha_i^{\pm}(t))(1 \pm e^{-i\pi\alpha_i^{\pm}(t)})(\frac{s}{s_0})^{\alpha_i^{\pm}(t)}. \tag{3.1.15}$$

To get from (3.1.13) to (3.1.15) we have also reabsorbed some extra factors into β and introduced an energy scale s_0, because it is bad taste to raise a dimensionful quantity to a power.

The expression we derived, (3.1.15), is the asymptotic form of the $2 \to 2$ scattering amplitude in the Regge limit. We see that it is a sum of powers in s. Since we are considering $s \to \infty$ we can keep just the leading term in this sum (the term with the largest value of $\Re\alpha(t)$), which would finally give us

$$A^{\pm}(s,t) \sim (1 \pm e^{-i\pi\alpha^{\pm}(t)})\beta(t)(\frac{s}{s_0})^{\alpha^{\pm}(t)}. \tag{3.1.16}$$

All the factors of t have now been absorbed into $\beta(t)$, for simplicity. We see that the amplitude goes as $s^{\alpha(t)}$, compared to s^j for exchange of a particle of spin j. Therefore, as promised, now a whole trajectory of particles $\alpha(t)$ is being exchanged in the process. The mass of the particles is given by t, where t solves the equation (3.1.7) for integer j. Note that from equation (3.1.15) the $\Gamma(-\alpha^{\pm}(t))$ term will have a pole in this case, so indeed the scattering amplitude will have a pole corresponding to the exchange of a particle of spin j and mass $\sqrt{t}$.

We can equivalently view the exchange of a trajectory $\alpha(t)$ as an exchange of an object with angular momentum equal to $\alpha(t)$. Such an object is called a 'Reggeon'.

3.2 Pomeron and Odderon

The derivation in the previous section was general, without making reference to any particular theory telling us how hadrons interact. Still, we were able to conclude the general asymptotic form of the amplitude, (3.1.16), in the Regge limit. Applying the optical theorem, (2.2.10), we can also conclude that the total cross section will behave as

$$\sigma_{tot} \sim (\frac{s}{s_0})^{\alpha^{\pm}(0)-1}. \tag{3.2.1}$$

However, we cannot calculate from first principles the intercept $\alpha(0)$. Therefore the hunt is on to determine the trajectory. First of all, notice that in equation (3.1.16) we have a factor

$$1 \pm e^{-i\pi\alpha^{\pm}(t)}. \tag{3.2.2}$$

When $\alpha^{+}(t)$ is odd, $1 + e^{-i\pi\alpha^{+}(t)} = 0$, and similarly when $\alpha^{-}(t)$ is even, $1 - e^{-i\pi\alpha^{-}(t)} = 0$. Hence we will have two sets of trajectories, one with only particles with even non-negative spin (the positive signature trajectory), and one with particles with odd positive spin (the negative signature trajectory). Plotting the masses versus spins of mesons we see that they

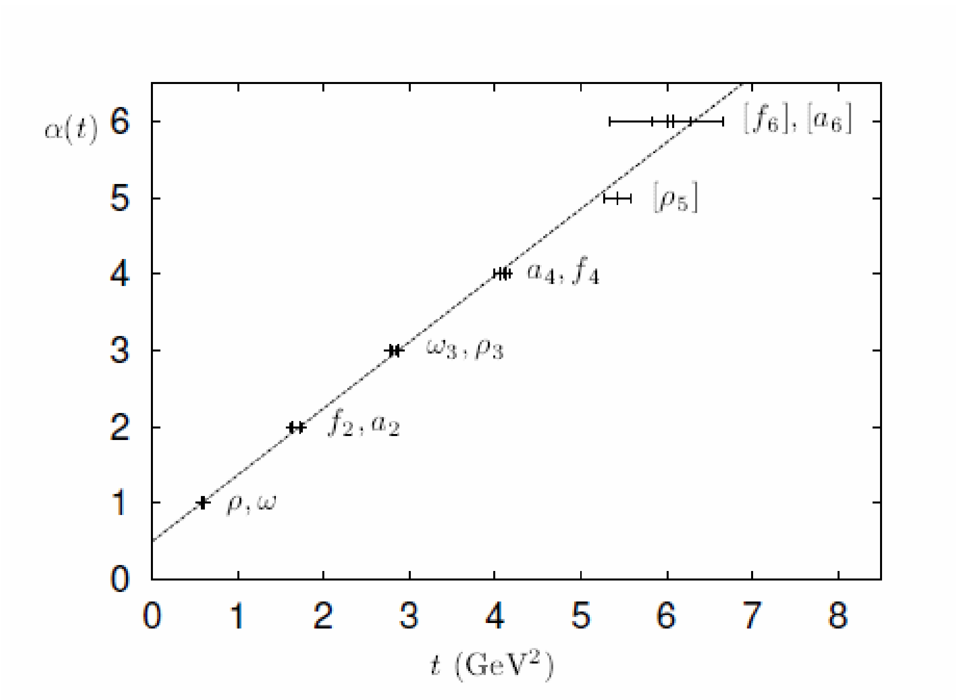

Figure 3.1: Regge trajectories.

lie on straight line trajectories, with the mesons on the trajectory having same external quantum numbers. Moreover, for trajectories which contain particles with isospin greater than 0, it has been determined experimentally that the intercept $\alpha(0) < 1$. This will lead to the cross section (3.2.1) to vanish asymptotically as $s \to \infty$. However, experimentally the cross section does not go to 0 for interactions that occur via exchange of resonances with quantum numbers of the vacuum. The leading Reggeon which has the quantum numbers of the vaccuum, $C = +1$ and $I = 0$, is known as the Pomeron. It is the dominant contribution in non-vanishing total cross sections, and as such is very important in high energy processes.

The states that lie on the Pomeron trajectory are glueballs, or bound states of gluons. With the physics developed so far, the intercept for the Regge trajectory cannot be calculated. However, by fitting experimentally to data, it was found that the intercept is equal to 1.08 [19], leading to a cross section

$$\sigma_{tot} \sim (\frac{s}{s_0})^{0.08}. \tag{3.2.3}$$

This is the so called 'soft' or non-perturbative Pomeron. When we revisit the Pomeron in chapter 4 from the point of view of QCD and the BFKL equation, we will see that in perturbative QCD we can calculate the intercept, and it is close to 1.40. This has been thought of as a second, 'hard', Pomeron. However, finally it is string theory on AdS space which shows how these two objects are the same. In chapter 6 we will develop the Pomeron in string theory, and in chapter 8 we will see how it leads to a whole set of effective Pomerons, with intercepts starting at around 1.40 and decreasing down to close to 0.08. See also figure 8.2.

The Odderon is the Pomeron's less well known cousin. Whereas the Pomeron corresponded to the exchange of a positive signature trajectory, corresponding to states with even spin, and $C = +1$, the Odderon corresponds to the exchange of the leading negative signature trajectory, thus having states with odd spin, and $C = -1$. These states still have isospin $I = 0$.

The Odderon has been much more elusive experimentally, having a trajectory lying below the Pomeron. Its intercept is either slightly below 1 or exactly 1. We will have much more to say about the Odderon from the point of view of string theory in chapter 7.

We can draw a Feynman diagram for Pomeron and Oderon exchange [20]:

where

$$\beta(t) = \beta_{ac}(t)\, \beta_{bd}(t) \tag{3.2.4}$$

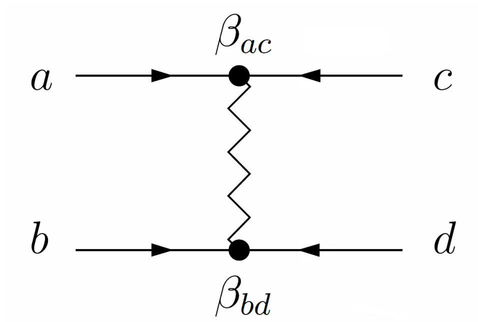

Figure 3.2: A Feynman diagram for Pomeron or Odderon exchange.

and $\beta_{ij}(t)$ are couplings of the particles to the Pomeron/Odderon. The propagator is given by

$$(-i)i(\frac{-is}{s_0})^{\alpha^+(t)-1} \tag{3.2.5}$$

for the Pomeron and

$$(-i)\eta_O(\frac{-is}{s_0})^{\alpha^-(t)-1} \tag{3.2.6}$$

for the Odderon, where $\eta_O = \pm 1$ is a phase factor which is process dependent.

3.3 The Pomeron and the Eikonal Approximation

We saw in equation (3.1.5) that the exchange of a spin j state leads to an amplitude that grows as a power of $j-1$, which violates the Froissart unitarity bound (2.4.4). Then in the last section we saw that summing an infinite number of exchanges, with higher and higher spin, or equivalently exchanging one Pomeron, gives a slower growth than any of the individual terms. But alas, although dramatically slower, the growth of the cross section was still like a power, and hence to fast for the Froissart bound. But this suggests that maybe the answer can be summing an infinite number of Pomerons? So let us try to perform this sum.

First, as is more common in the literature, we will replace t with $-\mathbf{q}_\perp{}^2$, according to (A.2.12). Next let us define the amplitude in impact parameter space by a Fourier transform

$$\tilde{A}(s, \mathbf{b}_\perp{}^2) = \frac{1}{16\pi^2} \int d^2 q e^{i\mathbf{q}_\perp \cdot \mathbf{b}_\perp} A(s, -\mathbf{q}_\perp{}^2) \,. \tag{3.3.1}$$

Since A does not depend on the direction of $\mathbf{q}_\perp$, we can perform the angular integral

$$= \frac{1}{8\pi} \int q dq \, J_0(bq) A(s, -\mathbf{q}_\perp{}^2) \,. \tag{3.3.2}$$

We now want to use the partial wave expansion (2.3.5) for $A(s, -\mathbf{q}_\perp{}^2)$, and use the representation (2.3.6). At large s, $\rho(s) \to 1$ and

$$A_j(s) \approx -\frac{i}{2}(e^{2i\delta_j} - 1) \,. \tag{3.3.3}$$

Now we need to make some approximations. At large j

$$P_j(z_s) \approx J_0(j\theta_s) \,. \tag{3.3.4}$$

According to (A.1.17) at large s $\cos\theta_s \approx 1 - 2\mathbf{q}_\perp{}^2/s$, giving us $\theta \approx 4q_\perp/\sqrt{s}$. Then if we change the integration variable to $z_s \cos\theta_s$, $qdq = \frac{s}{4} dz_s$, and we will need to evaluate

$$\sum_j (2j+1) \int dz \, J_0(\frac{b\sqrt{s}}{2}\sqrt{1-z}) J_0(j\sqrt{1-z}) \,. \tag{3.3.5}$$

Besides large s, for the eikonal approximation to work b also cannot be too small, so that we can use ${}^{b\sqrt{s}}\!/_2 \gg 1$. In that case the value of j closest to ${}^{b\sqrt{s}}\!/_2$ (note this is consistent with (3.3.4)) will dominate in the above sum and (since $2j \gg 1$) our integral will be

$$\begin{aligned} &\approx \quad b\sqrt{s}\int_{-1}^{1} dz\, J_0^2(\tfrac{b\sqrt{s}}{2}\sqrt{1-z}) \\ &= \; b\sqrt{s}\,2(J_0^2(b\sqrt{2s}) + J_1^2(b\sqrt{2s}))\,. \end{aligned} \tag{3.3.6}$$

For $b\sqrt{2s} \gg 1$

$$\begin{aligned} J_0^2(b\sqrt{2s}) &\approx \tfrac{\sqrt{2}}{\pi b\sqrt{s}}\cos^2(b\sqrt{2s}) \\ J_1^2(b\sqrt{2s}) &\approx \tfrac{\sqrt{2}}{\pi b\sqrt{s}}\cos^2(b\sqrt{2s} - \tfrac{\pi}{2}) \end{aligned}$$

and therefore our expression above is approximately a constant. Putting everything back in we get

$$\tilde{A}(s, \mathbf{b}_\perp{}^2) = -\frac{is}{2}(e^{i\chi(s,b)} - 1) \tag{3.3.7}$$

where

$$\chi(s,b) = 2\delta_{j_0(s,b)}(s)\,. \tag{3.3.8}$$

Then, to express $A(s, -\mathbf{q}_\perp{}^2)$ in terms of $\tilde{A}(s, \mathbf{b}_\perp{}^2)$ we do an inverse Fourier transform

$$\begin{aligned} A(s, -\mathbf{q}_\perp{}^2) &= 4\int d^2b\, e^{-i\mathbf{b}_\perp\cdot\mathbf{q}_\perp}\tilde{A}(s, \mathbf{b}_\perp{}^2) \\ &= -2is\int d^2b\, e^{-i\mathbf{b}_\perp\cdot\mathbf{q}_\perp}\,(e^{i\chi(s,b)} - 1)\,. \end{aligned} \tag{3.3.9}$$

We recognize the eikonal form from section 2.5 from chapter 2. We can expand the exponential to get

$$A(s, -\mathbf{q}_\perp{}^2) = -2is\int d^2b e^{-i\mathbf{b}_\perp\cdot\mathbf{q}_\perp}(i\chi + \frac{(i\chi)^2}{2} + \cdots)\,. \tag{3.3.10}$$

Then we see the amplitude is an infinite sum of terms. See figures 6.1-6.3 for a Feynman diagram representation.

If we identify the first level term with the single Pomeron exchange amplitude, which we calculated in (3.1.15) and (3.1.16), we can once again Fourier transform and express χ in terms of the one Pomeron amplitude

$$\chi(s,b) = \frac{1}{2\pi} s^{\alpha(0)-1} \int d^2q e^{i\mathbf{b}_\perp \cdot \mathbf{q}_\perp} \beta(-{\mathbf{q}_\perp}^2)\Gamma(-\alpha(-{\mathbf{q}_\perp}^2))(1+e^{-i\pi\alpha(-{\mathbf{q}_\perp}^2)})e^{-{\mathbf{q}_\perp}^2\alpha' \log s} \,. \tag{3.3.11}$$

However, the above identification seems to be a guess. See [16] for more details. We will return to the eikonal approximation in AdS space in section 6.3, and then apply it in chapter 8.

Chapter 4

QCD

During the 1960's a large group of physicists studied the strong interaction just by examining general properties of the S matrix and Regge theory. This program was able to give satisfactory explanations for several phenomena, and in the past decade many of the ideas from this period are being revisited, and studied anew. During the 1970's, a new theory came about, called quantum chromodynamics, or QCD, and eventually gained more prominence than the study of S matrix theory.

QCD is built as a quantum field theory of quarks and gluons. It has had tremendous success in explaining and predicting a whole range of physical phenomena. However, the theory is nonlinear, and sometimes very difficult to work with.

In this chapter we will not try to give a thorough overview of QCD, which would require multiple volumes. Some good places to start such a study would be for example [21, 22, 23]. Instead we introduce some basic features of QCD, followed by a short study of topics which are directly relevant to our previous discussion on Regge theory, and which will be relevant when we reexamine some of the same ideas from the point of view of string theory and the AdS/CFT correspondence.

4.1 The QCD Lagrangian

We will begin by reviewing a few of the main properties of the theory. To begin with, let us examine the QCD Lagrangian. As mentioned before, QCD is a theory of quarks and gluons. Quarks are spin-$\frac{1}{2}$ particles. Omitting spinor and color indices, the free quark Lagrangian is

$$\mathcal{L}_q = \bar{q}(x)\,(i\partial\!\!\!/ - m)\,q(x), \tag{4.1.1}$$

with m the quark mass, and $q(x)$ the quark wave function. The above Lagrangian is invariant under global $SU(N)_c$ transformations, with $N = 3$ in the case of QCD. To make it invariant under local $SU(N)_c$ we introduce the gluon fields A_μ, where

$$A^\mu = \sum_{a=1}^{8} A_a^\mu T_a\,, \tag{4.1.2}$$

and T_a are the generators of $SU(N)$ in the fundamental representation. We then replace the partial derivative ∂_μ with the covariant derivative defined by

$$D_\mu = \partial_\mu + igA_\mu, \tag{4.1.3}$$

where g is a coupling constant that we will say much more about later. If we make the replacement (4.1.3) we would get a Lagrangian that is invariant under local gauge transformations and includes quark-gluon interactions. But we also need to add the

Lagrangian for the gluon field

$$\mathcal{L}_g = -\frac{1}{2}\mathrm{Tr}[F_{\mu\nu}^2(x)], \tag{4.1.4}$$

with the field strengths given by

$$F_{\mu\nu} = \partial_\mu A_\nu - \partial_\nu A_\mu + ig[A_\mu, A_\nu]. \tag{4.1.5}$$

We already see part of the reason why QCD is highly non-trivial. The non-vanishing commutator $[A_\mu, A_\nu]$ means the theory is non-Abelian, and the F^2 term in (4.1.5) will lead to three-point and four-point gluon interactions. In contrast, QED does not include interactions with just photons. Adding the gluon Lagrangian to the Lagrangian with the quark-gluon interatcion, we finally get

$$\mathcal{L}_{QCD} = \sum_{n_f} \bar{q}_f(x)(i\not{D} - m)q_f(x) - \frac{1}{2}\mathrm{Tr}[F_{\mu\nu}^2]. \tag{4.1.6}$$

The sum over f in the above goes over the different types, or 'flavors', of quarks. Based on the current experimental data, the quarks come in six flavors, most commonly called the up, down, strange, charm, top and bottom. The renormalized masses of the quarks are [24] $1.7 \leq m_u \leq 3.3$ MeV, $4.1 \leq m_d \leq 5.8$ MeV, $80 \leq m_s \leq 130$ MeV, $1.18 \leq m_c \leq 1.34$ GeV, $4.13 \leq m_b \leq 4.28$ GeV and finally $m_t \simeq 172$ GeV. We see that there is a clear difference in the order of magnitude of the mass of the first three quarks and the next three quarks. Hence the first group is usually called the light quarks, and the second the heavy quarks (later on we will talk about an energy scale in the theory, and we will see that also the light quarks have a mass below this scale, while the heavy ones have a mass above this scale).

It can be easily checked that the Lagrangian (4.1.6) is invariant under the local gauge transformations

$$A_\mu \to A'_\mu = U(x)A_\mu(x)U^{-1}(x) + \frac{i}{g}(\partial_\mu U(x))U^{-1}(x), \tag{4.1.7}$$

$$q(x) \to q'(x) = U(x)q(x). \tag{4.1.8}$$

$U(x)$ are unitary unimodular matrices belonging to the fundamental representation of $SU(N)_c$.

The gauge invariance of the QCD Lagrangian also makes it difficult to quantize. As in other gauge theories, we are using more degrees of freedom than is needed to describe the theory, and the gauge condition eliminates the spurious information. There are several ways to proceed in the quantization. One very common method is to add to the Lagrangian a gauge fixing term. This term would lead to the presence of non-physical ghost fields, so we would need to add the ghost Lagrangian as well. The result we get by following this procedure is

$$\mathcal{L} = \mathcal{L}_{QCD} - \frac{\lambda}{2}(B_a)^2 + \bar{c}_b \left[\frac{\delta B_b}{\delta \alpha_a}\right] c_a \ . \tag{4.1.9}$$

The second term in the left hand side include the function B_a which fixes the gauge, and the last term includes the ghost fields c_a. There are many gauges one can choose, offering advantages and disadvantages based on the specific calculations that need to be done. In one class of gauges, the so-called physical gauges, there are no ghost fields. These are useful for qualitative discussion, but often difficult to do calculations in. For a thorough discussion of different gauges and their advantages and disadvantages, see chapter 1.4 of [22] and references therein. Of course, the important physical quantities, such as the S matrix elements, will be gauge invariant. Note that some authors refer to the Lagrangian

(4.1.9), rather than (4.1.6), as the QCD Lagrangian.

4.2 Asymptotic Freedom

Even though QCD is built up from quarks and gluons, the fact is that these have never been directly observed as free particles. Instead the particles that have been observed are all color singlet states of quarks and anti-quarks. If we label with q_i, the quark with color i $(= 1, 2, 3)$, the only simple color singlet combinations possible are [15] (ϵ_{ijk} is the totally anti-symmetric Levi-Civita symbol) :

$$\bar{q}^i q_i, \;\; \epsilon^{ijk} q_i q_j q_k, \;\; \epsilon_{ijk} \bar{q}^i \bar{q}^j \bar{q}^k. \tag{4.2.1}$$

The first of these combinations, consisting of a quark-antiquark pair is called a meson, and the combination with three quarks or three antiquarks is called a baryon. More exotic combinations, with five or more quarks, are also possible, but have not been observed yet. It can be shown, using group theory, that although colorless gluons exist, a color singlet gluon does not exist. This property, that quarks and gluons cannot exist as free particles under long time scales is referred to as confinement. More precisely we can say that the underlying fields of QCD never appear as asymptotic states, while color singlet composite fields invariant under gauge transformations can appear as asymptotic states in the infinite past or future, and we can associate them with plane waves [25].

We now should give some explanation for this phenomenon. First, let us begin by replacing the coupling g that appears in (4.1.3) with

$$g = \sqrt{4\pi\alpha}, \tag{4.2.2}$$

where from now on we will use α as the coupling, which is common in the literature, for the analysis to follow. This coupling is the bare coupling, and is not what is actually measured in experiments. What is measured in experiments is the renormalized coupling constant, which will depend on the energy scale μ at which the experiment is performed. For an introduction to renormalization see [26, 27]. To distinguish the renormalized from the bare coupling, we will write the μ dependence of the former explicitly, $\alpha(\mu)$. The scale μ must be such that $\alpha(\mu) \ll 1$, in which case we can express any cross section as a perturbative series in $\alpha(\mu)$

$$\sigma(p,\mu) = \sum_n^N a_n(p,\mu)\alpha(\mu)^n, \tag{4.2.3}$$

where N is the order of perturbation theory up to which we expand the the cross section, and p are the momenta of the external particles. After measuring the cross section experimentally, we can solve (4.2.3) for $\alpha(\mu)$, which would then give us the value of the coupling at scale μ up to order N. However, μ is an arbitrarily chosen parameter (as long as $\alpha(\mu) \ll 1$) in equation (4.2.3), and the physical cross section cannot depend on it. Therefore we can write

$$\mu\frac{d\sigma(p,\mu)}{d\mu} = 0, \tag{4.2.4}$$

which we can express as an equation in $\alpha(\mu)$

$$\mu^2\frac{d\alpha(\mu)}{d\mu^2} = -b_0\frac{\alpha(\mu)^2}{4\pi} - b_1\frac{\alpha(\mu)^3}{(4\pi)^2} + \cdots \stackrel{\text{def}}{=} \beta(\alpha). \tag{4.2.5}$$

This is the so called β-function, which tells us how our coupling constant depends on the scale μ. Once we know the value of $\alpha(\mu)$, which we obtain from an experimental measurement using (4.2.3), we can then use (4.2.5) to calculate the coupling at any value of μ. Hence one experimental measurement of any cross section provides us with the information needed to calculate other cross sections. For details of the derivation of (4.2.5) see for example [23].

The constants b_0 and b_1 are not arbitrary, but can also be calculated. Their values are

$$\begin{aligned} b_0 &= \frac{11}{3}N - \frac{2}{3}n_f \\ b_1 &= \frac{34}{3}N^2 - (\frac{13}{3}N - \frac{1}{N})n_f, \end{aligned} \tag{4.2.6}$$

which in case of QCD gives $b_0 = 7$. For calculations beyond second order, see for example [28].Note that N in the above equation is the number of colors, introduced at the beginning of the chapter, and not the N of equation (4.2.3). Keeping only the term of order $\alpha(\mu)^2$ in (4.2.5) the expression for $\alpha(\mu)$ at any scale μ_1 in terms of the arbitrary initial scale μ_0 is

$$\alpha(\mu_1) = \frac{\alpha(\mu_0)}{1 + (b_0/4\pi)\ln(\mu_1^2/\mu_0^2)}. \tag{4.2.7}$$

It is more common to express this equation after eliminating the coupling at the arbitrary scale μ_0 by writing

$$\alpha(\mu_1) = \frac{4\pi}{b_0 \ln(\mu_1^2/\Lambda_{QCD}^2)}, \tag{4.2.8}$$

where we have just introduced a new scale parameter, the famous Λ_{QCD}, defined to lowest order by

$$\Lambda_{QCD} = \mu_0 e^{-2\pi/b_0\alpha(\mu_0^2)}. \tag{4.2.9}$$

Now let us examine what happens to equation (4.2.8) as we change μ_1. It is easy to see that as μ_1 goes to infinity, corresponding to large energies or short distances,

$$\alpha(\mu_1) \to 0. \tag{4.2.10}$$

This is the celebrated phenomenon of asymptotic freedom - as the quarks get closer to each other the interaction between them gets switched off, and they act as if they are free particles. This depends crucially on the fact that $b_0 < 0$. In fact, we have defined $\alpha(\mu)$ as a positive quantity and hence equation (4.2.8) is defined for $\mu_1 > \Lambda_{QCD}$. If b_0 was less than 0, we would have to take the $\mu \to 0$ limit to keep $\alpha(\mu)$ positive. On the other hand, as $\mu_1 \to \Lambda_{QCD}$, we see that

$$\alpha(\mu_1) \to \infty. \tag{4.2.11}$$

Thus as we are decreasing the energy, and thus increasing the distance between the particles, the coupling between them becomes stronger and stronger, until we get close to Λ_{QCD} which is when all Hell starts to break loose. This is what leads to the phenomenon of confinement. Of course, retracing the derivation of (4.2.8) we see that this was valid only to first order in perturbation theory, and thus we cannot just naively set $\mu_1 = \Lambda_{QCD}$ and get infinite coupling. Effects beyond the first order would become important, and in fact since the coupling constant is indeed becoming very strong, perturbation theory begins to fail, and non-perturbative effects begin to dominate. Hence Λ_{QCD} can be estimated experimentally as the energy at which lowest order perturbation theory no longer gives us valid results, and the current estimates give approximately $\Lambda_{QCD} \simeq 200$ MeV.

The proof that non-Abelian gauge theories exhibit asymptotic freedom was a very important step in the development of physics. Indeed it has also been proven that the only theories in four dimension with asymptotic freedom are the non-Abelian gauge theories. This is what led to the ascendancy of QCD. Prior to the proof of asymptotic freedom, most physicists expected all interactions to be like QED, where the coupling runs in the other direction - at small distances the coupling is extremely large, and as we increase the distance it effectively gets switched off.

4.3 Deep Inelastic Scattering

In many ways, deep inelastic scattering, or DIS, is the quintessential QCD process. Since it is scattering between a lepton and a hadron, it can be easier to work with than some of the other QCD processes, which study hadron hadron scattering, but at the same time it contains many of the fundamental features and subtleties of hadron dynamics. It also introduces most of the strategies and the language used in studying perturbative QCD. Historically, the need to explain the data collected in DIS experiments has led to the advancement of the theory, and indeed it was extremely important as a catalyst for QCD to come about in the first place.

We will now introduce the basics of DIS, and through that the basics of some of the other processes we will study. We will return to DIS in chapter 8, where we will se what insights string theory can provide into this important window to the structure of the nucleons.

Deep inelastic scattering is scattering between a lepton and a hadron. In the original experiments done at SLAC in the late 1960's, the lepton was an electron, and the hadron was a proton. In the rest of this section we will mostly refer to the lepton as electron, as is common in most of the literature. In experiments, such as the recent ones done at HERA, the lepton is often a positron, or a muon, but that will not affect any of our discussion.

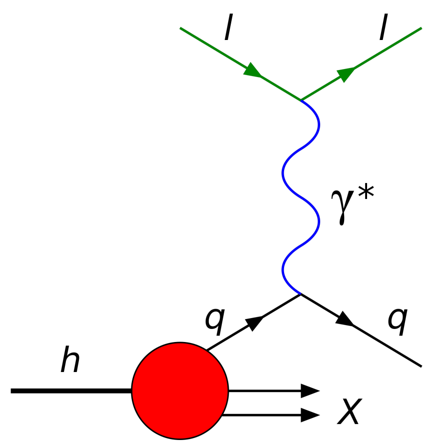

Figure 4.1: A basic DIS process.

If we call the initial electron momentum k and the final electron momentum k', then the momentum transfer between the electron and the hadron is clearly $q^\mu = k^\mu - k'^\mu$, and we can further define $Q^2 = -q^\mu q_\mu$. This is equal to our Mandelstam variable t from equation (2.1.9), but in DIS language it is more common to use Q^2. This momentum is carried by a virtual photon γ^*, radiated by the electron. It was found experimentally, in the original DIS experiments, that by studying the cross section at large Q^2 (compared to Λ_{QCD}), that the scattering happens as if the electrons interacts with a hard constituent within the proton, and not the proton itself. In fact, we will call large Q^2 scattering hard scattering, and low Q^2 scattering soft scattering. This was analogous to Rutherford's experiments half a century earlier which determined that the atom also has a substructure.

Hence the parton model was formulated by Feynman and others. The nucleon is made out of many pointlike parts, or 'partons'. We now know that these partons are actually quarks, antiquarks and gluons. Deep inelastic scattering is actually elastic scattering between the electron and a parton. The parton is then knocked out, and through the process of hadronization recombines with other partons to form a new hadron or hadrons. Hence we can write

$$\sigma_{tot}(e(k)+p(P)\to e(k')+X)=\int_0^1 dx\sum_i \phi_i(x)\sigma_{el}(e(k)q_i(xP)\to e(k')+q_i(p')). \quad (4.3.1)$$

This equation requires some explanation. The variable x is the fraction of the total momentum of the proton carried by the parton, and hence its range is from 0 to 1. The function $\phi_i(x)$, called the parton distribution function (PDF), represents the probability of finding a parton of type i inside the hadron, carrying a fraction x of its momentum. σ_{el} is just the aforementioned elastic scattering cross section.

To the passing glance, equation (4.3.1) may appear logical. However, the observant reader would notice something is wrong immediately. We are summing over all the PDFs, which as we just said represent probabilities, and quantum mechanics teaches us that we should add amplitudes and not probabilities. However, the reason we can write this expression is based on the discussion in section 4.2 of confinement and asymptotic freedom. At large Q^2, from the point of view of the virtual photon, it will see the hadrons as free and frozen in time. It will then scatter off of this hadron, knocking it out. The hadron will then stabilize through lower energy processes and form a color singlet state [23, 15]. Recall that the masses of the light quarks are below Λ_{QCD}, and hence in the region where perturbation theory no longer applies.

We will come back to this comment and PDFs later. First, let us return to equation (4.3.1) and write it in terms of differential cross sections:

$$\frac{d\sigma_{tot}}{dtdu} = \int_0^1 dx \sum_i \phi_i(x) \frac{d\sigma_{el}}{dtdu}. \tag{4.3.2}$$

The elastic scattering cross section can be easily computed (see chapter 2 or [29])

$$\frac{d\sigma_{el}}{dtdu} = x \frac{2\pi\alpha^2 e_i^2}{t^2} \frac{s^2+u^2}{s^2} \delta(t + x(s+u)). \tag{4.3.3}$$

Now let us look at the total cross section, the left hand side of (4.3.1). It can be written in terms of a leptonic scattering, involving an electron-electron-photon vertex, and a hadronic scattering, involving an electromagnetic current and a hadron. The leptonic part can be calculated from QED (see [23, 21, 15]), and for the hadronic tensor we can write

$$\begin{aligned} W_{\mu\nu}(p,q) = \frac{1}{8\,\pi} \sum_\sigma \sum_X \langle h(p,\sigma)| j_\mu^\dagger(0) |X\rangle \, \langle X| j_\nu(0) | h(p,\sigma)\rangle \times \\ \times \, (2\,\pi)^4 \, \delta^4(p + q - p_X) \; . \end{aligned} \tag{4.3.4}$$

Here j_μ is the appropriate electromagnetic current (in general the scattering can happen with Z exchange instead of γ in which case we would have a weak current, but this will not be the subject of this thesis), and we are summing the expression over all intermediate states X, and averaging over the spins of the particles. However, due to symmetry properties and gauge invariance, we can write $W_{\mu\nu}$ completely generally in the form

$$W^{\mu\nu}(p,q) = -(g^{\mu\nu} + \frac{q^\mu q^\nu}{Q^2}) F_1(x,Q^2) + \frac{2x}{Q^2}(p^\mu + \frac{1}{2x} q^\mu)(p^\nu + \frac{1}{2x} q^\nu) F_2(x,Q^2). \tag{4.3.5}$$

F_1 and F_2 are called the structure functions. In fact in the parton model, they are only function of x, and not of Q^2. However, the parton model is just a first order in $\alpha(\mu)$ approximation of QCD, and we are keeping the explicit Q^2 dependence in anticipation of higher order corrections we will consider later on.

We can now express the cross section in terms of the hadronic tensor. It will also depend on the flux of the virtual photon γ^*. There is some ambiguity in how this is defined. Using the convention from [16] we have

$$\sigma_\lambda^{\gamma^* p} = \frac{4\pi^2 \alpha_{em}}{{}^{Q^2}\!/_{2x} + 2mx^2} n_\lambda^\mu n_\lambda^\nu W_{\mu\nu}. \tag{4.3.6}$$

The index λ corresponds to the polarization of the photon. Since the photon is virtual, it can have three polarizations. The vector n_λ is the polarization vector. In Appendix A we will include more detailed calculations with the explicit form of the polarization vector and more precise kinematics.

We can write the total cross section as the sum of the transverse and the longitudinal cross sections

$$\sigma_{total} = \sigma_T + \sigma_L. \tag{4.3.7}$$

By using transverse and longitudinal polarization vectors, we can then calculate these (see appendix)

$$\sigma_T^{\gamma^* p} = \frac{4\pi^2 \alpha_{em}}{{}^{Q^2}\!/_{2x} + 2mx^2} F_1, \tag{4.3.8}$$

and

$$\sigma_L^{\gamma^* p} = \frac{4\pi^2 \alpha_{em}}{Q^2} (F_2 - \frac{Q^2}{{}^{Q^2}\!/_{2x} + 2xm^2} F_1). \tag{4.3.9}$$

It is customary to define

$$F_L = F_2 - \frac{Q^2}{Q^2/2x + 2xm^2} F_1, \tag{4.3.10}$$

in which case

$$\sigma_L^{\gamma^* p} = \frac{4\pi^2 \alpha_{em}}{Q^2} F_L. \tag{4.3.11}$$

These are the expressions for the polarized cross section in terms of the structure functions.

We can easily solve this system to reexpress instead the structure functions in terms of the cross section. The result is

$$F_1 = \frac{Q^2/2x + 2xm^2}{4\pi^2 \alpha_{em}} \sigma_T^{\gamma^* p}, \tag{4.3.12}$$

and

$$F_2 = \frac{Q^2}{4\pi^2 \alpha_{em}} (\sigma_L^{\gamma^* p} + \sigma_T^{\gamma^* p}). \tag{4.3.13}$$

So far all these relations have been exact. We have not made use of any approximation. If, however, we would like to work in the Regge limit we can take $x \ll 1$, which will simplify some of our calculations. The cross section (4.3.6) is now given by

$$\sigma_\lambda^{\gamma^* p} \simeq \frac{4\pi^2 \alpha_{em}}{Q^2} 2x n_\lambda^\mu n_\lambda^\nu W_{\mu\nu}, \tag{4.3.14}$$

$$\sigma_T^{\gamma^* p} \simeq \frac{4\pi^2 \alpha_{em}}{Q^2} 2x F_1, \tag{4.3.15}$$

$$\sigma_L^{\gamma^* p} \simeq \frac{4\pi^2 \alpha_{em}}{Q^2} F_L, \tag{4.3.16}$$

$$F_L \simeq F_2 - 2x F_1. \tag{4.3.17}$$

Turning things around again so that we have the structure functions instead, we see that

$$F_1 \simeq \frac{Q^2}{4\pi^2\alpha_{em}}\frac{1}{2x}\sigma_T^{\gamma^* p} \tag{4.3.18}$$

and

$$F_2 = \frac{Q^2}{4\pi^2\alpha_{em}}(\sigma_L^{\gamma^* p} + \sigma_T^{\gamma^* p}). \tag{4.3.19}$$

This expression is important. By taking into account (4.3.7) we see that it gives us the structure function F_2 in terms of the total cross section. We will use this in chapter 8 to derive an expression for F_2 from string theory. In Appendix A we will give more details of the above derivation, and show that in the $Q^2 \to 0$ limit, in which the photon becomes real, we get the expected result.

We have expressed the structure functions in terms of the total cross section. To give a physical interpretation of their meaning, we have to connect them to equations (4.3.1) and (4.3.2). The equations we derived here correspond to just the hadronic scattering part

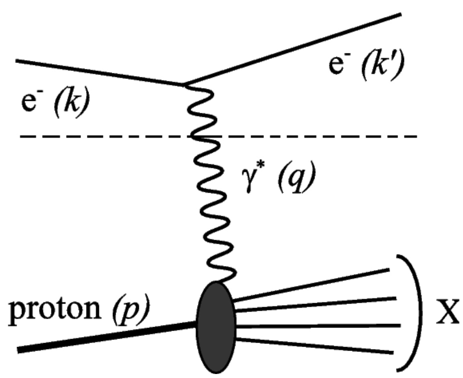

Figure 4.2: We are only interested in the part below the dashed line.

The leptonic tensor can be calculated easily using QED, and we can combine it with the above results to express the differential cross section for scattering of $e + P \to e + X$ as

$$\frac{d\sigma_{tot}}{dtdu} = \frac{4\pi\alpha^2}{t^2 s^2}\frac{1}{s+u}[(s+u)^2 xF_1 - usF_2]. \tag{4.3.20}$$

By comparing this equation to (4.3.2) and (4.3.3), we get the desired physical meaning for the structure functions

$$2xF_1(x) = F_2(x) = \sum_i e_i^2 x\phi_i(x). \tag{4.3.21}$$

This is the most important formula of the parton model. The first equality on the left is known as the Callan-Gross relation. It leads to the vanishing of the longitudinal structure function (4.3.17). Recall that $\phi_i(x)$ is the probability of finding a parton with momentum x inside the hadron. In (4.3.21) we wrote the structure functions as only dependent on x, while before we were writing them as functions of both x and Q^2. The reason is that, as mentioned before, the parton model is only a first order approximation of QCD. In fact, this prediction of the parton model, that F_1 and F_2 only depend on the dimensionless variable x, is known as Bjorken scaling, and x is often called the Bjorken x. Indeed, the Q^2 dependence is supposed to be weak, and using perturbative QCD can be calculated beyond the first order, where Bjorken scaling will be violated, but only slowly in Q^2. This dependence will be much of the subject of the next section.

Equation (4.3.1) has the important property of soft-hard factorization. Which is common in many QCD processes, and not just a feature of DIS (even when we go beyond the leading order). The elastic scattering cross section depends on the hard scattering scale Q, and can be calculated perturbatively. On the other hand, the parton distribution functions depend on soft processes, for which perturbation theory is not valid. These cannot be calculated using perturbative QCD. However, these are universal, and do not depend on the details of the elastic scattering. They are the same for all processes. However, they do depend on the momentum scale. Using the equations (4.3.12) and (4.3.13) we can relate the experimentally measured cross section to determining the PDFs. The common strategy in QCD is to determine the PDFs experimentally at some scale, and then use evolution equations to calculate them at all energies.

4.4 DGLAP and BFKL equations

To take into account the dependence of the parton distribution functions on Q^2, and therefore the violation of Bjorken scaling, we can use the approach known in the literature by various combinations of the names of Dokshitzer, Gribov, Lipatov, Altarelli and Parisi. We will refer to it as the DLGAP approach, and call the corresponding equations we obtain the DGLAP equations.

First, let us make some comments about gluons. In equation (4.3.1) and the subsequent discussion, the functions $\phi_i(x)$ correspond to quarks, and in this chapter we will instead label them $q(x)$, and the sum will run over both quarks and antiquarks. This is because initially it was uncertain whether these 'partons' of the parton model correspond to quarks or not. However now we know that they do, because they also match the quantum numbers that quarks carry. We do not have gluons in this sum, because the gluons are electrically neutral, and therefore do not interact with the photons.

Nevertheless, if there are gluons inside the proton, they will carry some of its momentum and we can calculate

$$\sum_i \int_0^1 dx x \phi_i(x) = 1 - \epsilon_g, \tag{4.4.1}$$

where ϵ_g is the missing momentum fraction, carried by the gluons. By measuring the structure functions in electron proton and electron neutron scattering, and integrating them from 0 to 1 over x, we do find from experiments that the missing momentum is not zero, and indeed is significant. Therefore besides the quark and antiquark distribution functions inside the proton, we must also consider the gluon distribution functions, which we will label as $g(x)$.

Even though the photon will not interact directly with the electrically neutral gluon, it does not mean we should completely ignore the presence of gluons. A quark struck by the photon can radiate a gluon, or we could have a $\gamma^* + g \to q + \bar{q}$ process, see figure.

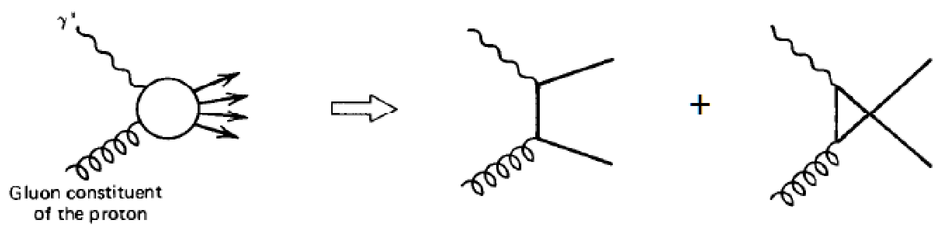

Figure 4.3: The lowest order contributions of $\gamma^* + g \to q + \bar{q}$ processes to DIS cross section.

These diagrams will be of lower order at large Q^2, justifying what we said in the previous section. A $\gamma^* + q \to \gamma^* + q$ diagram is of order α_{em} while the diagrams of figure 4.3 will be of order $\alpha_{em}\alpha(\mu)$.

It can be shown [29] that by including these diagrams in the scattering amplitude will modify F_2, (4.3.21)

$$F_2(x, Q^2) = \sum_i x e_i^2 (q_i(x) + \Delta q_i(x, Q^2)). \tag{4.4.2}$$

The first term is just what we had before, while the second term

$$\Delta q_i(x,Q^2) \stackrel{\text{def}}{=} \frac{\alpha(\mu)}{2\pi}\log\frac{Q^2}{\mu^2}\int_x^1 \frac{dy}{y} q_i(y) P_{qq}(\frac{x}{y}), \tag{4.4.3}$$

gives us the Bjorken scaling violation we mentioned previously, to first order in $\alpha(\mu)$. The function $P_{qq}(\frac{x}{y})$ is called a splitting function, and represents the probability that the quark with momentum py emits a gluon, giving us a quark with momentum px. Clearly we need $y > x$, explaining the limits of the integral.

By considering how this equation changes with $\log Q^2$ we derive

$$\frac{d}{d\log Q^2} q_i(x,Q^2) = \frac{\alpha(\mu)}{2\pi}\int_x^1 \frac{dy}{y} q_i(y,Q^2) P_{qq}(\frac{x}{y}). \tag{4.4.4}$$

This included just the contribution from the $\gamma^* + q \to q + g$ diagrams. Similarly, by including the $\gamma^* + g \to q + \bar{q}$ contributions as well, we can show that the structure function would pick up an additional term to (4.4.2) equal to

$$\sum_i x e_i^2 \log\frac{Q^2}{\mu^2}\int_x^1 \frac{dy}{y} g(y) \frac{\alpha(\mu)}{2\pi} P_{qg}(\frac{x}{y}), \tag{4.4.5}$$

with the splitting function $P_{qg}(\frac{x}{y})$ being the probability that a gluon of momentum py disintegrates into a $q\bar{q}$ pair, in such a way that the quark carries the momentum px.

Including these contributions in equation (4.4.4) we would get

$$\frac{d}{d\log Q^2} q_i(x,Q^2) = \frac{\alpha(\mu)}{2\pi}\int_x^1 \frac{dy}{y} (q_i(y,Q^2) P_{qq}(\frac{x}{y}) + g(y,Q^2) P_{gq}(\frac{x}{y})), \tag{4.4.6}$$

and similarly for the gluon distribution function

$$\frac{d}{d\log Q^2}g_i(x,Q^2) = \frac{\alpha(\mu)}{2\pi}\int_x^1 \frac{dy}{y}(\sum_i q_i(y,Q^2)P_{gq}(\frac{x}{y}) + g(y,Q^2)P_{gg}(\frac{x}{y})). \tag{4.4.7}$$

The index i runs over all quark and antiquark flavors. In the limit that the quark masses can be neglected, P_{qq} will not depend on i.

Equations (4.4.6) and (4.4.7) are the celebrated DGLAP evolution equations. They are clearly integro-differential equations. If we know the values $q_i(x,Q_0^2)$ and $g(x,Q_0^2)$ at some scale Q_0^2, we can then solve these equations using these values as boundary conditions, and calculate the values at any Q^2. This rounds out the strategy discussed in the previous section.

The DGLAP equation depends on using perturbative QCD, hence on the smallness of $\alpha(\mu)$. Furthermore, it also depends on terms of order $\alpha_{em}\alpha(\mu)$ being smaller than the terms of order $\alpha(\mu)$. However, according to the discussion in 4.2, as $Q^2 \to \Lambda_{QCD}^2$, the coupling becomes large. The moral is that we should only use the DGLAP equations at large values of Q^2, and there is excellent agreement between theory and experiment in this regime. Precisely at what point the DGLAP equation breaks down is subject to intense ongoing study.

Somewhat similar to the DGLAP equation is the BFKL equation, named after Balitsky, Fadin, Kuraev and Lipatov. It describes the evolution of quark and gluon distribution functions, but instead of evolution in Q^2, it looks at evolution in x. It is applicable when x is small, and Q^2 large, but not too large.

To lowest order, it only considers gluons (because at small x gluons are the dominant partons [22]), and assumes that the strong coupling is fixed. It is given by [16]

$$x\frac{\partial}{\partial x}g(x,Q^2) = x\frac{\partial}{\partial x}g^{(0)}(x,Q^2) + \alpha\int dk^2 K(Q^2,k^2)g(x,k^2). \tag{4.4.8}$$

The function $g^{(0)}$ is a non-perturbative distribution, and the second term on the right hand side is the perturbative correction. It can be shown to correspond to a sum of Reggeised gluon ladders, with leading order behavior in $\alpha \log s$. The function $K(Q^2, k^2)$ is referred to as the BFKL kernel. Its eigenfunctions are powers of momentum

$$\int dk^2 K(Q^2,k^2)(k^2)^\nu = K(\nu)(Q^2)^\nu. \tag{4.4.9}$$

It is usual, for calculational simplicity, to work with the function $g(j,\nu)$ instead, defined by

$$g(j,\nu) = \int_0^1 dx x^{j-1}\int_0^\infty dQ^2(Q^2)^{(-\nu-1)}g(x,Q^2). \tag{4.4.10}$$

Care must be taken in choosing the contour in the complex plane for the above integrations [16]. The x integration above ranges up to $x = 1$, while the BFKL equation is only applicable at small x. We can separate g into a part that satisfies the BFKL equation and a remainder, only important when x is not small

$$g(j,\nu) = g^{BFKL}(j,\nu) + g^{rem}(j,\nu). \tag{4.4.11}$$

Taking into account only the BFKL part, we have

$$jg^{BFKL}(j,\nu) = jg^{(0)}(j,\nu) - \alpha K(\nu)g^{BFKL}(j,\nu). \tag{4.4.12}$$

An explicit calculation for $K(\nu)$ to lowest order would give

$$K(\nu) = \frac{3}{\pi}(2\psi(1) - \psi(\nu) - \psi(1-\nu)), \tag{4.4.13}$$

with $\psi(\nu) = \frac{\Gamma'(\nu)}{\Gamma(\nu)}$. It can be shown that this will lead to the total cross section going as

$$\sigma \simeq s^{\lambda}, \tag{4.4.14}$$

where

$$\lambda = \frac{4\alpha N}{\pi} \log 2\,. \tag{4.4.15}$$

Recall our discussion of the Pomeron in section 3.2, and equation (3.2.3). We see that we can identify the above as happening with the exchange of a Pomeron, with intercept equal to $1 + \lambda \simeq 1.4 - 1.5$. It also interprets the Pomeron as a tower of Reggeized gluon ladders.

The BFKL equation is applicable at Q^2 large which corresponds to high momentum transfer, or hard scattering. Our discussion in chapter 3 relied on the limit of low momentum transfer, or soft scattering. These were thought as two distinct object, a non-perturbative Pomeron with intercept around 1.08 and a perturbative Pomeron with intercept around 1.4. Experimentally, indeed at small values of Q^2 the data can be parametrized with the soft Pomeron, and at high Q^2 with the hard Pomeron. We will see however that these are unified through string theory in the AdS/CFT correspondence.

The BFKL equation has several problems. It is valid only in a small range of x and Q^2, and even there it was found that the second order correction is large compared to the leading order term, and of opposite sign. It also does not properly take into account conservation of energy, and since it leads to a power like behavior for the cross section, it violates unitarity.

Chapter 5

String Theory

String theory is another very complex and diverse subject. We will focus on those apsects which are important for later work. In particular, we will work out the massless states of the closed string, which we will later relate to the Pomeron and the Odderon, and see how we can use string vertex operators to study their scattering, which we will apply in AdS space.

It is interesting to note that string theory started out as a candidate for explaining just strong interactions. Historically the first success of the theory was the derivation of the Veneziano amplitude, which was able to fit the Regge trajectories of chapter 3. It turned out that once we quantize the theory, it must include a massless spin 2 state, not found in the theory of strong interactions. This was at first thought to be a bug, but was later instead declared a feature. We will indeed use the graviton state in a higher dimensional string theory to describe a theory of strong interactions, and no gravity, in a lower number of dimensions.

5.1 Spectrum of States

A one dimensional object moving through spacetime describes a two dimensional sheet, which we will refer to as the world sheet. We can parametrize it using two independet coordinates, let us call them σ and τ. The simplest reparametrization invariant action for such an object is proportional to its area, and called the Nambu-Goto action:

$$S_{NG} = \frac{1}{2\pi\alpha'}\int d\sigma d\tau \sqrt{(\partial_\tau X)^2(\partial_\sigma X)^2 - (\partial_\tau X \cdot \partial_\sigma X)^2}. \tag{5.1.1}$$

Here α' is a constant, called the Regge slope. $X(\tau, \sigma)$ are the target space string coordinates.

To get an action that is simpler to work with, we can introduce an auxiliary world sheet metric field γ_{ab} and use the Polyakov metric:

$$S_P[X,\gamma] = -\frac{1}{4\pi\alpha'}\int d\tau d\sigma \sqrt{-\gamma}\gamma^{ab}\partial_a X^\mu \partial_b X_\mu, , \tag{5.1.2}$$

and $\gamma = \det \gamma_{ab}$. By varying the action with respect to $\delta\gamma_{ab}$ we would get the equation of motion for γ_{ab} which we can then use to eliminate it from (5.1.2) and recover (5.1.1).

The action (5.1.2) is left invariant by Poincaré, diffeomorphisms, and two dimensional Weyl transformations. These will lead to some constraints on the allowed states. We will come back to the constraints later.

By varying the action with respect to δX^μ we can obtain the Euler-Lagrange equations of motion. The general form will be complicated, but as usual fixing a gauge will considerably simplify the equations. We can in fact exploit all three symmetries we mentioned in the above paragraph, but for now we will only spend two. Using the diffeomorphism and Weyl invariance, we can simplify the metric γ_{ab} to

$$\gamma_{ab} = \eta_{ab}, \tag{5.1.3}$$

where $\eta_{ab} = diag(1, -1)$. This choice is called the covariant gauge. Of course there are many other options we can choose. In the covariant gauge, the Euler-Lagrange equation of motion for the string is just the one dimensional wave equation

$$\partial_a \partial^a X^\mu = (\partial_\tau^2 - \partial_\sigma^2) X^\mu = 0. \tag{5.1.4}$$

To get this result in the case of the open string, we would have to impose the boundary conditions on the endpoints

$$X^\mu(\tau, \{\sigma = 0, \pi\}) = 0, \tag{5.1.5}$$

known as the Dirichlet boundary condition, or

$$\partial_\sigma X^\mu(\tau, \{\sigma = 0, \pi\}) = 0, \tag{5.1.6}$$

known as the Neumann boundary condition. In the case of the closed string, it is enough to know that since the string is closed

$$X^\mu(\tau, \sigma + \pi) = X^\mu(\tau, \sigma). \tag{5.1.7}$$

The general solution of (5.1.4) for a closed string can be written in terms of oscillator coefficients

$$X^\mu = x^\mu + 2\alpha' p^\mu \tau + \frac{i}{2}\sqrt{(}2\alpha') \sum_{n\neq 0} (\frac{1}{n}\alpha_n^\mu e^{-2in(\tau-\sigma)} + \frac{1}{n}\tilde{\alpha}_n^\mu e^{-2in(\tau+\sigma)}). \tag{5.1.8}$$

The zero mode,

$$\alpha_0^\mu \stackrel{\text{def}}{=} \sqrt{\frac{\alpha'}{2}}\, p^\mu \tag{5.1.9}$$

has been pulled out from the sum.

We can now quantize the theory by promoting the oscillators α^μ to operators, and imposing commutation relations

$$[\alpha_m^\mu, \alpha_n^\nu] = -m\,\delta_{m+n,0}\,\eta^{\mu\nu} \tag{5.1.10}$$

$$[\tilde{\alpha}_m^\mu, \tilde{\alpha}_n^\nu] = -m\,\delta_{m+n,0}\,\eta^{\mu\nu} \tag{5.1.11}$$

$$[\alpha_m^\mu, \tilde{\alpha}_n^\nu] = 0\ . \tag{5.1.12}$$

These are analogous to creation and annihilation operators, only with a different normalization. In fact, we can show that oscillators with negative n will correspond to creation operators, while those with positive n to annihilation operators:

$$\begin{aligned} a_n^\mu &= \frac{1}{\sqrt{n}}\alpha_n^\mu\,, \quad \tilde{a}_n^\mu = \frac{1}{\sqrt{n}}\tilde{\alpha}_n^\mu \\ a_n^{\dagger\mu} &= \frac{1}{\sqrt{n}}\alpha_{-n}^\mu\,, \quad \tilde{a}_n^{\dagger\mu} = \frac{1}{\sqrt{n}}\tilde{\alpha}_{-n}^\mu\,. \end{aligned} \tag{5.1.13}$$

Acting with these operators on the string vacuum will produce all the states of string theory.

We derived these results in the conformal gauge, (5.1.3). However we cannot just pick a gauge of γ_{ab} and forget about it. The symmetries of the problem will impose constraints on our theory. To implement these, analogously to the Euler-Lagrange equation for X^μ, we also need to find the equation of motion for γ_{ab} before applying our choice of gauge (5.1.3), and then after fixing the gauge the thus obtained equation will be the necessary constraint. As usual, we vary the action with respect to the field and set it to zero:

$$\frac{\delta S_P[X,\gamma]}{\delta\gamma_{ab}} = 0. \tag{5.1.14}$$

It is more common to slightly adjust this, by first defining the world sheet energy-momentum tensor of the theory

$$T_{ab} \stackrel{\text{def}}{=} \frac{-2\pi}{\sqrt{-\gamma}}\frac{\delta S_P[X,\gamma]}{\delta\gamma_{ab}}, \tag{5.1.15}$$

in which case the equation of motion for γ_{ab} gives us its vanishing

$$T_{ab} = 0. \tag{5.1.16}$$

Quantum mechanically, this condition means that for a physical state $|\phi>$ we must have $T_{ab}|\phi>= 0$. Properly implementing this condition will involve some subtleties, for which we refer the reader to standard treatments [30, 31]. What is clear is that this will limit the states we can form by acting on the vacuum with the raising and lowering operators. We cannot just take every possible combination and get a physical state.

The physical state condition (5.1.16) is most commonly expressed in terms of the so called Virasoro operators. First let us define

$$L_m = -\frac{1}{2}\sum_{n=-\infty}^{+\infty}\alpha^\mu_{m-n}\alpha_{\mu n} \quad m \neq 0, \tag{5.1.17}$$

$$\tilde{L}_m = -\frac{1}{2}\sum_{n=-\infty}^{+\infty} \tilde{\alpha}^{\mu}_{m-n}\tilde{\alpha}_{\mu n} \quad m \neq 0. \tag{5.1.18}$$

The case $m = 0$ requires special treatment. In this case we can first define two expressions

$$L_0 = -\frac{1}{2} : \sum_{n=-\infty}^{+\infty} \alpha^{\mu}_{-n}\alpha_{\mu n} :, \tag{5.1.19}$$

and

$$L_0' = -\frac{1}{2}\sum_{n=-\infty}^{+\infty} \alpha^{\mu}_{-n}\alpha_{\mu n}, \tag{5.1.20}$$

and similarly for $\tilde{L}_0$, with $: \cdot :$ denoting normal ordering. Then the difference between equations (5.1.19) and (5.1.20) is

$$L_0 - L_0' = a, \tag{5.1.21}$$

where a is a formally infinite constant. Operators (5.1.17)-(5.1.19) are the Virasoro operators. In terms of them, the physical state conditions (5.1.16) are

$$L_m|\phi >= \tilde{L}_m|\phi >= 0, \tag{5.1.22}$$

and

$$L_0|\phi >= \tilde{L}_0|\phi >= a|\phi > . \tag{5.1.23}$$

Writing equation (5.1.23) in terms of the ladder operators (5.1.13), it is easy to see that we can express L_0 in terms of the number operator:

$$L_0 = \frac{\alpha'}{4}p^2 + N\,, \quad \tilde{L}_0 = \frac{\alpha'}{4}p^2 + \tilde{N}\,, \tag{5.1.24}$$

where, as in quantum mechanics

$$N = \sum_{n=1}^{\infty} n a_n^{\mu\dagger} a_{n,\mu} \,. \tag{5.1.25}$$

The $p^\mu p_\mu$ term above appears from the zero mode (5.1.9) $\alpha_0^\mu \alpha_{0\mu}$. Therefore equations (5.1.23) imply that a physical state must always be composed out of an equal number of left moving modes and right moving modes (recall from equation (5.1.8) the modes α_n^μ multiply $e^{-2in(\tau-\sigma)}$ while $\tilde{\alpha}_n^\mu$ multiply $e^{-2in(\tau+\sigma)}$, hence we can call them right moving and left moving). Now any physical state can be formed by acting on the vacuum $|0>$ with the raising and lowering operators, as long as (5.1.22) and (5.1.23) are obeyed. We can use (5.1.24) together with (5.1.23) to calculate the masses of the physical states:

$$M^2 = -p^2 = \frac{4}{\alpha'}(N - \frac{L_0}{2} + \tilde{N} - \frac{\tilde{L}_0}{2}) = \frac{4}{\alpha'}(N + \tilde{N} - 2a) \,. \tag{5.1.26}$$

We can also write the string Hamiltonian in terms of $L_0, \tilde{L}_0$

$$H = L_0 + \tilde{L}_0 - 2a. \tag{5.1.27}$$

For bosonic closed string, the lowest level state is the tachyon, and from (5.1.26) its mass squared is

$$M_T^2 = -\frac{4}{\alpha'} a \tag{5.1.28}$$

which is negative (a is positive). We usually would like to avoid having such a state in a stable theory. If we were to consider superstrings, the tachyon can be eliminated using the GSO projection [30]. However, bosonic string theory is simpler to use, and the quickest way to extract information out of problems, and the tachyon is the simplest state we can use. Although not present in the final theory, it is useful to work with. Of course, some times care must be taken to make sure that the conclusions drawn still hold after transitioning to superstrings.

The next level state would be created out of the combination of α_{-1} and $\tilde{\alpha}_{-1}$

$$\xi_{\mu\nu}\alpha^{\mu}_{-1}\tilde{\alpha}^{\nu}_{-1}|0> . \tag{5.1.29}$$

Any rank two tensor $\xi_{\mu\nu}$ can be decomposed in terms of irreducible representations of $SO(D-1)$ into

$$\xi_{\mu\nu} = \frac{1}{2}(\xi_{\mu\nu} + \xi_{\nu\mu} - 2\eta_{\mu\nu}(D-2)^{-1}\xi^{\beta}_{\beta}) + \frac{1}{2}(\xi_{\mu\nu} - \xi_{\nu\mu}) + \eta_{\mu\nu}(D-2)^{-1}\xi^{\beta}_{\beta}), \tag{5.1.30}$$

corresponding to the traceless symmetric representation, antisymmetric representation and the trace.

Using equation (5.1.26) we see that these states are massless. Hence the massless sector of string theory is made up of three states. The traceless symmetric state corresponds to the aforementioned massless spin 2 particle, and we can identify it with the graviton. This is a crucial result. We see that we always have a graviton present in closed string theory. The antisymmetric state has spin 1, and corresponds to the so called Kalb-Ramond state. Finally, the trace is spin 0, and corresponds to the dilaton.

We will later see, when we apply Regge theory to strings, that the graviton will give rise to the Pomeron Regge trajectory, while the Kalb-Ramond state will give rise to the Odderon Regge trajectory.

We have written things in this chapter in the conformal gauge, (5.1.3). Sometimes the physical results can be arrived at most quickly in the light cone gauge, where we set $X^+ = \tau$. In this gauge it can be most easily seen that the states (5.1.30) have precisely the right number of independent components to confirm our identification above. We shall represent the three massless states by

$$|h\rangle = \sum_{I,J} h^{IJ}|I,J;k\rangle \quad , \quad |B\rangle = \sum_{I,J} B^{IJ}|I,J;k\rangle \quad , \quad |\phi\rangle = \sum_{I,J} \eta^{IJ}|I,J;k\perp\rangle \ . \tag{5.1.31}$$

For reference, the most general state is [31]

$$|N,\tilde{N};k\rangle = \left[\prod_{i=2}^{D-1}\prod_{n=1}^{\infty} \frac{(\alpha^i_{-n})^{N_{in}}(\tilde{\alpha}^i_{-n})^{\tilde{N}_{in}}}{(n^{N_{in}}N_{in}!\,n^{\tilde{N}_{in}}\tilde{N}_{in}!)^{1/2}}\right]|0,0;k\rangle. \tag{5.1.32}$$

In our discussion, in order to quickly sketch the main steps, we have skipped many of the subtleties involved in the quantization of strings and imposing the Virasoro constraints (5.1.22) and (5.1.23). We refer the interested reader to [31, 30], where he can find all the necessary details, as well as a discussion of open strings. One very important point is that in order to regularize the theory, the above procedure will only work in $D = 26$ spacetime dimensions for the bosonic string. In this case, the constant a of equation (5.1.23) will be equal to 1. Then equation (5.1.23) can be expressed in the form in which we will use it in chapters 6 and 7:

$$L_0|\phi>=\tilde{L}_0|\phi>=|\phi>\ . \tag{5.1.33}$$

In the case of superstring theory, a similar calculation will lead to $D = 10$ spacetime dimensions.

5.2 String Interactions

Now that we have learned some of the basics of string theory, and seen what states lie at the lowest level of the string spectrum, let us also learn how strings interact. Here we will present just the basic ideas, and in appendix C we will work out in considerable detail some specific examples. Rather than starting from the interacting string Lagrangian, the theory of which is still not very well understood, it is common to use quantum field theory to motivate some general rules that string scattering should follow, and then see how we can implement those rules.

In quantum field theory of point particles, we can study their scattering amplitudes by using Feynman diagrams. Similarly for string we can consider string diagrams. These are two dimensional surfaces parametrized by coordinates τ and σ. Loops in string interactions would correspond to holes in these surfaces. The process we show in figure 5.1 starts out with two string, which join to become a single string, and then later split and give us two string again. All strings considered are closed. Unlike Feynman diagrams, there is no invariant spacetime point where the interaction occurs. Observers in different reference frames will see the string joining and splitting at different points in spacetime.

Using the conformal invariance of the world sheet metric, we can use the transformation $\gamma_{ab} \to e^{\phi}\gamma_{ab}$ to transform these surfaces into Riemann surfaces. The states in the infinite past and future would now be just points. Since we can never propagate to the infinite past or future, these points should not belong to the surface, and in fact they will correspond to punctures. Hence we can classify string interactions by topology of punctured Riemann surfaces. These surfaces will be the same irrespective of what string states we are looking at. We also need an operator to keep track of the quantum numbers of these states, which

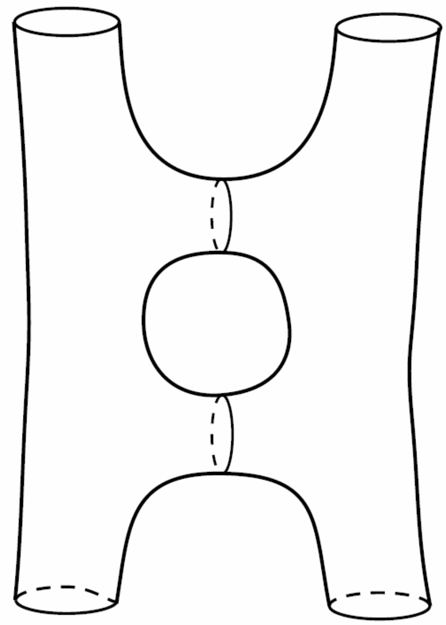

Figure 5.1: A one loop string scattering diagram.

is what will distinguish the scattering of different states. We will call these operators vertex operators.

Let us first change variables from σ, τ to

$$z = \tau + i\sigma \quad \bar{z} = \tau - i\sigma. \tag{5.2.1}$$

Our vertex operator for state Λ must contain a local operator W_Λ which has the same Lorentz quantum numbers as Λ. W_Λ must be a polynomial in X^μ and its derivatives. To take into account global translation symmetry $X^\mu \to X^\mu + a^\mu$ we also include a factor of $e^{ik\cdot X}$ for a state of momentum k^μ. We also have to take into account that the punctured point can be anywhere on the Riemann surface. Taking all of this into account, we define the vertex operator for state Λ [30]

$$V_\Lambda(k) = \int d^2z\sqrt{-\gamma} : W_\Lambda(z,\bar{z})e^{ik\cdot X(z,\bar{z})} : . \tag{5.2.2}$$

The function W_Λ can be calculated based on how the quantum numbers of Λ and its behavior under scale transformation. In the case of the tachyon, a spin 0 state, $W_\Lambda = 1$ and the vertex operator is

$$V_T = e^{ik\cdot X} \tag{5.2.3}$$

(we will omit writing the normal ordering operator and the integral common to all vertex operator). At the massless level, we saw in (5.1.29) and (5.1.30) that we have three states, with spin 2, 1 and 0. The corresponding vertex operators are

$$\begin{aligned} V_G &= h_{\mu\nu}\partial_a X^\mu \bar{\partial}_a X^\nu e^{ik\cdot X} && (5.2.4)\\ V_{KR} &= B_{\mu\nu}\partial_a X^\mu \bar{\partial}_a X^\nu e^{ik\cdot X} && (5.2.5)\\ V_D &= \eta_{\mu\nu}\partial_a X^\mu \bar{\partial}_a X^\nu e^{ik\cdot X} && (5.2.6) \end{aligned}$$

corresponding to the graviton, the Kalb-Ramond field, and the dilaton respectively. $\partial = \partial_z$, $\bar{\partial} = \partial_{\bar{z}}$ and $h_{\mu\nu}$ and $b_{\mu\nu}$ are traceless symmetric and antisymmetric tensors respectively, corresponding to the polarizations of the states.

Now that we have our basic vertex operators, let us see how we can use them to calculate a scattering amplitude. We will focus only on tree level amplitudes. The vertex operators, $V_\Lambda(k)$ will characterize the absorption or emission of string state of momentum k. We also need a propagator, Δ, describing the propagation of the string between vertices. The general form for the N-particle scattering amplitude is

$$A_N = g_s^{N-2} < \Lambda_1; k_1 | V_{\Lambda_2}(k_2) \Delta V_{\Lambda_3}(k_3) \cdots \Delta V_{\Lambda_{N-1}}(k_{N-1}) | \Lambda_N; k_n > + permutations. \quad (5.2.7)$$

In particle physics, the propagator is given by $(-p^2 + m^2 + i\epsilon)^{-1}$. Similarly, using the mass formula (5.1.26) we can write

$$\Delta = \frac{1}{2}(L_0 + \bar{L}_0 - 2)^{-1} \quad (5.2.8)$$

and introduce an integral representation for Δ

$$\Delta = \frac{1}{2} \int_0^1 d\rho \rho^{L_0 + \bar{L}_0 - 3}. \quad (5.2.9)$$

However, this will propagate all possible states, whereas we want to include just the physical string states, satisfying the Virasoro constraints. Using the first equality in (5.1.33) we can write

$$(L_0 - \bar{L}_0)|\phi >= 0 \quad (5.2.10)$$

which we then use to write the representation for the propagator

$$\begin{aligned} \Delta &= \frac{1}{4\pi} \int_0^1 d\rho \int_0^{2\pi} d\phi \rho^{L_0 + \bar{L}_0 - 3} e^{i\phi(L_0 - \bar{L}_0)} \\ &= \frac{1}{4\pi} \int_{|z| \leq 1} d^2 z z^{L_0 - 2} \bar{z}^{\bar{L}_0 - 2}. \end{aligned} \quad (5.2.11)$$

If we were to integrate (5.2.7) over all the intermediate $z, \bar{z}$ we would get an infinite answer. The reason is that even after a conformal transformation of the world sheet metric γ_{ab} to get a Riemann surface, we still have a leftover $SL(2,C)$ symmetry

$$z \to \frac{az+b}{cz+d} \tag{5.2.12}$$

which we can use to fix any three point on the Riemann sphere to any arbitrary value. By fixing these three points, we would no longer be integrating over the volume of $SL(2,C)$, and our amplitude would be finite. By taking into account also the possible permutations of the points where we insert the vertex operators, it can be shown that we can write the amplitude

$$A_N = 4\pi(\frac{g}{4\pi})^{N-2}\int d\mu_N(z)\langle V_1 V_2 \cdots V_N\rangle \tag{5.2.13}$$

where we have introduced an integration measure

$$d\mu_N(z) = |z_A - z_B|^2|z_A - z_C|^2|z_B - z_C|^2\delta^2(z_A - z_A^0)\delta^2(z_B - z_B^0)\delta^2(z_C - z_C^0)\prod_{i=1}^{N} d^2 z_i. \tag{5.2.14}$$

A common choice for fixing the arbitrary points A, B, C, which we will use throughout, is

$$\begin{aligned} &A = 1,\ B = N-1,\ C = N \\ &z_A^0 = 0,\ z_B^0 = 1,\ z_C^0 = \infty\ . \end{aligned} \tag{5.2.15}$$

The vertex operators in (5.2.13), using our choice (5.2.15), are ordered

$$0 < |z_2| < |z_3| < \cdots < |z_{N-2}| < 1 < \infty. \tag{5.2.16}$$

In Appendix C we have calculated several amplitudes in detail, where the reader can see how the above procedure works. One of these, (C.0.1), is the amplitude for scattering of four closed string tachyons:

$$A_4 = \frac{g^2}{4\pi} \int d^2z |z|^{\alpha' k_1 \cdot k_2} |1-z|^{\alpha' k_2 \cdot k_3} \tag{5.2.17}$$

which we can rewrite using Mandelstam variables (2.1.9) and tachyon mass (5.1.28)

$$A_4 = \frac{g^2}{4\pi} \int d^2z |z|^{-2-\alpha(s)} |1-z|^{-2-\alpha(t)} \tag{5.2.18}$$

and we defined

$$\alpha(x) = 2 + \frac{\alpha' x}{2}. \tag{5.2.19}$$

This result is well known as the Virasoro-Shapiro amplitude. The integral in (5.2.18) is equal to

$$A_4 = \frac{g^2}{4\pi} B(-\frac{\alpha(s)}{2}, -\frac{\alpha(t)}{2}, 1 + \frac{\alpha(s)}{2} + \frac{\alpha(t)}{2}) \tag{5.2.20}$$

and

$$B(a,b,c) = \pi \frac{\Gamma(a)\Gamma(b)\Gamma(c)}{\Gamma(a+b)\Gamma(b+c)\Gamma(c+a)}. \tag{5.2.21}$$

In the Regge limit, $s \gg t$, we can use the Stirling formula for the Γ function and see that (5.2.20) gives

$$A_4 \simeq g^2 2\pi \frac{\Gamma(-\frac{\alpha(t)}{2})}{\Gamma(1+\frac{\alpha(t)}{2})} (e^{-i\pi/2} \frac{\alpha' s}{4})^{\alpha(t)}. \tag{5.2.22}$$

Comparing this result to (3.1.16) we see that it has the form of a Reggeon exchange amplitude with Regge trajectory $\alpha(t)$ (which also explains the name 'Regge slope' for α'). In fact, string theory started when Veneziano wrote down the open string version of four tachyon amplitude:

$$A_4^{open} = \kappa^2 \frac{\Gamma(-\alpha(s))\Gamma(-\alpha(t))}{\Gamma(-\alpha(s) - \alpha(t))} \stackrel{\text{def}}{=} \kappa^2 B(-\alpha(s), -\alpha(t)). \tag{5.2.23}$$

Again by using Stirling's formula for the asymptotic behavior of Γ functions we can see that in the Regge limit this amplitude would lead to Regge trajectories. These Regge trajectories fit well with early experimental observations, and it was later realized that the amplitude (5.2.23) corresponds to scattering of strings. We invite the reader, as an exercise, to follow the steps of Appendix C, but for open strings, and derive the above equation.

Chapter 6

Gauge/String Duality

The goal of this chapter is to summarize the key results of the papers [1, 2, 3]. These present recent developments in applying string theory to the study of scattering by the strong interaction. The results will then be used in chapters 7-8 to develop some new physics. We begin with a lightning review of gauge/string duality. For better, more detailed reviews see for example [32, 33].

6.1 The Bare Necessities

The gauge/gravity duality relates a theory of gravity, in $d+1$ dimensions, to a gauge field theory, with no gravity, in d dimensions. A particular example is the AdS/CFT correspondence, which claims that type IIb superstring theory on $AdS_5 \times S^5$ is dual to $\mathcal{N} = 4SYM$ theory. In a sense, gravity emerges as the square of the gauge interaction. A graviton will be a bound state of two gluons, and the extra dimension that the graviton lives in roughly corresponds to the separation between gluons [32]. A theory with gravity has less observables than a theory without gravity, which is why we can get the number of degrees of freedom of theories in different dimensions to match.

The metric of $AdS_5 \times S^5$ space can be written in several different ways, depending on the choice of coordinates. One popular expression is

$$ds^2 = \frac{r^2}{R^2} dr^2 + \frac{R^2}{r^2} \eta_{\mu\nu} dx^\mu dx \nu + R^2 d\Omega_5 \tag{6.1.1}$$

where R is the radius of S^5. Upon change of coordinate $z = R^2/r$ the metric is

$$ds^2 = \frac{R^2}{z^2}(dz^2 + \eta_{\mu\nu} dx^\mu dx^\nu) + R^2 d\Omega_5. \tag{6.1.2}$$

This is the form we will make most use of in this work. Technically, this is just the metric of Poincaré wedge of AdS space, but this will not matter much to our discussion. The space (6.1.2) has for the boundary the 4 dimensional Minkowski space at $z = 0$ plus a single point at $z = \infty$. The gauge theory lives in the Minkowski space on the $z = 0$ boundary. Sometimes we will also make a change of variable $z = R \exp(-u)$ (in the case of the hard-wall model discussed below $z = z_0 \exp(-u)$), which will give us the metric

$$ds^2 = R^2 du^2 + e^{2u} \eta_{\mu\nu} dx^\mu dx^\nu + R^2 d\Omega_5. \tag{6.1.3}$$

If g_{YM} is the coupling on the gauge theory side, then as 't Hooft showed, in the large N limit, with N the number of colors, it is useful to study the theory by doing an expansion in coupling

$$\lambda = g_{YM}^2 N \tag{6.1.4}$$

by taking $g_{YM} \to 0$,$N \to \infty$ in such a way that λ is fixed. The string coupling g is related to g_{YM} by $4\pi g = g_{YM}^2$. The correspondence relates the 't Hooft coupling to the AdS radius and string tension

$$\lambda = \frac{R^4}{\alpha'^2}. \tag{6.1.5}$$

The aspect of the correspondence we will want to use is applying the gravity (string) side to learning new things about the gauge side. It is possible to go in the other direction as well, but is not the subject of this work. The direction we want to apply works in the 't Hooft large N fixed λ limit, but we also need the AdS space to be weakly curved and $R \gg \sqrt{\alpha'}$, in order to be able to approximate the string theory by type IIb supergravity. In this case we have $\lambda \gg 1$ and $g \ll 1$ (since $g_{YM} \to 0$), so that the gauge theory is strongly coupled, but the string theory is weakly coupled. Therefore we can use perturbation theory on the string side to get non-preturbative answers on the gauge side - a very useful tool indeed.

The correspondence claims that generating functionals of the string theory and the CFT are related by

$$Z_{string}[\phi_0(x)] = \langle \exp(\int d^4x \phi_0(x)\mathcal{O}(x))\rangle_{CFT} \tag{6.1.6}$$

where

$$\phi_0(x) \stackrel{\text{def}}{=} \phi(x, z) \tag{6.1.7}$$

and $\mathcal{O}(x)$ is an operator in the gauge theory, while ϕ is the corresponding field on the gravity side. If we can apply the supergravity limit, $\lambda \gg 1$ then we can approximate the string partition function

$$Z_{string} \simeq \exp(-S_{sugra}), \tag{6.1.8}$$

where S_{sugra} is the classical supergravity action.

We should note that the correspondence has not been rigorously proven as of yet, but nevertheless it has accumulated a lot of circumstantial evidence, and juries often convict solely on circumstantial evidence.

Another model we will use is the so called hard-wall model [34]. It involves putting a 'wall at the end of space', or in other words a cutoff, in the z coordinate. We use the metric (6.1.2) but with the understanding

$$0 < z < z_0 \tag{6.1.9}$$

where z_0 is the position of the cutoff. This is not a fully consistent theory, as the metric does not satisfy the supergravity equations, but it is a useful toy model. It will lead to a discrete spectrum of states and a mass gap. Its advantage is that by cutting off the space, we break scale invariance, which leads to a more realistic theory with confinement. In particular, as we will see in later chapters, especially chapter 8, the cutoff position will roughly correspond to

$$z_0 \simeq \frac{1}{\Lambda_{QCD}}. \tag{6.1.10}$$

The advantage of the hard-wall model is that it is a (relatively) simple model of confinement. On the other hand, it is not the final answer, and care must be taken to separate features which are model dependent, and those which are model independent. Results that depend on the precise way the metric is cutoff will be most likely model dependent.

6.2 The AdS Pomeron

In this section we review the approach to the Pomeron in AdS called the BPST Pomeron, after its authors Brower, Polchinski, Strassler and Tan. Due to the importance of the Pomeron in high energy scattering (see chapter 3), the BPST Pomeron is a very important object. Furthermore their string theory approach has the advantage of uniting the soft non-perturbative Pomeron and the hard, perturbative BFKL Pomeron (chapter 4.4).

First, let us present an intuitive derivation. For scattering in d flat spacetime dimensions we can write the S matrix

$$\mathcal{S} = \mathbb{1} + i\,(2\pi)^d\,\delta^d(\sum k_i)\,\mathcal{T}_d\,. \tag{6.2.1}$$

By separation of variables we can write the wavefunctions for external hadrons

$$\Phi(x,y) = \phi(x)\psi(y)\,, \tag{6.2.2}$$

and $\phi(x)$ is determined by the coupling to $\mathcal{O}$, equation (6.1.6). x represents the 4 Minkowski space coordinates on the boundary, while y represents the other 6 dimensions. For example in the case of scattering of scalar glueballs,

$$\phi(x) = \exp(i\,p\cdot x)\,. \tag{6.2.3}$$

BPST argued that for $d=10$ dimensions we can represent $\mathcal{T}_4$ as a coherent superposition over all possible scattering locations in the other 6 dimensions:

$$\mathcal{T}_4 = \int d^4y \sqrt{-G}\, \mathcal{T}_{10}(\tilde{p}) \prod \psi_i(y) \tag{6.2.4}$$

where the product runs over the i external states (in the case considered, $i = 4$).

The momenta with a tilde, $\tilde{p}^\mu$ represent the momenta as seen by a local inertial observer sitting at a given value z

$$\tilde{p}^\mu = \frac{z}{R} p^\mu \,, \tag{6.2.5}$$

and p^μ are the standard 4 dimensional gauge theory momenta, associated with conserved Nöther currents. Note that $\sqrt{-G}$ is the full 10 dimensional metric.

If we were considering states with spin, $\mathcal{T}_{10}$ and $\phi(x)$ would carry appropriate indices, which would be contracted with each other. With the substitution (6.2.4), the S matrix (6.2.1) is

$$\mathcal{S} = \mathbb{1} + i\,(2\pi)^4\, \delta^4(\textstyle\sum p)\, \mathcal{T}_4 \,. \tag{6.2.6}$$

This approximation is appropriate for tree level scattering, in the limit $R \gg \alpha'$, which we saw was appropriate for the AdS/CFT correspondence.

To evaluate the integral (6.2.4) we need to know the expression for the T-matrix in 10 dimensions. We begin by calculating this expression using flat space string theory, by methods described in section 5.2. For example, applying it to Regge scattering of scalars, using equation (5.2.22) we can replace

$$\mathcal{T}_{10} \to f(\alpha'\tilde{t})\,(\alpha'\tilde{s})^{\alpha(\tilde{t})} \tag{6.2.7}$$

with the Mandelstam variables replaced with the local forms according to (6.2.5)

$$\tilde{s} = \frac{z^2}{R^2}\, s \quad \tilde{t} = \frac{z^2}{R^2}\, t\,. \tag{6.2.8}$$

As a first,'ultralocal', approximation, which will be shown later to correspond to the supergravity limit $\lambda \to \infty$ we can plug this result into (6.2.4)

$$\mathcal{T}_4(s,t) = \int d^6y\, \sqrt{-G}\, f(\frac{\alpha' z^2}{R^2} t)(\frac{\alpha' z^2}{R^2} s)^{2+\frac{\alpha' z^2}{2R^2}t} \prod_{i=1}^{4} \psi_i(y). \tag{6.2.9}$$

We can now use this result to examine the structure of the amplitude. We see, from the exponent of s, that the Pomeron intercept is at 2, the same as in flat space. The Regge slope now depends on the position in the 5th dimension z

$$\alpha'_{eff}(z) = \frac{\alpha' z^2}{R^2} = \frac{z^2}{\sqrt{\lambda}}\,. \tag{6.2.10}$$

The next step is to study what happens at λ large, but finite. To do this, we must keep some terms of order $1/\sqrt{\lambda}$ which we have implicitly dropped previously. To this end, we promote the momenta $\tilde{s}$, $\tilde{t}$ to differential operators:

$$\alpha' \tilde{t} \to \alpha' \nabla_P^2 \stackrel{\text{def}}{=} \frac{z^2}{\sqrt{\lambda}} t + \alpha' \nabla^2_{\perp P}\,. \tag{6.2.11}$$

The operator $\nabla^2_{\perp P}$ is the curved space transverse Laplacian acting in the t-channel, therefore on the product of wavefunctions Φ_1 and Φ_3. There are some subtleties involved in precisely how this operator is defined, but BPST show that to order $1/\sqrt{\lambda}$ for Pomeron exchange the appropriate replacement in lightcone coordinates is

$$\begin{aligned}
&\nabla_P^2 \to \Delta_2\,, \\
&\Delta_2 = (\frac{R}{z})^2 \nabla_0^2 \left[(\frac{R}{z})^{-2} \right]\,, \\
&\nabla_0^2 = (-G)^{1/2}\, \partial_M \left[(-G)^{1/2} G^{MN} \partial_N \right]\,.
\end{aligned} \tag{6.2.12}$$

The indices M, N run over the 10 AdS coordinates. The last definition above is just the 10 dimensional scalar Laplacian. In other words, this would lead to $\tilde{t}$ being replaced by the differential operator

$$\alpha' \tilde{t} \to \frac{1}{\sqrt{\lambda}} \left[z\partial_z z \partial_z + t z^2 - 4 \right] + O(1/\lambda)\,. \tag{6.2.13}$$

We should do a similar replacement for $\tilde{s}$, with a differential operator acting on the product of wavefunctions Φ_1 and Φ_2. However in the high energy limit we are working in, $s \to \infty$, and s is so large that we do not have to keep any other term, as they would all be subleading:

$$\alpha' \tilde{s} \to \frac{1}{\sqrt{\lambda}} s z^2\,. \tag{6.2.14}$$

Applying equations (6.2.14) and (6.2.13) in equation (6.2.4) for $\mathcal{T}_4$ we would have the term

$$(\frac{z^2}{\sqrt{\lambda}} s)^{2 + \frac{1}{2\sqrt{\lambda}} \left[z\partial_z z\partial_z + t z^2 - 4 \right]} \psi_1(z) \psi_3(z)\,. \tag{6.2.15}$$

To study the structure of the amplitude we therefore need to know how the differential operator in the exponent acts on the product $\psi_1(z)\psi_3(z)$. We can ascertain this by writing

$$\psi_k(z) = \int dz' \psi_k(z')\delta(z-z') \;\; k = 1,3\,, \tag{6.2.16}$$

which would lead to the amplitude

$$\Im A(s,t) \propto \int dz\, dz'\, \psi_2(z)\psi_4(z)\mathcal{K}(z,z',t,\tau)\, \psi_1(z')\psi_2(z')\,, \tag{6.2.17}$$

where we have define the Pomeron exchange kernel

$$\mathcal{K}(z,z',t,\tau) \stackrel{\text{def}}{=} e^H \delta(z-z')\,, \tag{6.2.18}$$

and

$$H = \frac{1}{2\sqrt{\lambda}}\left[z\partial_z z\partial_z + tz^2 + 4\sqrt{\lambda} - 4\right]\,. \tag{6.2.19}$$

We can then find $\mathcal{K}$ by expanding the δ function into the eigenvalues of H

$$\delta(z-z') = \int d\nu c(\nu)\phi_\nu(z)\,, \tag{6.2.20}$$

where ϕ_ν satisfy

$$H\phi_\nu(z) = E_\nu\phi_\nu(z)\,. \tag{6.2.21}$$

Using the orthonormality of ϕ_ν we can solve (6.2.20) for $c(\nu)$ giving us

$$\delta(z-z') = \int d\nu \phi_\nu^*(z')\phi_\nu(z) \tag{6.2.22}$$

which using (6.2.18) finally gives us

$$\mathcal{K}(z, z', t, \tau) = \int d\nu \phi_\nu^*(z')\phi_\nu(z) e^{E_\nu} \,. \tag{6.2.23}$$

Hence we see that finding the Pomeron propagator reduces to solving Schrödinger's equation in Liouville quantum mechanics (6.2.21), with H given by (6.2.19). Computationally it is probably simplest to solve this problem using the u variable (6.1.3), which turns

$$\begin{aligned} H &= \frac{1}{2\sqrt{\lambda}}(-\partial_u^2 + V(u))\,, & (6.2.24)\\ V &= -2\sqrt{\lambda}\, j_0 - z_0^2 t e^{-2u} & (6.2.25)\\ j_0 &= 2 - \frac{2}{\sqrt{\lambda}} & (6.2.26)\end{aligned}$$

where we made it look more like a Schrödinger's equation. Let us begin by introducing a dimensionless variable

$$\begin{aligned} \xi &= \rho e^{-u} & (6.2.27)\\ \rho &= z_0\sqrt{|t|}\,, & (6.2.28)\end{aligned}$$

and write the eigenvalues as

$$E_\nu = \frac{-2\sqrt{\lambda}\, j_0 + \nu^2}{2\sqrt{\lambda}}\,. \tag{6.2.29}$$

We can then rewrite the differential equation

$$\xi^2\psi'' + \xi\psi' - (\xi^2 + (i\nu)^2)\psi = 0\,. \tag{6.2.30}$$

Right now we are working in the conformal theory, so we have an implied boundary condition that

$$\psi \to finite \;\; u \to \infty \,. \tag{6.2.31}$$

The above equation has the form of a modified Bessel equation. The general solution with the above boundary condition is given by

$$c(\nu) I_{i\nu}(\xi) \,. \tag{6.2.32}$$

To fix c, we require the eigenfunctions to be normalized

$$\int_0^\infty d\nu \psi^*_\nu(u) \psi_\nu(u') = \delta(u - u') \,. \tag{6.2.33}$$

This gives

$$|c|^2 = \frac{\nu}{2 \sinh(i\nu)} \,. \tag{6.2.34}$$

To fix the phase of c we require the limit $t \to 0$ to be well defined, which gives

$$c(\nu) = i \, (\frac{\rho}{2})^{-i\nu} \frac{\nu \Gamma(i\nu)}{\sqrt{2\pi}} \,. \tag{6.2.35}$$

We can use identities between Bessel functions to simplify this to

$$\psi_\nu(u) = c(\nu) I_{i\nu}(\xi) = \sqrt{\frac{2}{\pi}} \frac{K_{i\nu}(z_0 \sqrt{|t|}\, e^{-u})}{\Gamma(i\nu)}, \;\; \nu > 0 \,, \tag{6.2.36}$$

and the corresponding eigenfunctions

$$j = -E = j_0 - \frac{\nu^2}{2\sqrt{\lambda}} \,, \tag{6.2.37}$$

where we used equation (6.2.29). We see that the amplitude will have a cut starting at

$$j = j_0 = 2 - \frac{2}{\sqrt{\lambda}} \tag{6.2.38}$$

independently of the value of t. The Pomeron exchange kernel, (6.2.23), would therefore be equal to in this (conformal) model

$$\mathcal{K}(u, u', \tau, t) = \frac{2}{\pi^2} e^{j_0 \tau} \int_0^\infty d\nu\, \nu\, \sinh(\pi\nu)\, K_{i\nu}(z_0 |t|^{1/2} e^{-u}) K_{-i\nu}(z_0 |t|^{1/2} e^{-u'}) e^{-\nu\tau^2} \tag{6.2.39}$$

with

$$\tau \stackrel{\text{def}}{=} \frac{1}{2\sqrt{\lambda}} \log\left(\frac{z_0^2}{\sqrt{\lambda}} e^{-(u+u')} s\right). \tag{6.2.40}$$

In the case $t = 0$, the wavefunctions simplify

$$\psi_\nu(u) \to e^{i\nu u} \tag{6.2.41}$$

and the integral in $\mathcal{K}$ can be explicitly evaluated to give

$$\mathcal{K}(u, u', \tau, 0) = \frac{1}{\sqrt{2\pi\tau}} e^{j_0 \tau} e^{-\frac{(u-u')^2}{4\tau}}. \tag{6.2.42}$$

Plugging this into (6.2.17) would give us the imaginary part of the forward scattering elastic amplitude, which we know from the optical theorem, (2.2.10), is equal to the total scattering cross section. We will make extensive use of this in chapter 8.

We can repeat the same calculation starting from (6.2.24) but working in the hard-wall model. In terms of the u coordinate the space is cut off at $u = 1$, $0 < u < 1$, so we no longer have the boundary condition (6.2.31) as $u \to \infty$. The general solution of equation

(6.2.30) in this case is

$$\psi_\nu(u) = c(\nu)(I_{i\nu}(\xi) + R(\nu,\rho)I_{-i\nu}(\xi) \tag{6.2.43}$$

with $c(\nu)$ the same as before (6.2.35). The boundary condition that ψ_ν must satisfy is now

$$\partial_\xi(\xi^2\psi)|_{\xi=\rho} = 0\,. \tag{6.2.44}$$

This is the Neumann boundary condition which enforces energy momentum conservation at the wall. The condition above determines

$$R(\nu,\rho) = -\frac{\partial_\xi(\xi^2 I_{i\nu}(\xi))}{\partial_\xi(\xi^2 I_{-i\nu}(\xi))}|_{\xi=\rho} = -\frac{4I_{i\nu}(\rho) + \rho I_{i\nu-1}(\rho) + \rho I_{i\nu+1}(\rho)}{4I_{-i\nu}(\rho) + \rho I_{-i\nu-1}(\rho) + \rho I_{-i\nu+1}(\rho)}\,. \tag{6.2.45}$$

Following the same procedure as before, we can calculate the imaginary part of the amplitude, with the Pomeron exchange kernel given by

$$\begin{aligned}\mathcal{K}_{HW}(u,u',\tau,t) = e^{j_0\tau}\int_0^\infty d\nu\,|c(\nu,\tau)|^2\,[I_{i\nu}(\xi) + R(\nu,\tau)I_{-i\nu}(\xi)]^* \times \\ \times\,[I_{i\nu}(\xi') + R(\nu,\tau)I_{-i\nu}(\xi')]\,e^{-\tau\nu^2}\,.\end{aligned} \tag{6.2.46}$$

In the forward scattering limit, $t = 0$, the result will again simplify. The wavefunction will be

$$\psi_\nu(u) \to \frac{1}{\sqrt{2\pi}}\,(e^{-i\nu u} + \frac{\nu - 2i}{\nu + 2i}e^{i\nu u}) \tag{6.2.47}$$

which will give for the Pomeron exchange, after performing the integral in (6.2.46)

$$\mathcal{K}_{HW}(u,u',\tau,0) = \frac{1}{\sqrt{\pi\tau}}e^{j_0\tau}\left(\exp(-\frac{(u-u')^2}{4\tau}) + \mathcal{F}(u,u',\tau)\exp(-\frac{(u+u')^2}{4\tau})\right) \tag{6.2.48}$$

with

$$\mathcal{F}(u, u', \tau) = \quad 1 - 4\sqrt{\pi\tau}\, e^{\eta^2} \operatorname{erfc}(\eta) \tag{6.2.49}$$

$$\eta = \quad \tfrac{u+u'+4\tau}{\sqrt{4\tau}} \,. \tag{6.2.50}$$

In chapter 8 we will return to use this result to calculate the total cross section in DIS. We will discuss the physical meaning of the function F there, and the difference between the expressions with confinement and without confinement.

A more formal derivation of the above results can be performed, using the discussion in section 5.2. Let us commence at equation (5.2.7) and write it as

$$A_{W_L W_R} = \int d^2 w \langle W_R w^{L_0 - 2} \bar{w}^{\tilde{L}_0 - 2} W_L \rangle \tag{6.2.51}$$

where $W_{R,L}$ contain the vertex operators and the associated propagators, and we just separated out one integration. The momenta in W_R have a large $-$ component, while those in W_L have a large $+$ component in light cone coordinates. We can insert a complete set of states (5.1.32) in the middle, and act on it with L_0 and $\tilde{L}_0$, keeping only the leading term in the Regge limit

$$\begin{aligned} A_{W_L W_R} \sim \sum_{n=0}^{\infty} \int d^2 w \frac{2^{m+n} w^{m-2-\frac{\alpha' t}{4}} \bar{w}^{n-2-\frac{\alpha' t}{4}}}{\alpha'^{m+n} m! n!} \times \\ \langle W_R e^{ik\cdot X} (\partial X^-)^m (\bar{\partial} X^-)^n \rangle \langle e^{-ik\cdot X} (\partial X^+)^m (\bar{\partial} X^+)^n W_L \rangle \,. \end{aligned} \tag{6.2.52}$$

If we expand X in terms of modes (5.1.8) we can readily see that $\partial X(0)$ contains only α_{-1} and analogously for $\bar{\partial} X(0)$. All the m and n dependent terms combine to form an exponential

$$\exp(2w\partial X^-_R \partial X^+_L/\alpha' + 2\bar{w}\bar{\partial}X^-_R\bar{\partial}X^+_L/\alpha') \,. \tag{6.2.53}$$

We can integrate over w above, which gives

$$A_{W_L W_R} \sim \Pi(\alpha' t) \times \langle W_R e^{ik\cdot X}\left(\frac{2}{\alpha'}\partial X^-_{-1}\bar{\partial}X^-_{-1}\right)^{1+\frac{\alpha' t}{4}}\rangle\langle e^{-ik\cdot X}\left(\frac{2}{\alpha'}\partial X^+_{-1}\bar{\partial}X^+_{-1}\right)^{1+\frac{\alpha' t}{4}} W_L\rangle \,. \tag{6.2.54}$$

Comparing with equation (5.2.4) we see that the amplitude factorizes into a product of two amplitudes, with an insertion of the Pomeron vertex operator

$$\mathcal{V}_P \stackrel{\text{def}}{=} \left(\frac{2}{\alpha'}\partial X^{\pm}\bar{\partial}X^{\pm}\right)^{1+\frac{\alpha' t}{4}} e^{\mp ik\cdot X} \,. \tag{6.2.55}$$

Comparing with the graviton vertex operator, (5.2.4), we see that at $t = 0$ the Pomeron vertex operator gives the graviton. Hence the Pomeron is the graviton's Regge trajectory.

In Appendix C we will give more detailed calculations, showing how we can extract computationally the Regge limit of the scattering amplitudes by the insertion of this vertex operator.

In AdS space we would again insert a complete set of states. We also need to impose the physical state condition (5.1.33)

$$L_0\mathcal{V}(j) = \tilde{L}_0\mathcal{V}(j) = \mathcal{V}(j) \tag{6.2.56}$$

where to diagonalize L_0 we went to a basis of definite spin

$$\mathcal{V}(j) = (\partial X^+\bar{\partial}X^+)^{j/2} e^{ik\cdot X}\phi_{+j}(Y) \,. \tag{6.2.57}$$

We work in the Gaussian limit, in which we can take the AdS vertex operator to be the product of the 4-dimensional flat space vertex operator multiplied by a function of the remaining coordinates. In terms of the string wavefunctions (6.2.3) this translates directly into $e^{ipX}\Psi(Y)$. Now to evaluate

$$\begin{aligned} L_0 V(j) &= (\partial X^+ \overline{\partial} X^+)^{\frac{j}{2}}[\frac{j}{2} - \frac{\alpha'}{4}\triangle_j]e^{ik\cdot X}\phi_+(Y) + O(\frac{1}{\lambda}) \\ &= (\partial X^+ \overline{\partial} X^+)^{\frac{j}{2}} e^{ik\cdot X}\phi_{+j}(Y) \end{aligned} \tag{6.2.58}$$

Once we write out the Laplacian this condition becomes (taking $\phi_{+j}(Y)$ to depend only on r)

$$[j - 2 - \frac{\alpha' R^2}{2r^2}t - \frac{1}{2\sqrt{\lambda}}(j(j-4) + r(5-2j)\partial_r + r^2\partial_r^2)]\phi_{+j}(r) = 0. \tag{6.2.59}$$

At $j = 2$ we should identify this state with the graviton. In this case the equation becomes

$$[-\frac{\alpha' R^2}{2}te^{-2u} - \frac{1}{2\sqrt{\lambda}}(\partial_u^2 - 4)]\phi_{++}(u) = 0\,. \tag{6.2.60}$$

This can lead us back to our previous solution, equation (6.2.24). In chapter 7 we will present a more detailed discussion, including keeping the next to leading order term.

6.3 The Eikonal Approximation in AdS Space

In this section we will review a few of the main results from papers [3, 7], that we will make use of in later chapters. Similar results appeared in [35, 36, 37, 38].

The eikonal approximation neglects all non-linear Pomeron interactions, and it is only valid when the scattering angle is small. In the previous section we calculated the Pomeron exchange kernel in the conformal model, equation (6.2.39), and we expressed it as a function of s, t, z and z'. This is actually only the imaginary part of the kernel, $\Im\mathcal{K}(s,t,z,z')$. To build the eikonal exchange, we need both the real and imaginary parts, and it is computationally simplest to do after we express the kernel as a function of $j, b^{\perp}, z$ and z', with $b^{\perp} = x^{\perp} - x'^{\perp}$ the impact parameter. Then the results can be obtained by a whole chain of integral transforms. First, we do a Mellin transform to take us from the s plane to the j plane:

$$\mathcal{K}(j,t,z,z') = \int_0^{\infty} d\hat{s}(\hat{s})^{-j-1}\Im\mathcal{K}(s,t,z,z')\,. \tag{6.3.1}$$

The transform is done with respect to a dimensionless variable $\hat{s} \overset{\text{def}}{=} zz's$. Next, we do a Fourier transform with respect to $q_{\perp}^2 = -t$:

$$\mathcal{K}(j,x^{\perp}-x'^{\perp},z,z') = \int \frac{d^2q_{\perp}}{(2\pi)^2} e^{iq_{\perp}\cdot(x^{\perp}-x'^{\perp})}\mathcal{K}(j,-q_{\perp}^2,z,z')\,. \tag{6.3.2}$$

We now have the desired form of $\mathcal{K}$, starting from results we calculated in the previous section. Eventually, we will want to go back to the s plane from the j plane, to connect our results with physical measurements. We are able to this by means of an inverse Mellin transform

$$\mathcal{K}(s,x^{\perp}-x'^{\perp},z,z') = -\int \frac{dj}{2\pi i}\,(\frac{\hat{s}^j - (-\hat{s})^j}{\sin \pi j})\,\mathcal{K}(j,x^{\perp}-x'^{\perp},z,z') \tag{6.3.3}$$

where the two summands allow us to reconstruct both the real and the imaginary parts of the amplitude.

The reason given for going to the j plane in the first place is that our expression simplifies there. Indeed, equation (6.3.2) can be integrated analytically giving

$$\mathcal{K}(j, x^{\perp} - x'^{\perp}, z, z') = (\frac{zz'}{R^4})\, G_3(j, v) \tag{6.3.4}$$

where $G_3(j, v)$ is the AdS_3 scalar Green's function, given by

$$G_3(j, v) = \frac{1}{4\pi} \frac{\left[1 + v + \sqrt{v(2+v)}\right]^{2-\Delta_+(j)}}{\sqrt{v(2+v)}}\,, \tag{6.3.5}$$

and v is the chordal distance in AdS_3 space

$$v = \frac{(x^{\perp} - x'^{\perp}) + (z - z')^2}{2zz'}\,. \tag{6.3.6}$$

The chordal distance appears as a natural generalization of the impact parameter. The presence of the extra AdS radial coordinate together with the two transverse coordinates in Minkowski space forms a transverse AdS_3 space. The exponent in (6.3.5) $\Delta_+(j) - 1$ is the AdS_3 conformal dimension

$$\Delta_+(j) = 2 + \sqrt{2\sqrt{\lambda}\,(j - j_0)}\,. \tag{6.3.7}$$

The eikonal approximation will work at large v. As $v \to 0$, we have a head on collision, which leads to large momentum transfers. $G_3(j, v)$ will become large and our approximations will break down. We now build the eikonal approximation as a sum to all orders of ladder and crossed ladder diagrams, figure 6.1, where each rung represents a Pomeron exchange, and neglecting all diagrams where Pomerons interact with each other. The authors of [3] work out this sum carefully. It is important to calculate the combinatorial factor at each level.

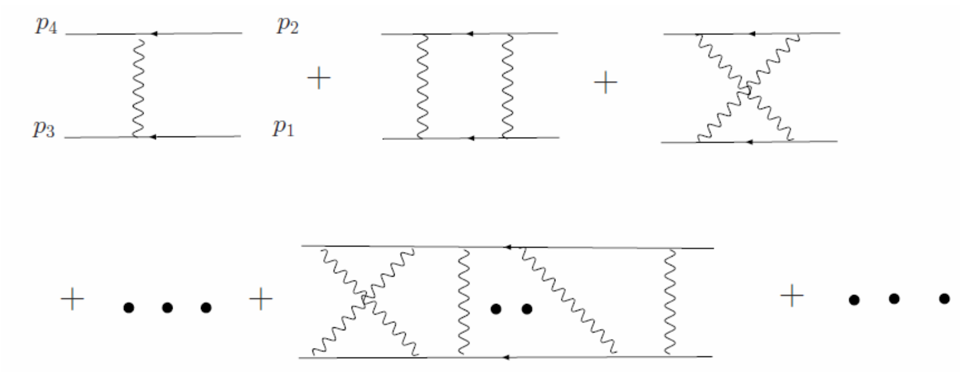

Figure 6.1: Some of the diagrams contributing to the eikonal approximation.

For example at one loop level the two diagrams that enter the sum are, figure 6.2. We can

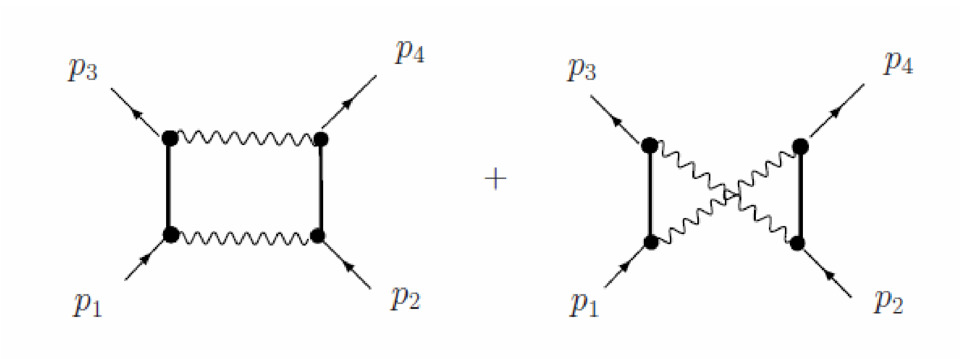

Figure 6.2: The one loop level diagrams of the eikonal expansion.

factorize this into a product where the factor $1/2!$ is included to avoid overcounting the diagrams we would obtain, figure 6.3. Doing a similar procedure at each level we would have

$$i\chi + \frac{(i\chi)^2}{2!} + \frac{(i\chi)^3}{3!} + \cdots = e^{i\chi} - 1 \tag{6.3.8}$$

which would lead to the $2 \to 2$ elastic scattering amplitude

$$A(s,t) \simeq -2is \int d^2 b e^{-ib^{\perp} q_{\perp}} \int dz dz' P_{13}(z) P_2 4z' \left[e^{i\chi(s,b^{\perp},z,z')} - 1 \right] \tag{6.3.9}$$

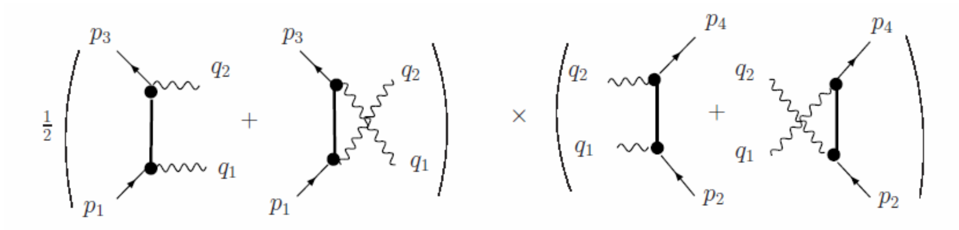

Figure 6.3: Factorization at one loop level.

where χ is given in terms of the Pomeron exchange kernel:

$$\chi(s, x^\perp - x'^\perp, z, z') = \frac{g_0^2 R^4}{2(zz')^2 s} \mathcal{K}(s, x^\perp - x'^\perp, z, z') \,. \tag{6.3.10}$$

The function P_{ij} appearing above are just products of the wavefunctions for the external hadrons

$$P_{ij}(z) = (\frac{z}{R})^2 \sqrt{g(z)}\, \phi_1(z)\phi_3(z) \,, \tag{6.3.11}$$

and $g(z)$ is the determinant of the metric of AdS_5, not the whole $AdS_5 \times S^5$ space.

We see from (6.3.9) that to get the amplitude $A(s,t)$ we need the kernel in the s plane, which we calculate using (6.3.3)

$$\begin{aligned} \mathcal{K}(s, b^\perp, z, z') = &- (\frac{zz'}{R^4})\, G_3(j_0, v) \\ &\times \hat{s}_0^j \int_{-\infty}^{j_0} \frac{dj}{\pi} \frac{1 + e^{-i\pi j}}{\sin \pi j} \hat{s}^{(j-j_0)} \sin\left[\xi(v)\sqrt{2\sqrt{\lambda}(j_0 - j)}\right] \end{aligned} \tag{6.3.12}$$

where we introduced a new variable

$$\xi = \log(1 + v + \sqrt{v(2+v)}\,) \,. \tag{6.3.13}$$

The imaginary part can be analytically integrated

$$\begin{aligned}
\Im K &= (\frac{zz'}{R^4})\, G_3(j_0,v)\, \hat{s}_0^j \int_{-\infty}^{j_0} \frac{dj}{\pi} \hat{s}^{(j-j_0)} \sin\left[\xi(v)\sqrt{2\sqrt{\lambda}(j_0-j)}\right] \\
&= (\frac{zz'}{R^4})\, G_3(j_0,v)\, \hat{s}_0^j \int_{-\infty}^{+\infty} \frac{dy}{2\pi i\sqrt{\lambda}} y e^{-\tau y^2/2\sqrt{\lambda}} e^{i\xi(v)y} \qquad (6.3.14)\\
&= (\frac{zz'}{R^4})\, G_3(j_0,v)\, (\frac{\sqrt{\lambda}}{2\pi})^{1/2} \xi\, e^{j_0\tau} \frac{e^{-\sqrt{\lambda}\xi^2/2\tau}}{\tau^{3/2}}
\end{aligned}$$

where we changed the integration variable to $y^2 = 2\sqrt{\lambda}(j_0 - j)$.

This is the imaginary part for the single Pomeron exchange propagator. As we know from optical theorem, (2.2.10), this is enough for calculating the total cross section, and we will use this result in chapter 8. To get the total cross section for exchange of the full eikonal amplitude, we need the real part of $\mathcal{K}$ as well. This cannot be calculated exactly, but in the limit $\tau \to \infty$, $\sqrt{\lambda}$ fixed and large, we can approximate

$$\Re\mathcal{K} \approx \cot\frac{\pi}{\sqrt{\lambda}}\,\Im\mathcal{K}\,. \qquad (6.3.15)$$

We will use this approximation in our eikonal models of chapter 8. For future reference, let us note that expanding (6.3.9) and keeping just leading order exchange, i.e. the single Pomeron, the $2 \to 2$ elastic amplitude written in terms of (6.3.10) is

$$A(s,t) = 2s \int d^2b e^{i\vec{q}\cdot\vec{b}} \int dzdz' P_{13}(z) P_{24}(z') \chi(s,b,z,z'), \qquad (6.3.16)$$

Chapter 7

Odderon in AdS/CFT

In the previous chapter, section 6.2 we saw how the Pomeron arises in string theory, and in 3.2 we saw that it has been conjectured for a long time that it might have a partner, odd under charge conjugation, called the Odderon [39, 40, 41, 42, 43]. In this chapter we will try to build a theory of the Odderon using string theory, and then apply it to QCD using the AdS/CFT correspondence. This chapter is completely based on [7].

7.1 Odderon at Weak Coupling

At weak coupling the classic study of Balitsky, Fadin, Kuraev and Lipatov (BFKL) [44, 45, 46, 47, 48], which we briefly reviewed in section 4.4, evaluated the Pomeron contribution to leading order in g^2_{YM} and all orders in $g^2_{YM} log(s/s_0)$. In the conformal limit, both the weak-coupling BFKL Pomeron and Odderon correspond to J-plane branch points. For instance, for the BFKL Pomeron, the cut is located at $j_0^{(+)} = 1 + (\ln 2)\, \lambda/\pi^2 + O(\lambda^2)$, where $\lambda = g^2 N_c$ is the 't Hooft coupling. Under the same leading log approximation investigations for the Odderon in the weak coupling were first carried out by Bartels, Kwiecinski and Praszalowicz (BKP) [49, 50]. Interestingly, two leading Odderon solutions have been identified. Both are branch cuts in the J-plane. One has an intercept slightly below 1, at $j^{(-)}_{0,(1)}$, [51, 52], and the second, denoted by $j^{(-)}_{0,(2)}$, [53], has an intercept precisely at 1 [1]. These are summarized in Table 7.1.

To illustrate the difference between the Pomeron ($C = +1$) and the Odderon ($C = -1$) sectors, consider the path ordered trace operator, $TrP_\sigma \exp[i \oint d\sigma x'_\mu(\sigma) A_\mu(x)]$, which is the source for the closed string on the boundary of AdS_5. On the string world sheet, charge conjugation is given by parity ($\sigma \to -\sigma$), so that the $C = \pm 1$ sectors correspond to symmetric/anti-symmetric (or real/imaginary) combinations,

$$TrP_\sigma[e^{i \oint d\sigma x'_\mu(\sigma) A_\mu(x)} \pm e^{-i \oint d\sigma x'_\mu(\sigma) A_\mu(x)}] ,$$

respectively. Expanding to lowest order in perturbation theory, these reduce to two- and three-gluon source, where charge conjugation is $A_\mu(x) \to -A^T_\mu(x)$ with $A_\mu = \lambda^a A^a$, the Hermitian gauge field generators. Thus the Pomeron Green's function for exchanging two gluons between hadrons can be written as a correlator, $\langle \mathcal{P}_{\mu\nu}(x,y)\mathcal{P}_{\mu'\nu'}(x',y')\rangle$, of two color-singlet operators,

$$\mathcal{P}_{\mu\nu}(x,y) = tr(A_\mu(x)A_\nu(y)) = (1/2)\delta_{ab}A^a_\mu(x)A^b_\nu(y) \tag{7.1.1}$$

with $C = +1$. For three gluons exchange, the Green's function can again be written as a correlator of color-singlet operators, $\langle \mathcal{O}_{\mu\nu\rho}(x,y,z)\mathcal{O}_{\mu'\nu'\rho'}(x',y',z')\rangle$. Unlike the case of two

[1]The fact that the second solution has $j^{(-)}_{0,(2)} = 1$ up to $O(\lambda^3)$ in the conformal limit was communicated to us by Cyrille Marquest.

gluons, we now have two possibilities. One involves the totally symmetric d-coupling,

$$\mathcal{O}_{\mu\nu\rho}(x,y,z) = tr\left(\{A_\mu(x), A_\nu(y)\}\, A_\rho(z)\right) = (1/2) d_{abc} A^a_\mu(x) A^b_\nu(y) A^c_\rho(z) \quad (7.1.2)$$

which is odd under C and therefore is the lowest order contribution to the Odderon. The second possibility involves the totally anti-symmetric coupling, $tr\left([A_\mu(x), A_\nu(y)]\, A_\rho(z)\right) = (i/2) f_{abc} A^a_\mu(x) A^b_\nu(y) A^c_\rho(z)$. Under C, $f_{abc} \to f_{cba} = -f_{abc}$ and C even, leading to a three gluon contribution to the Pomeron.

In the weak coupling leading logarithmic approximation, the $C = +1$ BFKL Pomeron and the $C = -1$ Odderon [49, 50] are given by the ladder approximation for two and three Reggeized gluons in the t-channel. Rapid advances have been made recently by exploring the consequences of conformal invariance. It is possible to treat each sector with fixed number, n_g, of Reggeized gluons exchanges in the large N_c limit, $n_g = 2, 3, \cdots$. The leading intercept for each n_g-sector can be found as the ground state eigenvalue of a Hamiltonian, $H_{\rm BFKL}$, where

$$H_{\rm BFKL} = \frac{1}{4} \sum_{i=1}^{n_g} [\mathcal{H}(J^2_{i,i+1}) + \mathcal{H}(\bar{J}^2_{i,i+1})], \quad (7.1.3)$$

is a sum over two-body operators with holomorphic and anti-holomorphic functions of the Casimir. It has been shown in [54] that this is a spin chain with a sufficient number of conserved charges to be completely integrable. In [55] it was then identified as an $SL(2,C)$ XXX Heisenberg spin chain. For the $n_g = 3$ Odderon, explicit solutions were found in [51, 52, 53]. (For a comprehensive review on Odderon, see [56]. Other related works include [57, 58, 59].)

7.2 Introduction

Let us start by generalizing the intuitive argument of section 6.2 to the case of crossing odd amplitudes. Consider a $2 \to 2$ scattering process,$a + b \to c + d$, and a process related to it by crossing, section 2.3, $\bar{c} + b \to \bar{a} + d$, where $\bar{a}$ and $\bar{c}$ denote anti-particles of a and c respectively. In terms of the Mandelstam variables (2.1.9), $s = -(p_a + p_b)^2$ and $t = -(p_a + p_c)^2$. Let us denote amplitudes for these two processes by F and $\bar{F}$ and consider the combinations $F^{\pm} \equiv (\bar{F} \pm F)/2$, i.e.,

$$\begin{aligned} F_{\bar{c}b \to \bar{a}d} &\equiv \bar{F} = F^+ + F^- \ , \\ F_{ab \to cd} &\equiv F = F^+ - F^- \ . \end{aligned} \tag{7.2.1}$$

However, since F and $\bar{F}$ are also related by crossing, $s \leftrightarrow u$, $u = -(p_a + p_c)^2$, $F^{\pm}$, at fixed t, will be even and odd ($C = \pm 1$) in the difference variable: $\nu = (s - u)/2$. At s large and t fixed, $\nu \simeq s$, and we shall therefore in what follows treat as if $F^{\pm}$ are even and odd in s.

For the most part, we will consider elastic scattering where $a = c$ and $b = d$. It follows that the average and the difference of total cross sections at high energies are related to $C = \pm 1$ amplitudes in the forward limit where $t = 0$ via the optical theorem, i.e.,

$$\begin{aligned} [\sigma_T(\bar{a}b) + \sigma_T(ab)] &\sim (2/s) \ \mathrm{Im} \ F^+ \ , \\ [\sigma_T(\bar{a}b) - \sigma_T(ab)] &\sim (2/s) \ \mathrm{Im} \ F^- \ . \end{aligned} \tag{7.2.2}$$

We already met the crossing even amplitude, related to the Pomeron, (6.2.7). Using the above, we can rewrite it in a form which makes explicit the crossing even form:

$$\mathcal{T}_{10}^{(+)}(s,t) \to f^{(+)}(\alpha' t)\left[\frac{(-\alpha' s)^{2+\alpha' t/2} + (\alpha' s)^{2+\alpha' t/2}}{\sin \pi(2+\alpha' t/2)}\right] , \tag{7.2.3}$$

where $f^{(+)}(\alpha' t)$ is process-dependent. Similarly, for the $C = -1$ sector the amplitude behaves as

$$\mathcal{T}_{10}^{(-)}(s,t) \to f^{(-)}(\alpha' t)\left[\frac{(-\alpha' s)^{1+\alpha' t/2} - (\alpha' s)^{1+\alpha' t/2}}{\sin \pi(1+\alpha' t/2)}\right] , \tag{7.2.4}$$

corresponding to the exchange of a closed string trajectory

$$\alpha_{-}(t) = 1 + \alpha' t/2 \, . \tag{7.2.5}$$

We saw that the Pomeron corresponded to the graviton's Regge trajectory. Similarly, the above trajectory will correspond the the Regge trajectory of the massless Kalb-Ramond field, B^{IJ} (5.1.31). We can then proceed to use this flat space amplitude in (6.2.4), and use the same arguments as for the Pomeron to build the ultralocal approximation in terms of the local inertial momenta $\tilde{s}$ and $\tilde{t}$ for the Odderon exchange amplitude in AdS. According to the arguments in section 6.2, this will lead to an effective intercept for the trajectory

$$\alpha_{\text{eff}}^{(-)}(t) \simeq 1 + \frac{1}{2\sqrt{\lambda}}\frac{R^4}{r^2} t \, . \tag{7.2.6}$$

and the amplitude in the supergravity limit having a cut at $j = 1$.

The next step would again be to promote the momenta $\tilde{s}$ and $\tilde{t}$ to operators, but, as before, in the high energy limit that we are working in it is enough to replace $\tilde{s}$ by (6.2.1). Let us replace the Odderon kernel by

$$\tilde{s}^{1+\alpha'\tilde{t}/2} = \int \frac{dj}{2\pi i}\, \tilde{s}^j\, G^{(-)}(j) = \int \frac{dj}{2\pi i}\, \frac{\tilde{s}^j}{j - 1 - \alpha'\Delta_O/2} \tag{7.2.7}$$

where we have again introduced a J-plane $C = -1$ propagator. The operator $\Delta_O(j)$ can be fixed by examining the EOM at $j = 1$ for the associated super-gravity fluctuations responsible for this exchange, i.e., the anti-symmetric Kalb-Ramond field, B_{MN}. There are two classes of EOM's:

$$(\Box_{Maxwell} - (k+4)^2)B^{(1)}_{IJ} = 0\ , \quad (\Box_{Maxwell} - k^2)B^{(2)}_{IJ} = 0 \tag{7.2.8}$$

$k = 0, 1, 2, \cdots$, where $\Box_{Maxwell}$ stands for the Maxwell operator defined in Eq. B.0.2. However, for $k \neq 0$, there would be associated fluctuations on W, which we ignore, thus leaving two solutions, both for $k = 0$. We also normalize the $\Box_{Maxwell}$ operator so that its component in flat transverse directions is $(R^4/r^2)\nabla_b^2$. For both cases, we have

$$G^{(-)}(j) = \frac{1}{j - 1 - (\alpha'/2R^2)(\Box_{Maxwell} - m^2_{AdS,i})} \tag{7.2.9}$$

where the AdS mass-squared are [2]

$$m^2_{AdS,1} = 16\ , \quad m^2_{AdS,2} = 0\ . \tag{7.2.10}$$

We are now in position to demonstrate that (7.2.9) leads to diffusion in AdS for the $C = -1$ sector, similarly to what we saw earlier for the Pomeron. Denote matrix elements by

[2] In our normalization, these are dimensionless. Formally, the second solution can be gauged away. However, we leave it here for now and will return to have a more careful discussion later.

$G^{(-)}(z, z,' ; j, t) = \langle z; t\, |G^{(-)}(j)|\, z'; t\rangle$, we adopt a normalization so that $(zz')^2 G^{(-)}$ satisfies a standard AdS_5 scalar equation. Indeed, at $j = 1$ this reduces precisely to the equation for an AdS_5 scalar propagator, up to a constant factor $2\sqrt{\lambda}$. It is actually simpler to deal with $G^{(-)}$ directly, and one finds

$$(1/2\sqrt{\lambda}) \left\{ -z\partial_z z \partial_z + z^2 t + m_-^2(j) \right\} G^{(-)}(z, z'; j, t) = z\, \delta(z - z') \tag{7.2.11}$$

where $m_-^2(j) = 2\sqrt{\lambda}(j-1) + m^2_{AdS,i}$. $G^{(-)}$ can now be found by a standard spectral analysis.

We will turn this problem into a Schrodinger eigenvalue problem, analogous to (6.2.21):

$$H^{(\pm)}\Psi_E(u) = [-\partial_u^2 + V(u,t)]\Psi_E(u) = E\Psi_E(u) \tag{7.2.12}$$

with $V(u,t) = -te^{-2u}$. We can simplify the problem further by considering $t = 0$ first. This has the same eigenstates as a free particle. The spectral representation for G^- at $t = 0$ is

$$G^{(-)}(z, z'; j, 0) = \frac{1}{\sqrt{\lambda}} \int_{-\infty}^{\infty} d\nu \frac{e^{2i\nu(u-u')}}{j - j_0^- + \mathcal{D}\nu^2} \tag{7.2.13}$$

with $j_0^{(-)}$ given by

$$j_0^{(-)} = 1 - m^2_{AdS}/2\sqrt{\lambda} + O(1/\lambda)\ . \tag{7.2.14}$$

and $\mathcal{D} = 2/\sqrt{\lambda}$.

Upon taking an inverse Mellin transform, it follows that

$$\langle z; 0|\tilde{s}^{\alpha_-(0)+\alpha'\tilde{t}/2}|z'; 0\rangle = e^{j_0^{(-)}\tau}\ \frac{e^{-2(u-u')^2/\mathcal{D}\tau}}{\sqrt{\pi\mathcal{D}\tau}} \tag{7.2.15}$$

where we have $\tau = \log \tilde{s}$. This is the same type of behavior found by BFKL in perturbative context. Here, it corresponds to diffusion in AdS. In particular, we can identify $j_0^{(-)}$ as the strong coupling limit of the Odderon intercept. Also from (7.2.13), one can verify that there is a branch point in the J-plane ending at $j_0^{(-)}$, as summarized in Table 7.1, for both $C = \pm 1$. The weak coupling intercepts have been calculate using the BFKL and BKP equations for the Pomeron and Odderon respectively.

	Weak Coupling	Strong Coupling
$C = +1$	$j_0^{(+)} = 1 + (\ln 2)\, \lambda/\pi^2 + O(\lambda^2)$	$j_0^{(+)} = 2 - 2/\sqrt{\lambda} + O(1/\lambda)$
$C = -1$	$j_{0,(1)}^{(-)} \simeq 1 - 0.24717\, \lambda/\pi + O(\lambda^2)$ $j_{0,(2)}^{(-)} = 1 + O(\lambda^3)$	$j_{0,(1)}^{(-)} = 1 - 8/\sqrt{\lambda} + O(1/\lambda)$ $j_{0,(2)}^{(-)} = 1 + O(1/\lambda)$

Table 7.1: Pomeron and Odderon intercepts at weak and strong coupling.

For $t \neq 0$, the eigenvalue problem can again be solved in terms of Bessel functions while the spectrum remains unchanged. Instead of (7.2.13), one has

$$G^{(-)}(z, z'; j, t) = \frac{2}{\sqrt{\lambda}\pi^2} \int_{-\infty}^{\infty} d\nu\, \nu \sinh 2\pi\nu \frac{K_{2i\nu}(|t|^{1/2} e^{-u}) K_{-2i\nu}(|t|^{1/2} e^{-u'})}{j - j_0^- + \mathcal{D}\nu^2} \tag{7.2.16}$$

Therefore, the spectrum in the J-plane remains a fixed cut at $j = j_0^{(-)}$.

To get the Odderon exchange kernel in the s and $b^\perp$ plane, we can do an inverse Mellin transform

$$\mathcal{K}^{(-)}(s, z, x^\perp, z', x'^\perp) \sim \left(\frac{(zz')^2}{R^4}\right) \int \frac{dj}{2\pi i} \left[\frac{(-\tilde{s})^j - (\tilde{s})^j}{\sin \pi j}\right] G^{(-)}(z, x^\perp, z', x'^\perp; j)\,. \tag{7.2.17}$$

To obtain scattering amplitudes, we simply fold this kernel with external wave functions. Eq. (7.2.17) also serves as the starting point for eikonalization, as we already saw for the

Pomeron in section 6.3.

7.3 World Sheet Analysis

7.3.1 Flat Space

At the end of section 6.2 we gave a quick review of a more formal derivation of Pomeron exchange kernel, using a BPST Pomeron vertex operator. We will now present a more thorough treatment of this approach. Previously, in the Regge limit we kept just the leading components in the light cone coordinate, which corresponded to graviton exchange. We will now keep terms corresponding to all massless level exchanges. We will once again see that the Odderon corresponds to the trajectory of the 2 form Kalb-Ramond field. Once again, we will work for simplicity with just bosonic string theory.

We start by working in flat space. We saw from equation (6.2.55) that we can insert a Pomeron vertex operator into the amplitude. To generalize this to the $C = -1$ sector we must go beyond elastic tachyon amplitude. Due to symmetry under crossing, $s \leftrightarrow u$, only $C = +1$ states, which are even under worldsheet parity, couple in the t-channel. The odd sector couples first in the four point amplitude involving two external $C = -1$ states, one initial and one final in the t-channel. This is due to world-sheet parity conservation. Hence more generally insert the operator,

$$\mathcal{V}(T) = (T_{MN}\partial X^M \bar{\partial} X^N/\alpha')^{1+\alpha' t/4} e^{\mp ik\cdot X} \tag{7.3.1}$$

and factorize the tensor and take the high energy limit. The leading term on-shell at $t = 0$

defines 3 vertex operators (cf. equations (5.2.4)-(5.2.6)) :

$$\begin{aligned}
\langle \mathcal{W}_R\, e^{ikX} h_{MN}\partial X^M \overline{\partial} X^N\rangle &\simeq \langle \mathcal{W}_R\, e^{ikX} h_{--}\partial X^- \overline{\partial} X^-\rangle = O(s)\ , \\
\langle \mathcal{W}_R\, e^{ikX} B_{MN}\partial X^M \overline{\partial} X^N\rangle &\simeq \langle \mathcal{W}_R\, e^{ikX} B_{-\perp}(\partial X^- \overline{\partial} X^\perp - \partial X^\perp \overline{\partial} X^-)\rangle = O(\sqrt{s})\ , \\
\langle \mathcal{W}_R\, e^{ikX} \eta_{MN}\partial X^M \overline{\partial} X^N\rangle &\simeq O(1)\ .
\end{aligned} \tag{7.3.2}$$

For $t \neq 0$ the leading term picks up a common factor of $(\partial X^- \bar{\partial} X^-)^{\frac{\alpha' t}{4}}$ on the left,

$$\begin{aligned}
[(h_{MN} &+ B_{MN})\partial X^M \overline{\partial} X^N]^{1+\frac{\alpha' t}{4}} \\
&\simeq \Big[h_{--}(\partial X^- \overline{\partial} X^-) + B_{-\perp}(\partial X^- \overline{\partial} X^\perp - \partial X^\perp \overline{\partial} X^-)\Big] (\partial X^- \overline{\partial} X^-)^{\frac{\alpha' t}{4}}\ .
\end{aligned} \tag{7.3.3}$$

For $\mathcal{W}_L$, we need to replace X^- by X^+, with a common factor $(\partial X^+ \bar{\partial} X^+)^{\frac{\alpha' t}{4}}$ on the right. When they are combined, the symmetric combination, i.e., the first term above, leads to the Pomeron vertex operator. The anti-symmetric combination, the second term, contributing to $1/s$ down relative to the first term, corresponds to an Odderon exchange.

In analogy with $\mathcal{V}_P^\pm$, we can now define an Odderon vertex operator

$$\mathcal{V}_O^\pm = (2\epsilon_{\pm,\perp}\partial X^\pm \bar{\partial} X^\perp/\alpha')(2\partial X^\pm \bar{\partial} X^\pm/\alpha')^{\alpha' t/4} e^{\mp ik\cdot X} \tag{7.3.4}$$

which characterizes the exchange of a leading Odderon. Here $\epsilon_{\pm,\perp} = -\epsilon_{\perp,\pm}$. Just as for the Pomeron, this is an on-shell vertex operator, satisfying the on-shell conditions

$$L_0 \mathcal{V}_O^\pm = \bar{L}_0 \mathcal{V}_O^\pm = \mathcal{V}_O^\pm \tag{7.3.5}$$

In particular, this leading Regge trajectory interpolates those states created by level-one oscillators, $\alpha_{-1,M}$ and $\tilde{\alpha}_{-1,M}$, with $j = 2n+1$, $t_n = 4n\ \alpha'^{-1}$, $n = 0, 1, \cdots$, and can be characterized by an Odderon trajectory

$$\alpha^{(-)}(t) = 1 + \alpha' t/2\ , \quad \text{or} \quad L_0(j,t) = \bar{L}_0(j,t) = (j+1)/2 - \alpha' t/4 = 1 \tag{7.3.6}$$

Let us next briefly comment on the the couplings of the Odderon, i.e., $\langle \mathcal{W}_R\, \mathcal{V}_O^- \rangle$ and $\left\langle \mathcal{V}_O^+\, \mathcal{W}_L \right\rangle$. Note that $\mathcal{V}_P$ and $\mathcal{V}_O$ have opposite symmetry under $\partial \leftrightarrow \bar{\partial}$, even and odd for $\mathcal{V}_P$ and $\mathcal{V}_O$ respectively. For oriented closed strings, the theory should be invariant under $w \leftrightarrow \bar{w}$. It follows that non-vanishing coupling $\langle \mathcal{W}_R\, \mathcal{V}_O^- \rangle$ and $\langle \mathcal{W}_L\, \mathcal{V}_O^+ \rangle$ would require $\mathcal{W}_{R,L}$ to be odd under $w \leftrightarrow \bar{w}$. For example, tachyon and graviton vertex operators V_t and V_g are even under $w \leftrightarrow \bar{w}$. It follows that couplings involving n-tachyons and an Odderon vanish. To be precise, $\langle \mathcal{W}_R\, \mathcal{V}_O^- \rangle$ and $\langle \mathcal{W}_L\, \mathcal{V}_O^+ \rangle$ are non-zero only if $\mathcal{W}_{R,L}$ are odd under $w \leftrightarrow \bar{w}$. Conversely, $\langle \mathcal{W}_R\, \mathcal{V}_P^- \rangle$ and $\langle \mathcal{W}_L\, \mathcal{V}_P^+ \rangle$ are non-zero only if $\mathcal{W}_{R,L}$ are even under $w \leftrightarrow \bar{w}$.

The interested reader can turn to Appendix C for more calculations.

It is worth mentioning that our discussion for the Pomeron and Odderon vertex operators also apply to couplings with branes, which can be used to model “mesons”. It should also apply in the case of baryons.

7.3.2 AdS

We now extend the above analysis to AdS space. The starting point is similar as in the final part of section 6.2. We need to include a function with a dependence on the AdS radial coordinate in the vertex operator, and then enforce the physical state condition

(5.1.33). The vertex operator we introduce is

$$\mathcal{V}_O(j,\pm) = (\partial X^{\pm}\overline{\partial}X^{\perp} - \partial X^{\perp}\overline{\partial}X^{\pm})(\partial X^{\pm}\overline{\partial}X^{\pm})^{\frac{j-1}{2}} e^{\mp ik\cdot X}\phi_{\pm j\perp}(r). \tag{7.3.7}$$

The physical state condition, $L_0 V_O^{\pm}(j) = \tilde{L}_0 V_O^{\pm}(j) = V_O^{\pm}(j)$, will then give us

$$[\frac{j+1}{2} - \frac{\alpha'}{4}\Delta_{O,j}]\phi_{\pm j\perp}(r) = \phi_{\pm j\perp}(r). \tag{7.3.8}$$

We can again perform a similarity transformation, $\phi_{\pm j\perp} = (r/R)^{(j-1)}\phi_{\pm,\perp}$, and arrive at a J-plane Odderon propagator,

$$G^{(-)}(j) = \frac{1}{j - 1 - (R^2/2\sqrt{\lambda})\Delta_{O,1}}\ , \tag{7.3.9}$$

where $\Delta_{O,j} = (r/R)^{-(j-1)}(\Delta_{O,1})(r/R)^{(j-1)}$. To determine the diffusion operator for Odderon, $\Delta_{O,1}$, we can match the EOM at $j = 1$, appropriate in the infinite λ limit.

The EOM in this case involves a Maxwell operator, and in general will also involve an AdS mass. Both the Maxwell operator and the AdS mass squared, m^2_{AdS}, can be fixed by a proper identification of the $B_{\mu\nu}$ state of string theory at $j = 1$ using the AdS/CFT dictionary [4]. In [60, 4] it was found that a 2-form field in AdS space has two solutions, corresponding to $m^2_{AdS} = 16$ and $m^2_{AdS} = 0$.

As done for the Pomeron, to $O(1/\sqrt{\lambda})$, after writing out the Maxwell operator, we have, for $z \neq z'$, and for $j \simeq 1$, $G^{(-)}(j)$ satisfies the $C = -1$ part of Eq. (7.2.11). Again, the wave function, $\phi_{\pm\perp}$, satisfies the same DE. Changing variable to $u = -\ln(z/z_0)$, we get

$$[j - 1 - \frac{\alpha' t}{2}e^{-2u} - \frac{1}{2\sqrt{\lambda}}(\partial_u^2 - m^2_{AdS})]\phi_{\pm\perp}(u) = 0. \tag{7.3.10}$$

This equation can again be diagonalized by ν, with

$$\phi_{+j\perp} \sim e^{(j-1)u} K_{2i\nu}(|t|^{1/2} e^{-u}) \ , \quad \text{and} \quad G^{(-)}(j) = \frac{1}{j - j_0^{(-)} + \mathcal{D}\nu^2} \ . \tag{7.3.11}$$

where $j_0^{(-)} = 1 - m_i^2/2\sqrt{\lambda}$, Eq. (7.2.14). In this basis, the Odderon vertex operator takes on the form

$$\mathcal{V}_O(j, \nu, k, \pm) \sim (\partial X^{\pm} \overline{\partial} X^{\perp} - \partial X^{\perp} \overline{\partial} X^{\pm})(\partial X^{\pm} \overline{\partial} X^{\pm})^{\frac{j-1}{2}} e^{\mp ik\cdot X} e^{(j-1)u} K_{\pm 2i\nu}(|t|^{1/2} e^{-u}) \tag{7.3.12}$$

Following the same steps done for $C = +1$, we arrive at

$$\mathcal{T}^{(-)} \quad \sim \quad \int \frac{dj}{2\pi i} \int \frac{d\nu \nu \sinh 2\pi\nu}{\pi} \frac{\Pi_-(j) \ s^j}{j - j_0^{(-)} + \mathcal{D}\nu^2} \langle \mathcal{W}_{R0} \, \mathcal{V}_O(j, \nu, k, -) \rangle \, \langle \mathcal{V}_O(j, \nu, k, +) \, \mathcal{W}_{L0} \rangle \tag{7.3.13}$$

where we again have a signature factor appropriate for amplitude being odd in s. Closing the contour at $\nu = i\lambda^{1/4}\sqrt{(j - j_0^{(+)})/2}$ directly leads to the desired final result.

Recall that there are two solutions for the conformal Odderon. For $m_{AdS}^2 = 16$,

$$j_{0,(1)}^{(-)} = 1 - 8/\sqrt{\lambda} + O(1/\lambda) \ , \tag{7.3.14}$$

and, for $m_{AdS}^2 = 0$,

$$j_{0,(2)}^{(-)} = 1 + O(1/\lambda) \ , \tag{7.3.15}$$

as summarized in Table 7.1.

7.4 The Hard-Wall Model

In this section we will se the effects of the hard-wall model, and compute the masses for low mass glueballs. These lie on Regge trajectories of the Pomeron and Odderon, see chapter 3.

We will first consider glueball spectra in the supergravity limit, ($\lambda \to \infty$), before addressing the issue of the associated Regge trajectories, (λ large but finite.) Type-IIB string theory at low energy has a supergravity multiplet with several zero mass bosonic fields: a graviton $G_{\mu\nu}$, a dilaton ϕ, an axion (or zero form RR field) C_0, and two K-R tensors, the NS-NS and R-R fields $B_{\mu\nu}$ and $C_{2,\mu\nu}$ respectively. With a hard cutoff for AdS_5, modes for these fields become discrete.

Our first task is to find out all quadratic fluctuations in the $AdS_5 \times S^5$ background metric whose eigen-modes correspond to the discrete glueball spectra for QCD_4 at strong coupling for various J^{PC} sectors. We are only interested in the excitations that lie on the superselection sector for QCD_4. Thus for example we can ignore all non-trivial harmonics in S^5 that carry a non-zero R charge. The result of these considerations, discussed in detail below, is summarized in Table 7.2.

To count the number of independent fluctuations for a supergravity field, we imagine harmonic plane waves propagating in the AdS radial direction, r, with Euclidean time, x_4. For example, the metric fluctuations in AdS_5

$$G_{\mu\nu} = \bar{G}_{\mu\nu} + h_{\mu\nu}(x) \tag{7.4.1}$$

in the fixed background $\bar{G}_{\mu\nu}$ are taken to be of the form $h_{\mu\nu}(r, x_4)$. There is no dependence on the other spatial coordinates, $\vec{x} = (x_1, x_2, x_3)$. As we shall explain in more details in appendix B, there are 5 independent transverse metric fluctuations, h_{ij}, (spin 2), 3 each for NS-NS and R-R two-form tensors respectively, B_{ij} and $C_{2,ij}$, (spin 1), 1 for the dilaton ϕ (spin 0), and 1 for the Axion C_0 (spin 0).

We can consider perturbations of the following forms:

$$h_{ij}(r, x_4) = a_{ij}\; t(r)\; e^{ik_4x_4} \;, \tag{7.4.2}$$

$$B_{ij}(r, x_4) = b_{ij}\; q_1(r)\; e^{ik_4x_4} \;, \tag{7.4.3}$$

$$C_{2,ij}(r, x_4) = c_{ij}\; q_2(r)\; e^{ik_4x_4} \tag{7.4.4}$$

$$\phi(r, x_4) = S_1(r)\; e^{ik_4x_4} \;, \tag{7.4.5}$$

$$C(r, x_4) = S_2(r)\; e^{ik_4x_4} \;, \tag{7.4.6}$$

where $k = (0, 0, 0, k_4)$, a_{ij} a constant traceless-symmetric 3×3 tensor, and b_{ij}, c_{ij} anti-symmetric, with $i, j = 1, 2, 3$. Let $m^2 = -k^2 = -k_4^2$. From linearized Einstein's equations for h_{ij}, scalar wave-equations for ϕ and C_0, and a set of Maxwell equations for B and C_2, we arrive at

$$[-r\frac{d}{dr}r\frac{d}{dr} + 4]\; t(r) = \frac{m^2}{r^2}t(r) \;, \tag{7.4.7}$$

$$\left[-r\frac{d}{dr}r\frac{d}{dr} + m^2_{AdS}\right] q_i(r) = \frac{m^2}{r^2}q_i(r) \;, \tag{7.4.8}$$

$$-\frac{d}{dr}r^5\frac{d}{dr}\; S_i(r) = m^2\; r\; S_i(r) \;, \tag{7.4.9}$$

where m^2_{AdS} are AdS mass squared for the two-form. Note that, for h_{ij} and S_i, $m^2_{AdS} = 0$.

We can bring all three equations into the "scalar" form by scaling

$$\begin{aligned} T(r) &= r^{-2}\, t(r)\,, \\ Q_i(r) &= r^{-2}\, q_i(r)\,. \end{aligned} \tag{7.4.10}$$

One finds that, for T, Q_i and S_i,

$$\begin{aligned} -\frac{d}{dr}r^5\frac{d}{dr}T(r) &= m^2\, r\, T(r)\,, \\ \left[-\frac{d}{dr}r^5\frac{d}{dr} + (m_{AdS}^2 - 4)r^3\right] Q_i(r) &= m^2\, r\, Q_i(r)\,, \\ -\frac{d}{dr}r^5\frac{d}{dr}S_i(r) &= m^2\, r\, S_i(r)\,. \end{aligned} \tag{7.4.11}$$

Note that equations for T and S_1 and S_2 are degenerate, and also for Q_1 and Q_2. We will find it convenient later to work directly with t, q_i and s_i, where $s_i = r^2 S_i$. One finds an equivalent set of equations

$$\begin{aligned} \left[-r\frac{d}{dr}r\frac{d}{dr} + 4\right] t(r) &= (m^2/r^2)\, t(r)\,, \\ \left[-r\frac{d}{dr}r\frac{d}{dr} + m_{AdS}^2\right] q_i(r) &= (m^2/r^2)\, q_i(r)\,, \\ \left[-r\frac{d}{dr}r\frac{d}{dr} + 4\right] s_i(r) &= (m^2/r^2)\, s_i(r)\,. \end{aligned} \tag{7.4.12}$$

For definiteness, let us for now work with Eqs. (7.4.11). Normalizability also requires wave functions to vanish at $r \to \infty$. (The case $m_{AdS}^2 = 0$ requires a special treatment [3].) Once boundary conditions at $r = r_0$ are specified, Eqs. (7.4.11) for T, Q_i and S_i separately turn

[3] In that case, $Q = r^{-2}\log(r/r_1)$ is a zero mode, with r_1 determined by boundary condition at $r = r_0$.

into an eigenvalue problem, with orthonormal condition:

$$\int_{r_0}^{\infty} dr \; r \; \Phi_n \; \Phi_m = \delta_{n,m} \; . \tag{7.4.13}$$

and eigenvalues m_n^2 , $n = 0, 1, \cdots$. From these, one is led to a discrete spectrum for QCD_4 associated with each bosonic supergravity mode.

7.4.1 Parity and Charge Conjugation Assignments

Next we determine how the supergravity fields and therefore the glueballs couple to the boundary gauge theory. This allows us to unambiguously assign the correct parity and charge quantum numbers to the glueball states, following the analysis done in [4].

For this purpose, we consider the Born-Infeld action plus Wess-Zumino term, describing the coupling of a supergravity field to a single D3-brane,

$$S = \int d^4x \det[G_{\mu\nu} + e^{-\phi/2}(B_{\mu\nu} + F_{\mu\nu})] + \int d^4x (C_0 F \wedge F + C_2 \wedge F + C_4)\rangle \; ,$$

where $\mu, \nu \; = 1, 2, 3, 4$. We will find the charge conjugation and parity assignments with the help of the symmetries of the 4-d gauge theory. The Euclidean time is taken to be x_4 and the spatial co-ordinates, x_i, $i = 1, 2, 3$.

For the 4-d gauge fields, we define parity by

$$\begin{aligned} P &: \; A_i(x_i, x_4) \to -A_i(-x_i, x_4), \\ P &: \; A_0(x_i, x_4) \to A_0(-x_i, x_4). \end{aligned} \tag{7.4.14}$$

for $x_i \to -x_i$, $x_4 \to x_4$.

Charge conjugation for a non-Abelian gluon field is

$$C : \tfrac{1}{2}T_a A^a_\mu(x) \to -\tfrac{1}{2}T^*_a A^a_\mu(x) \tag{7.4.15}$$

where T^a are the Hermitian generators of the group. In terms of matrix fields ($A \equiv \frac{1}{2}T_a A^a$), $C : A_\mu(x) \to -A^T_\mu(x)$. This leads to a subtlety. For example consider the transformation of a trilinear gauge invariant operators,

$$C : Tr[F_{\mu_1\nu_1}F_{\mu_2\nu_2}F_{\mu_3\nu_3}] \to -Tr[F_{\mu_3\nu_3}F_{\mu_2\nu_2}F_{\mu_1\nu_1}] \ . \tag{7.4.16}$$

The order of the fields is reversed. Hence the symmetric products, $d^{abc}F^a_1F^b_2F^c_3$, have $C = -1$ and the antisymmetric products, $f^{abc}F^a_1F^b_2F^c_3$, $C = +1$. Of course using a single brane, we can only find symmetric products. For reasons explained for instance in [4], we will only encounter symmetric traces over polynomials in F, designated by $Sym\ \mathrm{Tr}[F_{\mu\nu}\cdots]$. Even polynomials have $C = +1$ and odd polynomials $C = -1$.

Graviton, Dilaton and Axion States

Expanding the Born-Infeld action, we can now read off the J^{PC} assignments. One finds that the graviton $G_{\mu\nu}$ couples as $G_{\mu\nu}T^{\mu\nu}$, where $T^{\mu\nu} \sim \mathrm{Tr}(F_{\mu\lambda}F^\lambda_\nu) + \cdots$. Because an even number of gluons occur in the field operators, the charge conjugation for all such states are $C = +$. For parity, we assume we are in a gauge where the indices of $G_{\mu\nu}$ do not point along x_0, r. From the coupling, $G_{\mu\nu}\mathrm{Tr}[F^{\mu\lambda}F^\nu_\lambda] + \cdots$, we get states

$$G_{ij} \ \to \ 2^{++} \tag{7.4.17}$$

The dilaton couples as $\phi\mathrm{Tr}F^2$, leading to

$$\phi \;\rightarrow\; 0^{++}\;, \tag{7.4.18}$$

and for the axion coupling $C_0\mathrm{Tr}(F_{12}F_{34})$,

$$C_0 \;\rightarrow\; 0^{-+} \quad . \tag{7.4.19}$$

Two-Form Fields

Consider first the NS-NS 2-form field $B_{\mu\nu}$. For $U(1)$ gauge theory in leading order this field couples as $B_{\mu\nu}F^{\mu\nu}$. More generally in the $SU(N)$ gauge theory, $tr(F) = 0$, we must have a multi-gluon coupling, $B_{\mu\nu}\ Sym\mathrm{Tr}[F_{\mu\nu}W]$, where W is an an even power of fields F and the trace is symmetrized. The first non-trivial coupling for $B_{\mu\nu}$ involves the totally-symmetric color-singlet operator, $Sym\ Tr(F_{\mu\nu}F^2)$, i.e., the d-coupling.

For parity, again assume that we are in a gauge where the indices of the 2-form do not point along x_4, r. With $i, j = 1, 2, 3$, the coupling $B_{ij}\ Sym\mathrm{Tr}[F^{ij}W]$ leads to

$$B_{ij} \;\rightarrow\; 1^{+-} \quad , \tag{7.4.20}$$

For the Ramond-Ramond 2-form $C_{2,\mu\nu}$, we have the coupling $\epsilon^{ijk}C_{2,ij}\ Sym\mathrm{Tr}[F_{k4}W]$, so

$$C_{2,ij} \;\rightarrow\; 1^{--}\;. \tag{7.4.21}$$

The first non-trivial coupling for the RR tensor $C_{2,\mu\nu}$ is $Sym\ Tr(\tilde{F}_{\mu\nu}F^2)$.

The complete parity and charge conjugation assignments are now summarized in table 7.2.

G	ϕ	C_0	B	C_2
2^{++}	0^{++}	0^{-+}	1^{+-}	1^{--}

Table 7.2: J^{PC} Classification for QCD_4 glueball states from IIB Gauge/String Duality. The identification here differs slightly from that in [4] where one starts from an 11-d M-theory description with confinement modeled by an AdS^7 black hole metric.

7.4.2 Glueball Spectrum at $\lambda = \infty$

Let us next examine the boundary conditions at $r = r_0$. Recall that the hard-wall model is not a fully consistent theory. However, it does capture key features of confining theories with string theoretic dual descriptions. The main advantage of the hard-wall model is that it can be treated analytically. The boundary condition at the wall on the five-dimensional graviton (and its trajectory for general J) is constrained by energy-momentum conservation in the gauge theory. We must impose the boundary condition, $\partial_r(r^{-2}t_{ij}) = 0$, or, equivalently, Neumann boundary condition for $T(r)$,

$$\partial_r T(r) = 0 \tag{7.4.22}$$

at $r = r_0$. The logic is the same as in deriving the wave equation $\nabla_P \; h_{ij} = 0$: the pure gauge solution $t(r) = r^2$ must be retained as a zero mode, else conservation of the energy-momentum tensor will be violated. This condition extends to the Pomeron for small $|j - 2|$, which will be the regime we will mainly consider below.

J^{PC}:	2^{++}	0^{++}	0^{-+}	1^{+-}	1^{--}
Lattice	1	0.52	1.17	1.50	2.57
Modes:	T	S_1	S_2	Q_1	Q_2
Bdry C.	$\partial_u T\|_0 = 0$	$\partial_u s_1\|_0 = 0$	$\partial_u S_2\|_0 = 0$	$\partial_u q_1\|_0 = 0$	$\partial_u Q_2\|_0 = 0$
n = 0	1.00	0.64	1.00	1.93	2.44
n = 1	3.35	3.06	3.35	5.87	6.20
n = 2	7.05	6.77	7.05	10.95	11.25
n = 3	12.09	11.81	12.09	17.36	17.65

Table 7.3: The mass spectrum, m_n^2, $n = 0, 1, 2, 3$ for QCD_4 Glueballs vs Lattice calculations.

For simplicity, we shall assume a similar boundary conditions for Q_i and S_i, i.e., with Neumann conditions for all three,

$$\partial_r T = \partial_r S_i = \partial_r Q_i = 0 \ , \tag{7.4.23}$$

at $r = r_0$. Note, due to degeneracies noted earlier, we have, for the low-mass glueballs,

$$m_0^2(0^{++}) = m_0^2(0^{-+}) = m_0^2(2^{++}) < m_0^2(1^{+-}) = m_0^2(1^{--}) \ . \tag{7.4.24}$$

In Table 7.3, we have listed mass squared from lattice calculations for ground states, in ratios relative to $m_0^2(2^{++}) \simeq 5.76\text{GeV}^2$, e.g. $m_0^2(2^{++}) = 1$, $m_0^2(0^{++}) = .52$, etc. We have normalized our calculated mass squared with $m_0^2(2^{++}) = 1$, and presented result of this calculation, for $T:\ m_n^2(2^{++})$, $S_2:\ m_n^2(0^{-+})$, and $Q_2:\ m_n^2(1^{--})$, $n = 0, 1, 2, 3$. (For two-form fluctuations, we have considered only the case $m_{AdS}^2 = 16$, since the case of $m_{AdS}^2 = 0$ can be shown to correspond to pure gauge.)

In this dissertation, we are less concerned on how well the resulting spectrum agrees with the lattice result and will postpone further improvements to future investigations. Nevertheless, it is important to note the pattern of degeneracy between the lightest scalar

(0^{++}) glueball, the lightest tensor (2^{++}) and the pseudoscalar (0^{-+}), and the degeneracy between two spin-1 states, (1^{+-} and 1^{--}), are not shared by the lattice result. Within a hard-wall model, these patterns can only be broken by boundary conditions. There is *a priori* no reason to adopt the same boundary condition for S_i and Q_j, $i, j = 1, 2$. In fact, based on the results for a black hole background [61, 4, 62], it is suggestive that the physics of confinement could be better simulated by having different boundary conditions for S_1 vs. S_2, or Q_1 vs. Q_2, in the IR, thus breaking their degeneracies.

The spectrum can be changed if different boundary conditions for S_1 and Q_1 are adopted [4]. We find it amazing that it is possible to adjust the boundary conditions at $r = r_0$, so that $m_0^2\ (0^{++}) < m_0^2\ (2^{++}) \simeq m_0^2\ (0^{-+}) < m_0^2\ (1^{+-}) < m_0^2\ (1^{--})$. As noted earlier, this pattern is consistent with that followed from a constituent gluon and bag models. As an illustration, we adopt Neumann conditions for h_{ij}, s_1, S_2, q_1 and Q_2. This will change the masses for 0^{++} and 1^{+-}, and the resulting mass squared under Neumann conditions, $S_1 :\ m_n^2(0^{++})$, and $Q_1 :\ m_n^2(1^{+-})$, $n = 0, 1, 2, 3$, are also shown in table 7.3.

7.4.3 Regge Trajectories

At λ large but finite, $O(1/\sqrt{\lambda})$ corrections must be taken into account. Recall that, for the metric fluctuations, the on-shell conditions, $L_0 = \bar{L}_0 = 1$, receive corrections, and, operatorially, can be written as

$$\Big[j - 2 + (1/2\sqrt{\lambda})\nabla_P\Big]\, t(r) = \Big[j - 2 + (1/2\sqrt{\lambda})(-r\partial_r r\partial_r + 4 - \frac{t}{r^2})\Big]\, t(r) = 0 \qquad (7.4.25)$$

[4] Dirichlet boundary condition was used in [63] as a model for calculating the scalar glueball masses. Subsequently, both Dirichlet and Neumann boundary conditions were used in a holographic approach to glueballs masses [64]. For related works, see [65, 66].

For $j = 2$, this leads to Eq. (7.4.7), where, by applying the boundary condition at r_0, it turns into an eigenvalue condition on $t \to m_n^2$. For finite λ, we now have a generalized eigenvalue problem. Since j enters as a parameter, we find the glueball spectrum now can be considered as function of j and λ, $m_n^2(j, \lambda)$. Equivalently, we can treat t as a parameter, and consider this as an eigenvalue problem in j, i.e., we will have discrete spectrum in the J-plane. Since each eigenvalue is a function of t, one arrives at a set $j_n(t)$, $n = 0, 1, \cdots$, each specifying a Regge trajectory. Furthermore, this is also a continuous spectrum, corresponding to the BFKL cut. The J-plane spectrum is illustrated in Fig. 7.1, as a graph of j vs. t.

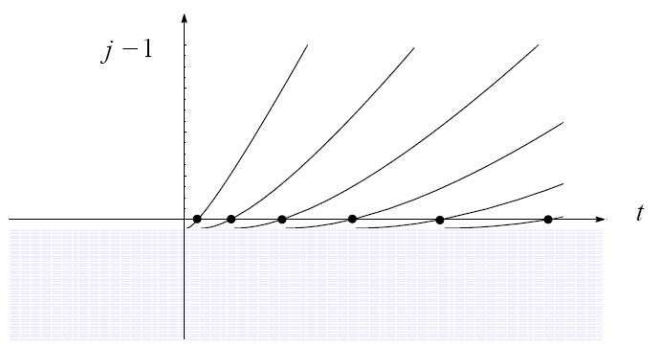

Figure 7.1: The J-plane structure for the $C = -1$ sector is schematically represented by the spectrum for hard-wall model. As t decreases, trajectories move under the fixed-cut at $j = j_0^{(-)}$ and disappear from the physical sheet. The transition region from moving-pole to fixed cut is model-dependent. At sufficiently large t each trajectory attains a fixed slope, corresponding to the tension of the model's confining flux tubes. This J-plane structure for the $C = -1$ sector is similar to that for the $C = +1$ sector, as depicted in Fig. 8 of Ref. [1].

It is now straight forward to generalize this to the whole supergravity modes. Using the variable $u = \log(r/r_0)$, it is possible to express all relevant extensions of Eqs. (7.4.12) in a standard Schrödinger form,

$$\begin{aligned}
\text{Pomeron :} \qquad & \left[-\partial_u^2 + 4 + (2\sqrt{\lambda})(j-2) - e^{-2u}(t/t_0)\right] t(u) &=& \ 0\ , \\
\text{Odderon :} \qquad & \left[-\partial_u^2 + m_{AdS}^2 + (2\sqrt{\lambda})(j-1) - e^{-2u}(t/t_0)\right] q(u) &=& \ 0\ , \\
\text{Scalar :} \qquad & \left[-\partial_u^2 + 4 + (2\sqrt{\lambda})(j-0) - e^{-2u}(t/t_0)\right] s(u) &=& \ 0\ ,
\end{aligned} \tag{7.4.26}$$

with boundary conditions, (7.4.23), becoming

$$\partial_u(e^{-2u}t) = \partial_u(e^{-2u}s_i) = \partial_u(e^{-2u}q_j) = 0\ , \tag{7.4.27}$$

at $u = 0$. We have also made use of the fact that $t_0 = 1/\alpha_0'\sqrt{\lambda} = \Lambda_{QCD}^2$ and $\alpha_0' \equiv \frac{\alpha' R^2}{r_0^2}$.

The spectra for all three cases are structurally identical. We can express these equations collectively as

$$\left[-\partial_u^2 + m^2{}_{(\gamma)}(j) - e^{-2u}(t/t_0)\right] \psi^{(\gamma)}(u) = 0 \tag{7.4.28}$$

with

$$m^2{}_{(\gamma)} = 2\sqrt{\lambda}(j - j^{(\gamma)}) \tag{7.4.29}$$

where $j^{(\gamma)} = 2 - 2/\sqrt{\lambda}, 1 - m_{AdS}^2/2\sqrt{\lambda}, -2/\sqrt{\lambda}$, for γ taking on t, q, s respectively. Note that $j^{(\gamma)}$ is the location of the BFKL cut for the t, q, s modes respectively. Note also that $m^2{}_{(t)}(j)$ and $m^2{}_{(q)}(j)$ are the same as $m^2{}_{(+)}(j)$ and $m^2{}_{(-)}(j)$ introduced earlier in Eq. (7.2.11). Since one can move from one equation to another by shifting the J value, they lead to same J-plane structure except for the intercepts at $t = 0$.

Let us examine the form of (7.4.28) as a Schrödinger equation. At $t \leq 0$, the potential is strictly positive and approaching zero, at $u = \infty$. We conclude that the spectrum consists of a continuum and there are no bound states. For $t > 0$, on the other hand, there is now an attractive potential well at $u = 0$, and bound states can now be formed, in addition to the continuum at $E_\gamma = 0$.

Changing back to the variable $z = e^{-u}$, our equation becomes a Bessel equation,

$$\left[z^2\partial_z^2 + z\partial_z + (t/t_0)z^2 - \nu^2\right]\psi = 0, \tag{7.4.30}$$

with

$$\nu^2 = m_{(\gamma)}^2 = 2\sqrt{\lambda}(j - j^{(\gamma)}) \tag{7.4.31}$$

The solutions are given by

$$\psi(z) = c_1 J_\nu(\sqrt{t/t_0}\, z) + c_2 Y_\nu(\sqrt{t/t_0}\, z), \tag{7.4.32}$$

where J_ν and Y_ν are the Bessel functions of the first and second kind respectively. At $z = 0$, Bessel functions of the second kind are singular, and since we want the solution that is regular at $z = 0$ we can conclude that $c_2 = 0$ and hence

$$\psi(z) = c_1 J_\nu(\sqrt{t/t_0}\, z) \tag{7.4.33}$$

We next impose boundary conditions (7.4.27) at $z = 1$, leading to an eigenvalue problem. There are two equivalent ways to proceed. One finds

- Given $j > j_\gamma$ real, solve spectrum $t_{\gamma,n}(j)$, $n = 0, 1, \cdots$.
- Given $t > 0$, solve spectrum $j_{\gamma,n}(t)$, $n = 0, 1, \cdots$.

Chapter 8

DIS in AdS/CFT

After developing the Odderon vertex operator, we now take a step back to the Pomeron. We calculate the structure function F_2, using techniques introduced in chapter 6. After finding the expression for $F_2(x, Q^2)$ we compare it to the most comprehensive set of recent small-x DIS experimental results, and find a very good agreement between the results obtained using string theoretic calculations and experiments. Furthermore, we see that the BPST Pomeron of section 6.2 can fit both the Donnachie-Landshoff soft Pomeron, with intercept ~ 0.08 and the BFKL hard Pomeron with intercept ~ 1.40. Even further more, we establish the importance of confinement and see that our results must account for it if we want to have a realistic theory. This chapter is wholly based on reference [10], after some aspects were foreshadowed in [8, 9]. For other recent studies see [67, 68, 69, 70, 71, 72, 73, 74, 75, 76, 77, 78, 79, 80, 81, 82, 83, 84, 85, 86, 87, 88].

8.1 Parton Phenomenology

As we saw in section 4.3, hadron structure functions $F_i(x, Q^2)$ follow from quark and gluon distributions, $q_i(x, Q^2)$, $\bar{q}_j(x, Q^2)$, and $g_k(x, Q^2)$. At LHC, proton gluon distribution is expected to play an increasingly important role at small-x and/or large Q^2. In a strong coupling approach, although it is no longer meaningful to speak of quarks and gluons as the effective partonic degrees of freedom, the dominance of gluon dynamics at small-x justifies treating a simpler situation where quarks are first ignored, i.e., considering the limit $N_c >> N_f$. In such a limit, Gauge/String duality can be applied directly [89, 1].

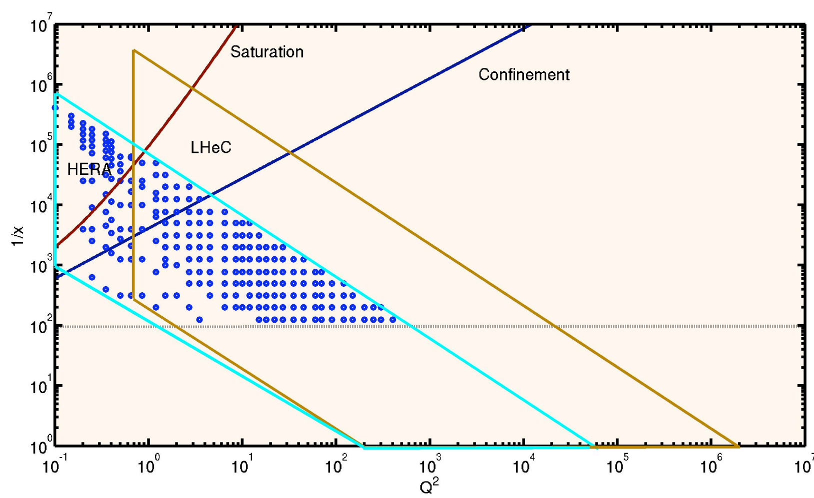

Figure 8.1: HERA and LHeC regions are labeled by trapezoids respectively. We have also shown the entire combined H1-ZEUS small-x data points as dots. Lines for confinement and saturation are discussed in Sec. 8.3 and Sec. 8.5 respectively.

In a naive parton picture, Bjorken scaling would lead to Q^2-independence for the DIS structure functions. In a perturbative treatment, due to QCD evolution, structure functions such as $F_2(x, Q^2)$ become Q^2-dependent, which can be derived by using the linear DGLAP evolution equation. This has indeed been carried out for the HERA data, starting with phenomenological inputs for structure functions at low Q^2, e.g., $Q^2 \simeq 3 - 4\ GeV^2$. Of course, an inclusive DIS cross section can also be treated directly as the total cross section of an off-shell photon, with mass squared $-Q^2$, scattered off a proton. The Bjorken x variable is then related to the center of mass energy squared s of the $\gamma^* p$ system by $x \approx {}^{Q^2}/_{s}$, at high s. The limit $x \to 0$, with Q^2 fixed, can then be considered as the Regge limit for $\gamma^* p$ two-body scattering. The off-shell $\gamma^* p$ total cross section in the limit $x \to 0$ can then be characterized by the exchange of Pomerons, as done for other hadronic total cross sections. This has been studied at weak coupling using the BFKL equation, which corresponds to summing over Reggeized gluon ladder graphs [90, 44, 45, 46]. It is therefore tempting to identify the rise of $F_2(x, Q^2)$ with $1/x$, for fixed Q^2, observed at HERA, as the onset of the Pomeron dynamics. In Fig. 8.1, we indicate in a $\log(Q^2) - \log(1/x)$ plot the kinematic region covered by HERA and also the region of particular interest at LHC, e.g., that for the proposed LHeC. We also identify, by dots, the small-x data points, with $x < 0.01$, for the combined H1-ZEUS data set, which has been released recently [6]. There are 249 data points, with Q^2 ranging from 0.1 to 400 GeV^2.

DGLAP provides a description for the evolution of the data in Q^2, given $F_i(x, Q^{*2})$ at some initial point Q^{*2}. The study of small-x, on the other hand, focuses on evolution in $1/x$, with Q^2 fixed. Indeed, for Q^2 ranging from $0.15\,GeV^2$ to $250\,GeV^2$, by fitting the data to

$$F_2(x, Q^2) \sim (1/x)^{\epsilon_{eff}}, \tag{8.1.1}$$

with Q^2 fixed, "effective Pomeron" intercept, $1+\epsilon_{eff}$, can be extracted [5], with ϵ_{eff} shown in Fig. 8.2. There are two intriguing aspects to this analysis. First, the effective intercept, except for that at small Q^2, is very large, with $1 + \epsilon_{eff} \simeq 1.2 \sim 1.4$. Even more puzzling is the fact that ϵ_{eff} is Q^2-dependent, contrary to a naive Regge expectation. This feature could seriously challenge the hypothesis of Pomeron dynamics at work in the HERA energy range. Indeed, this Q^2-dependence has been used to support the notion of "two-Pomeron" hypothesis [91]. (For related earlier work, see [92, 93, 94].)

As we have mentioned earlier, using AdS/CFT, the BPST Pomeron can provide a synthesis of both the "soft" and the "hard" Pomerons. Using the BPST Pomeron, we have found that the Q^2-dependence for ϵ_{eff} observed at HERA, Fig. 8.2, can be attributed primarily to diffusion for Q^2 large and to confinement effects for Q^2 small.

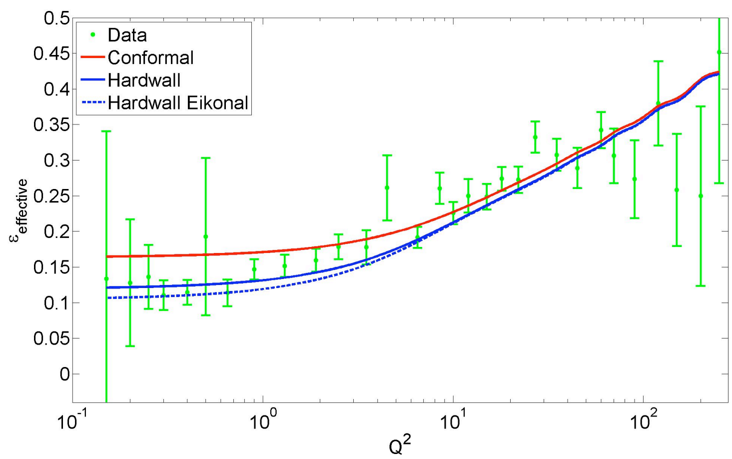

Figure 8.2: Q^2-dependence for effective Pomeron intercept, $\alpha_P = 1+\epsilon_{eff}$, from [5]. Various curves are fits based on strong/gauge duality described in Secs. 8.4 and 8.5.

8.2 Basic Setup

In our approach, two-body amplitudes are controlled by exchanging BPST Pomeron, with an intercept

$$j_0 \simeq 2 - \rho \tag{8.2.1}$$

where we have re-written Eq. (6.2.26) in terms of a more convenient parameter, $\rho \equiv 2/\sqrt{\lambda}$. It is useful to compare the dependence of the Pomeron intercept on the 't Hooft coupling at weak and strong couplings. It is worth noting that the BFKL Pomeron intercept for $\mathcal{N} = 4$ SYM, calculated to second order, meets with the BPST intercept near $\alpha_P \simeq 1.2 \sim 1.3$, as shown in Fig. 8.3, precisely in the range as extracted from the HERA data. At

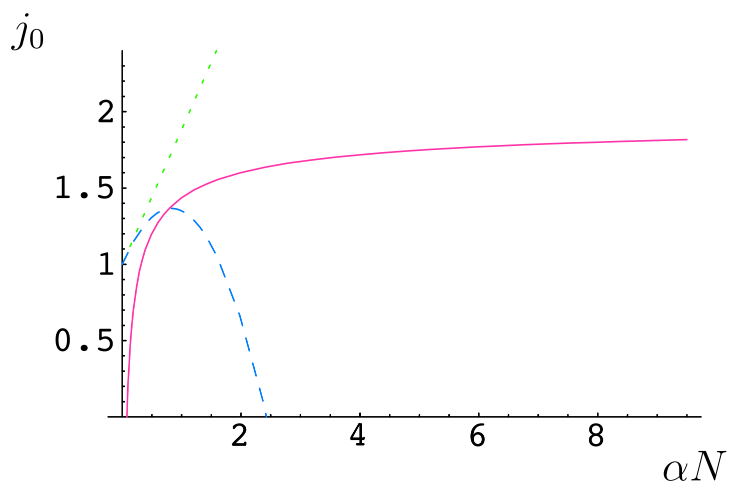

Figure 8.3: The Pomeron intercept in QCD viewed as a function of the 't Hooft coupling. ($\lambda = g^2_{YM} N_c$, with $\alpha = g^2_{YM}/4\pi$.) This is reproduced from Fig. 12 of Ref. [1].

these values, the 't Hooft coupling is relatively large, around $\lambda \simeq 10$. For such a large coupling value, it is important to explore the strong coupling approach as a more efficient procedure for addressing physical processes such as DIS. (There have already been several phenomenological studies of AdS/CFT which consider λ in this range. For example in [77], strong coupling is defined as $\lambda \geq 5$.)

QCD can be considered conformal only approximately at best. A conformal theory can never fully reproduce all experimental results due to the lack of a scale and the absence of confinement. However, at Q^2 sufficiently large, partons inside the proton are expected to be free, and a conformally invariant description could be a good approximation. Conversely, at smaller Q^2 values, it is reasonable to expect that confinement effects should be felt. Equally important is the phenomenon of "saturation", which should become important due to higher order Pomeron-exchanges. In AdS/CFT, these non-linear effects come from eikonalization. In contrast, in weak coupling, saturation has been addressed primarily by considering non-linear evolutions such as the BK equation [95, 96, 97].

In this chapter, we will extend the results of section 6.3 to the case involving two external currents, appropriate for DIS [89]. The structure functions in DIS can be extracted from the off-shell $\gamma^* p$ total cross sections, which, from optical theorem, are proportional to the imaginary part of the forward off-shell $\gamma^* p$ amplitudes, $\mathrm{Im}A(s, 0)$. We therefore need to consider the states of an offshell photon. This will require a replacement in P_{13} by wave functions divergent on the AdS boundary. As is well known, in closed string theory there is no photon state. In [89] Polchinski and Strassler have considered a $R-$boson propagating through the bulk that couples to leptons on the boundary. To be specific, for $F_2(x, Q)$, which corresponds to the sum of the transverse and longitudinal cross sections, the appropriate $R-$boson wave functions which mimic the vector currents involve both $K_0(Qz)$ and $K_1(Qz)$. After removing the associated polarization vectors and one factor of fine structure constant α_{em}, one arrives at

$$P_{13}(z) \to P_{13}(z, Q^2) = \frac{1}{z}(Qz)^2(K_0^2(Qz) + K_1^2(Qz)), \tag{8.2.2}$$

and, for x small where the Pomeron dynamics is applicable,

$$F_2(x, Q^2) = \frac{Q^2}{2\pi^2} \int d^2b \int dz \int dz' P_{13}(z, Q^2) P_{24}(z') \mathrm{Re}\left(1 - e^{i\chi(s,b,z,z')}\right) \tag{8.2.3}$$

(See also [72, 98]). A similar replacement would lead to the second structure function,

$F_1(x, Q^2)$,

$$2xF_1(x, Q^2) = \frac{Q^2}{2\pi^2} \int d^2b \int dz \int dz' P_{13}(z, Q^2) P_{24}(z') \mathrm{Re} \left(1 - e^{i\chi(s,b,z,z')}\right) \tag{8.2.4}$$

with

$$P_{13}(z) \to P_{13}(z, Q^2) = \frac{1}{z}(Qz)^2 K_1^2(Qz). \tag{8.2.5}$$

We shall next examine the usefulness of this strong coupling formalism by testing against the recently published combined H1-ZEUS data set. To simplify the discussion, we will focus primarily on F_2.

8.3 DIS at Strong Coupling and the BPST Kernel

Our goal is to calculate the structure function F_2, which is given in terms of the cross section by equation (4.3.13). From the Optical Theorem, (2.2.10), one can express the cross section in terms of the imaginary part of the forward scattering amplitude. We then calculate the scattering amplitude to first order using equation (6.3.16). For our present application, we consider deep inelastic scattering and the appropriate $R-$boson wave functions P_{13} for F_2 can be taken to be that given by (8.2.2). Note that, strictly speaking, the use of (8.2.2) is valid only for Q^2 large and near the AdS boundary where confinement effects can be ignored. This will give us the means to calculate F_2

$$F_2(x, Q^2) = (Q^2/2\pi^2) \int d^2b \int dz dz' P_{13}(z, Q^2) P_{24}(z') Im\ \chi(s, b, z, z'). \tag{8.3.1}$$

with $P_{13}(z, Q^2)$ given by Eq. (8.2.2). We see that for $Qz > 1$, $P_{13}(z, Q^2)$ rapidly decays to zero because of the Bessel functions K_0 and K_1. For small Qz, with $P_{13}(z, Q)$ bounded and, as we shall show shortly, $\int d^2b Im\, \chi(s,b,z,z')$ vanishing faster than $0(z^2)$, it follows that the integrand is peaked around $z \sim {}^1\!/_Q$. We also note that, after a simple calculation, $\int_0^\infty dz(zQ)^2 P_{13}(z,Q^2) = 1$.

8.3.1 DIS in the Conformal Limit

Let us begin by first considering the conformal limit. In this limit, the imaginary part of the BPST Pomeron kernel, $ImK(s,b,z,z')$ can be expressed in a closed form, [1], and, from Eq. (6.3.10), it leads to

$$Im\, \chi(s,b,z,z') = \frac{g_0^2}{16\pi}\sqrt{\frac{\rho}{\pi}} e^{(1-\rho)\tau} \frac{\xi}{\sinh\xi} \frac{\exp(\frac{-\xi^2}{\rho\tau})}{\tau^{3/2}}, \tag{8.3.2}$$

where τ and ξ are given by (6.2.40) and (5.1.30) respectively. The real part, $Re\, \chi(s,b,z,z')$, can be reconstructed via a dispersion integral, or, equivalently, by solving a derivative dispersion relation. As noted earlier, due to conformal invariance, $Im\chi(s,b,z,z')$ depends only on two variables, τ, (or $\hat{s}$), and ξ. The b-space integration of this kernel can be carried out explicitly [3], leading to

$$\int d^2b\, Im\, \chi(s,b,z,z') \;=\; \frac{g_0^2}{16}\sqrt{\frac{\rho^3}{\pi}}\, (zz')\, e^{(1-\rho)\tau} \frac{\exp(\frac{-(\log z - \log z')^2}{\rho\tau})}{\tau^{1/2}}. \tag{8.3.3}$$

This expression now takes on the familiar form of "diffusion" in $|\log z|$. This was first noted in Ref. [1].

Let us next turn to the factor P_{24}. For the proton, one is dealing with a normalizable state. Strictly speaking, this necessarily breaks the conformal limit, e.g., to model QCD we need to introduce a cutoff at $z_0 \sim 1/\Lambda$, where Λ is the confinement scale. This construct would be sufficient for describing glueballs. However, for baryons, one needs to go beyond the standard confining deformation and additional holographic prescriptions will have to be adopted [98, 99, 100]. It suffices to assume for now that the AdS wave-function for the proton is localized near the cutoff in the bulk, z_0.

Putting these two together, we have, for DIS in the strong coupling conformal limit, that the structure function F_2 can be expressed as

$$F_2(x, Q^2) = \frac{g_0^2 \rho^{3/2}}{32\pi^{5/2}} \int dz dz' P_{13}(z, Q^2) P_{24}(z')(zz'Q^2)\, e^{(1-\rho)\tau} \frac{\exp(\frac{-(\log z - \log z')^2}{\rho\tau})}{\tau^{1/2}} \tag{8.3.4}$$

where $x \simeq Q^2/s$ and P_{13} given by (8.2.2). Note that F_2 is uniquely determined once the parameter ρ and the overall strength factor g_0^2 are specified. There are two important features for Eq. (8.3.4). It is easy to verify, as noted earlier, that the integrand vanishes at least as fast as $z^{1-\rho}$ at $z = 0$ and is exponentially damped for $z >> 1/Q$. It follows that the dominant contribution to the integral coming from $z = O(1/Q)$. With $z' = O(1/\Lambda_{qcd})$, the factor $e^{(1-\rho)\tau}$ leads to

$$e^{(1-\rho)\tau} \sim (1/x)^{1-\rho} \;, \tag{8.3.5}$$

with Q^2 fixed. The limit $x \to 0$ will lead to a fast rising in F_2, violating the standard Froissart bound. In terms of the eikonal $\chi(\hat{s}, b, z, z')$, it is generally accepted that the condition $\chi = O(1)$ would signal the onset of "saturation". Note that this is a "local condition" in the three-dimensional transverse space, z and $\vec{b}$, with z' fixed. One of the main goal of our current analysis is to investigate the importance of saturation in the HERA range. We will come back to this discussion in Sec. 8.5.

The second key feature for (8.3.4) is the last exponential factor,

$$\exp\left(\frac{-(\log z - \log z')^2}{\rho\tau}\right) \tag{8.3.6}$$

With $z \sim 1/Q$, this corresponds to diffusion in $\log Q$, analogous to diffusion in "virtuality", found in weak coupling BFKL dynamics. As we shall see shortly, we find this diffusion effect playing a crucial role in understanding the Q^2 dependence for the $\epsilon_{eff}(Q^2)$ observed at HERA, as exhibited in Fig. 8.2.

8.3.2 Confinement

Let us next turn to the case with confinement, using the hard-wall model for illustration. In this model, we introduce a sharp boundary in the AdS z coordinate at some value z_0. This leads to a mass gap and a discrete spectrum of states. Our starting points are still Eqs. 4.3.13 and 8.3.1, but a modified Pomeron kernel has to be used. Such a kernel can formally be represented in a spectral representation, but it cannot be expressed in a simple closed form as the conformal case, i.e., (8.3.2). Fortunately, for a single Pomeron contribution, we only need to evaluate the total contribution after integration over the impact parameter $\vec{b}$. That is, if we go to momentum space,

$$\chi(s,t,z,z') = \int d^2b e^{iq_\perp b_\perp}\chi(s,b,z,z'), \tag{8.3.7}$$

where $t = -q_\perp^2$, we only need to know $\chi(s,t,z,z')$ evaluating in momentum space at $t = 0$. For this, a closed form has been found for the BPST hard-wall kernel, [3], leading to

$$Im\ \chi_{hw}(s,t=0,z,z') = Im\ \chi_c(\tau,0,z,z') + \mathcal{F}(z,z',\tau)\ Im\ \chi_c(\tau,0,z,z_0^2/z'), \tag{8.3.8}$$

where $Im\ \chi_c(\tau, 0, z, z')$ is the conformal expression given by the right hand side of Eq. (8.3.3), and $\mathcal{F}$ and η were already defined before, (6.2.50).

It follows that, with confinement,

$$F_2(x, Q^2) = \frac{g_0^2 \rho^{3/2}}{32\pi^{5/2}} \int dz dz' P_{13}(z, Q^2) P_{24}(z')(zz'Q^2)\ e^{(1-\rho)\tau} \left(\frac{e^{-\frac{\log^2 z/z'}{\rho\tau}}}{\tau^{1/2}} + \mathcal{F}(z, z', \tau) \frac{e^{-\frac{\log^2 zz'/z_0^2}{\rho\tau}}}{\tau^{1/2}} \right) \tag{8.3.9}$$

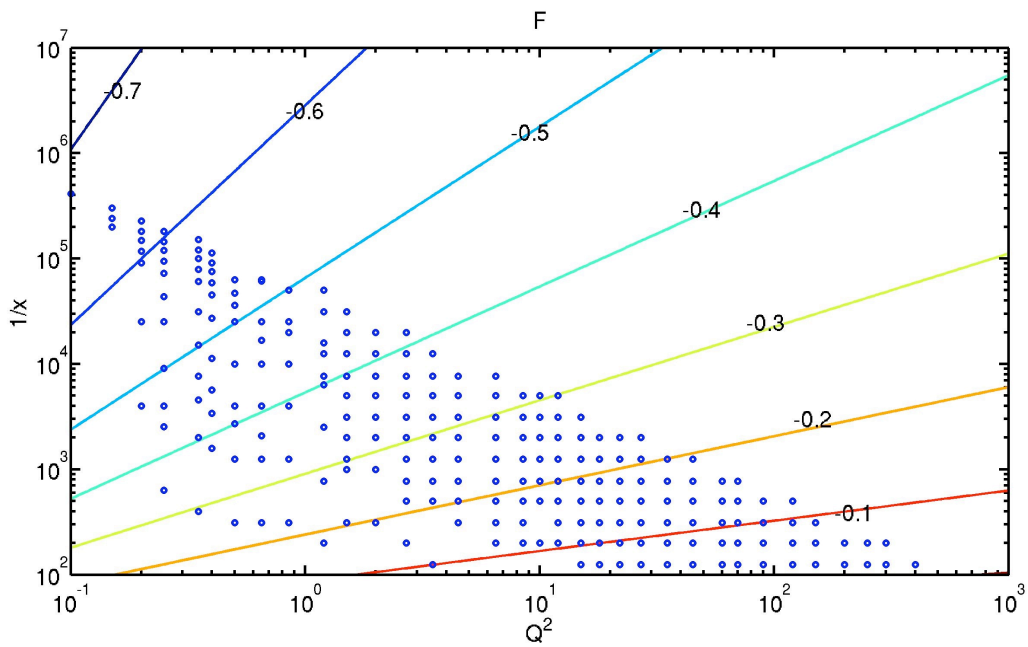

Figure 8.4: Contour plot for coefficient function $\mathcal{F}$ as a function of $log(1/z)$ and $\log(1/x)$, with $z' \simeq z_0$ fixed, $z_0 \sim \Lambda_{QCD}^{-1}$. Confinement effects become important in the region where $|\mathcal{F}| > 0.3 \sim 0.5$. We have also shown the entire combined H1-ZEUS small-x data points [6] as dots by identifying $Q = 1/z$.

The first term on the right-hand side of (8.3.9) is precisely the same as that in the conformal limit, (8.3.3) and is model independent. The second term, which can be expressed as a linear superposition of contributions from a set of image charges, is dependent upon the details of how the space is cutoff at z_0 and hence model dependent. Nevertheless it is reasonable to assume its presence can provide a qualitatively reliable estimate of the effects of confinement. The coefficient function, $\mathcal{F}(z,z',\tau)$, (6.2.50), at fixed z,z', goes to 1 as $\tau\to 0$ and to -1 as $\tau\to\infty$. Hence, at small x, i.e., τ large, $\mathcal{F}\to -1$ and confinement leads to a partial cancelation for the growth rate relative to that of the conformal BPST Pomeron. Moreover, since $\mathcal{F}$ is continuous, there will be a region over which $\mathcal{F}\sim 0$, and, in this region, there is little difference between the hard-wall and the conformal results.

In Fig. 8.4, we provide a contour plot for $\mathcal{F}$ as a function of $\ln x$ and $\ln z$, with z' fixed near z_0. Using the fact that, from $P_{13}(z,Q^2)$ is peaked at $z\simeq 1/Q$, this can also be interpreted as a contour plot in $1/x$ and Q^2, with $\ln Q\simeq -\ln z$. Anticipating our subsequent fit which fixes the scale with $z_0\sim\Lambda_{qcd}$, we have also exhibited the entire set of the recently combined ZEUS-H1 small-x data points as open dots on this plot. We note that, over a significant region, e.g., $Q^2>O(1)\ GeV^2$, $|\mathcal{F}|$ is small and the conformal kernel remains a reasonable approximation. Equally important is the observation that the region where confinement effects can be significant, roughly defined by the condition $|\mathcal{F}|>c$, $c\simeq 0.3-0.5$, goes beyond the narrow region of $Q^2=O(1)\ GeV^2$. The line for $c=0.5$ is also drawn in Fig. 8.1 indicating schematically the transition into confinement region. This observation goes against the conventional belief that confinement effects can be ignored for Q^2 large, independent of x. This also casts doubt on the assumption that saturation at Q^2 large can be understood without taking confinement into account.

Eq. (8.3.9) is the expression which we will use shortly for comparing with experimental results. This expression retains the two key features noted earlier for the conformal result, namely, the presence of the dominant term in τ, leading to $(1/x)^{1-\rho}$ rise, and the presence of diffusion in z.

8.4 Confronting the HERA Data – Linear Treatment

We now carry out a test of our strong coupling DIS analysis by fitting the recently published combined H1-ZEUS data set. We will first test single BPST Pomeron models, both conformal and with confinement, before trying the eikonal form in the next section. We restrict ourselves to the small-x region, i.e., $x < 0.01$. This remains a relatively large data set with 249 points, and in particular, the set extends to a large range of Q^2 values, from $0.1\,GeV^2$ to $400\,GeV^2$. We find that the confinement-improved treatment allows a surprisingly good fit to all HERA small-x data. In contrast, the fit based on the conformal BPST Pomeron breaks down in the low-Q^2 region.

Before proceeding further, we must specify more precisely the AdS wave function, $\phi_p(z)$, associated with the proton. Unfortunately, other than the expectation that it be normalizable, i.e., $\int dz\sqrt{-g(z)}(z/R)^2|\phi_p(z)|^2 = 1$, one cannot determine ϕ_p without an explicit strong coupling model for baryon. For the current analysis, we will assume that the wave function is sharply peaked near the IR boundary z_0, with $1/Q' \leq z_0$, with Q' of the order of the proton mass [98, 99, 100]. For simplicity, we will simply replace P_{24} by a sharp delta-function

$$P_{24}(z') \approx \delta(z' - 1/Q'). \tag{8.4.1}$$

Similarly, as noted earlier, the integral over $P_{13}(z, Q^2)$ in (8.3.4), and also in (8.3.9), is centered at $z = 1/Q$, with $\int dz(zQ)^2 P_{13}(z, Q^2) = 1$. As emphasized earlier, (8.3.4) follows only for Q^2 large, and there will be modifications coming from confinement for Q^2 small. To simplify the discussion below, we will again make the local approximation by replacing

$P_{13}(z, Q^2)$ by a delta-function

$$P_{13}(z) \approx C\delta(z - 1/Q), \tag{8.4.2}$$

with $C \simeq 1$. These constitute our model-dependent parametrizations. With these substitutions, the z and z' integrations can be performed trivially, leading to F_2 given essentially by the Pomeron kernel. It follows that the structure function, (8.3.4), becomes

$$F_2(x, Q^2) = \frac{g_0^2}{32\pi^{5/2}}\rho^{3/2}\frac{Q}{Q'}e^{(1-\rho)\tau} \left(\frac{\exp(-\frac{\log^2(Q/Q')}{\rho\tau})}{\sqrt{\tau}}\right). \tag{8.4.3}$$

with τ as a function of x and Q^2: $\tau(x, Q^2) = \log[(\frac{\rho Q}{2Q'})(\frac{1}{x})]$. The hard-wall single-Pomeron contribution, (8.3.9), can similarly be simplified, with η in (6.2.50) expressed as $\eta(x, Q^2) = \frac{\log(z_0^2 QQ') + \rho\tau(x,Q^2)}{\sqrt{\rho\tau(x,Q^2)}}$.

To see how well our strong coupling expression comes close to the experimental data, we begin by first restricting ourselves to a smaller set of ZEUS data with $x < 0.01$ and a range of Q^2 from 0.65 to 650 GeV^2. Although there are data at lower values of Q^2, we do not consider them initially since we would like to avoid the region where confinement effect can be expected to be important. We will also begin by first testing against the previously published ZEUS data [5, 101], so we can compare the goodness of our fit relative to other published fits done by others without invoking AdS/CFT [102, 103, 104]. Another reason for avoiding the small Q^2 region is because in our formalism it is natural to restrict $Q > Q'$, where $1/Q' \simeq z'$ characterizes the "size" of the proton and, as we shall see, will turn out to be $\approx 0.5\,GeV$.

We fit the F_2 to the ZEUS data using Matlab with 4 free parameters, which we choose to be : ρ, g_0, z_0, and Q'. We have carried out fits for both the conformal and the hard-wall models. In total we had 160 different data points with 32 different values of Q^2. Surprisingly, good fits can be achieved for both. To be specific, we obtain the "best fit" for the confining hard-wall model, with the following values: $\rho = 0.7716 \pm 0.0103$, $g_0^2 = 106.01 \pm 3.10$, $z_0 = 6.60 \pm 1.50\, GeV^{-1}$, $Q' = 0.5322 \pm 0.0465\ GeV$. These values are "reasonable", within our general expectations. For instance, the value of $\rho \simeq 0.77$ lies within the transition region between strong and weak coupling. The value of z_0 is also consistent with our expectation of $z_0 \sim O(\Lambda_{qcd}^{-1})$. With z_0 fixed, the value for Q' is again reasonable. The chi-square value per degree of freedom [1] we calculate for our best fit is $\chi^2_{d.o.f.} = 0.69$. An equally good fit can also be obtained using the conformal Pomeron, with best fit values: $\rho = 0.774 \pm 0.0103$, $g_0^2 = 110.13 \pm 1.93$, $Q' = 0.5575 \pm 0.0432\ GeV$, and the corresponding chi-square value is $\chi^2_{d.o.f.} = 0.75$.

Armed with this success, we next carried out an expanded study for the recently published combined H1-ZEUS data set [6], keeping only small-x data. With $x < 10^{-2}$, the set now extends to much smaller Q^2 values, with Q^2 ranging from $0.1\, GeV^2$ to $400\, GeV^2$, taking on 34 different Q^2 values. This is a larger data set than the ZEUS set considered above, increasing from 160 data points to 249 points. These are the data points shown in Fig. (8.4) as dots, with $z = Q^{-1}$.

With the inclusion of data at $Q^2 < 0.65 GeV^2$, we can no longer obtain acceptable fits by a single conformal BPST Pomeron. The best fit leads to an unacceptably large value of $\chi^2_{d.o.f.} = 11.7$. The fit cannot be improved by the sieve-procedure [105]. That is, one cannot attribute the poor fit to the presence of "outliers". In contrast, we find that the

[1] We calculated the $\chi^2_{d.o.f.}$ using a standard formula, $\chi^2_{d.o.f.} = \frac{1}{N-p} \sum_i \frac{(O_i - E_i)^2}{\sigma_i^2}$, where N is the number of points, p is the number of parameters, and O_i, E_i and σ_i are the observed, expected, and the total error of the observed values respectively. (See, for instance, P. Fornasini, "The Uncertainty in Physical Measurements", Springer 2008.)

confinement-improved (hard-wall) treatment allows a surprisingly good fit to all HERA small-x data, especially after applying the sieve-procedure. We obtain the "best fit" for the confining hard-wall model, with the following values

$$\rho = 0.7792\pm0.0034,\ g_0^2 = 103.14\pm1.68,\ z_0 = 4.96\pm0.14\,GeV^{-1},\ Q' = 0.4333\pm0.0243\,GeV, \tag{8.4.4}$$

These values differ from our earlier fit only slightly and they remain reasonable, within our general expectations. Without sieving, we obtain $\chi^2_{d.o.f.} = 1.34$. With the elimination of 6 data points as "outliers", each with $\chi^2 > 8$, the $\chi^2_{d.o.f.}$ improves to be 1.16. The best cutoff is for $\chi^2 > 4$, leading to a calculated chi-squared per degree of freedom $\chi^2_{d.o.f.} = 1.07$ for our best fit given above [2].

In Fig. 8.5 we show our fits to $F_2(x, Q^2)$ for all 34 different Q^2 as a function of x^{-1}. The fit for a single conformal BPST Pomeron is shown as blue curves and that for a single hard-wall BPST is shown as red curves. It is evident that, for Q^2 small, the conformal model does not fit the data well. However, for $Q^2 > 4 \sim 5\ GeV^2$, where data points exist, the conformal and the hard-wall models remain comparable.

We can further test our result by turning to the HERA effective Pomeron intercept plot, Fig. 8.2. Intercept values derived from the conformal Pomeron are in red and those from the hard-wall model are in blue. Much of the Q^2-dependence for the effective Pomeron intercept can be attributed to the diffusion effect. As Q^2 becomes large, diffusion is enhanced, leading to an increase to the effect rise in F_2 as $1/x$ increases. Let us next examine the hard-wall model, (8.3.9), where we see the effect of confinement is embodied in the second term. For $Q^2 >> 1\ GeV^2$, the difference between these two at HERA energy

[2] With a χ^2-cutoff at 8, we included a renormalization factor of $\mathcal{R} = 1.0433$. When the cut-off is at 4, one has $\mathcal{R} = 1.2924$.

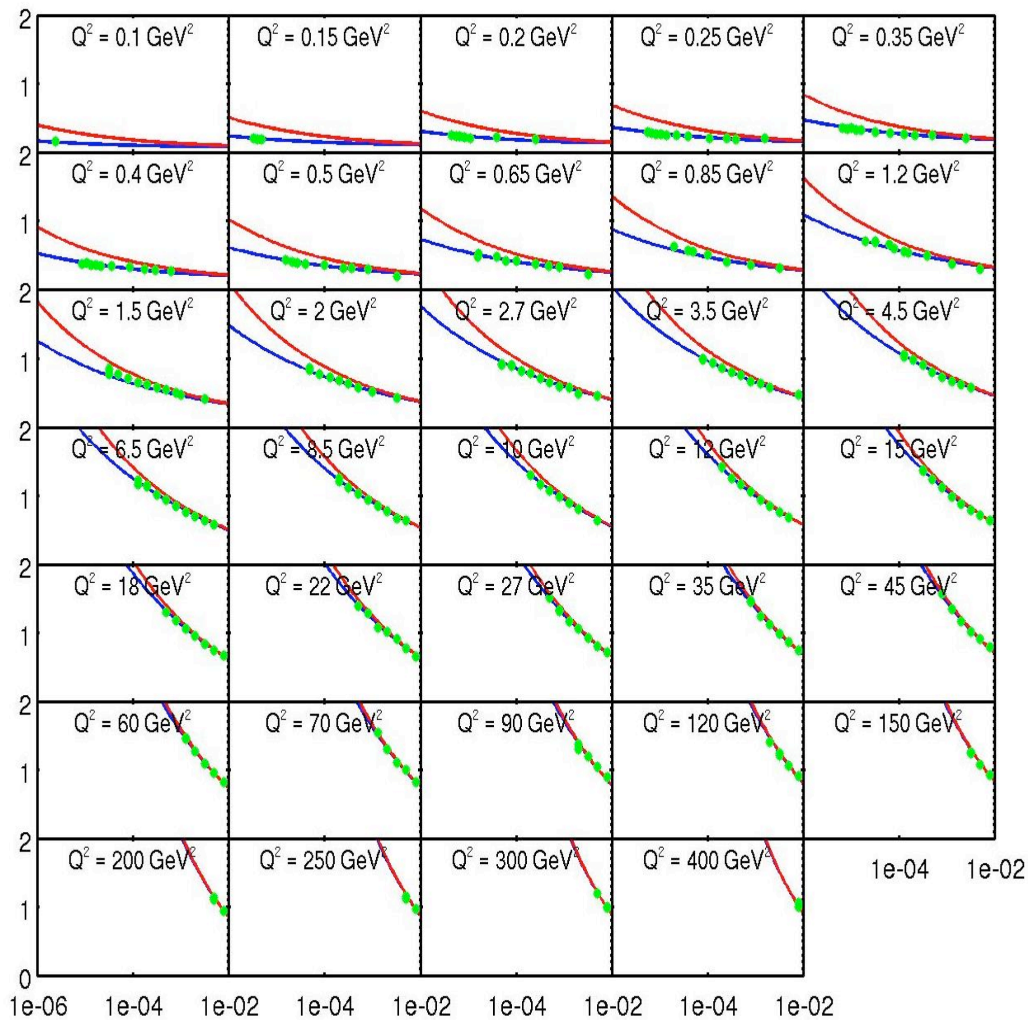

Figure 8.5: Global fits to the combined ZEUS-H1 small-x data. Dotted red lines are for single conformal BPST Pomeron and dotted blue lines are for single hard-wall BPST Pomeron.

range is small. As mentioned earlier, from Fig. 8.4, with $|\mathcal{F}| << 1$ mostly in this region, it is not surprising that the red and the blue lines converge as Q^2 increases. However, as Q^2 decreases, one finds $|\mathcal{F}|$ increases, and the effect of "destructive interference" is enhanced. In particular, in the extreme limit of $z \sim z' \sim z_0$, the leading order term from the denominator of the diffusion factor, $1/\sqrt{\tau}$, largely cancel, leading effectively to a $\tau^{-3/2}$ suppression. This enhanced suppression contributes to a lowered value for the effective Pomeron at small Q^2, which is reflected by the red-curve in Fig. 8.5. That is, using the hard-wall model as a guide, confinement leads to an effective lowering of the Pomeron intercept for scattering of two "soft" states, i.e., states with wave functions centered near the IR wall. This is consistent with the view of "soft Pomeron" dominance for hadronic cross sections in the near forward region, with an effective intercept $\alpha_P \simeq 1.08$. Of course, in the region, one also expects eikonalization would eventually become important. We turn to this issue in the next Section.

It is also worth noting that, under our local approximation where $z \simeq 1/Q$, one has, for $1/x$ large,

$$R = \frac{F_L}{F_T} \simeq \frac{\int_0^\infty dx x^{3-\rho}|K_0(x)|^2}{\int_0^\infty dx x^{3-\rho}|K_1(x)|^2} = \frac{2-\rho}{4-\rho}, \tag{8.4.5}$$

where $F_L = 2xF_1$ and $F_T = F_2 - 2xF_!$. With $0 < \rho < 1$, R ranges from 1/2 to 1/3, achieving the maximum in the supergravity limit when $\rho \to 0$. This differs significantly from that expected for x large due to Callan-Gross relation. This is consistent[3] with that found previously in Ref. [71].

[3]In [71], $R \simeq (1+\omega)/(3+\omega)$, with $\omega = 1-\rho$.

8.5 Nonlinear Evolution and Saturation

At strong coupling nonlinearity enters through eikonalization. When eikonalization becomes important, it also signifies the onset of "saturation". Instead of expanding Eq. (8.2.3) to first order in the eikonal, a fully non-perturbative treatment is now required. Clearly, nonlinearity becomes important only when

$$|\chi(s,b,z,z')| \geq O(1). \tag{8.5.1}$$

In general, both the real and the imaginary parts of the eikonal will have to be taken into account. Note that this is a local condition, in the three-dimensional transverse $(\vec{b}, z)$ space. (For a more traditional weak coupling approach, see [106, 95, 96, 97]. See also [72], [78], and references therein.)

Using the conformal eikonal as a guide, it is easy to convince ourselves that, for the HERA range, it is adequate to treat Pomeron linearly and one is far away from saturation. In Fig. 8.6a, we show a contour plot for the conformal eikonal, using the parameters given in Eq. (8.4.4), at zero impact parameter, $\vec{b} = 0$. We have also made use of the fact that $z \simeq 1/Q$, which allows one to label all the HERA data set on the same plot. Note that, for $\vec{b} = 0$, where the eikonal is the largest, the maximal value in the HERA range remains less than $0.2 \sim 0.3$. The conformal eikonal decreases with increasing $|\vec{b}|$ as a power, when $|\vec{b}| >> z$. We have carried out an eikonal analysis using the conformal eikonal. Not surprisingly, there is no improvement in the quality of the fit. We again find with unacceptable chi-square per degree of freedom, due primarily to the inadequate fit in the region of small Q^2. In order to answer the question regarding the onset of saturation, we next turn to an eikonal treatment for the hard-wall model.

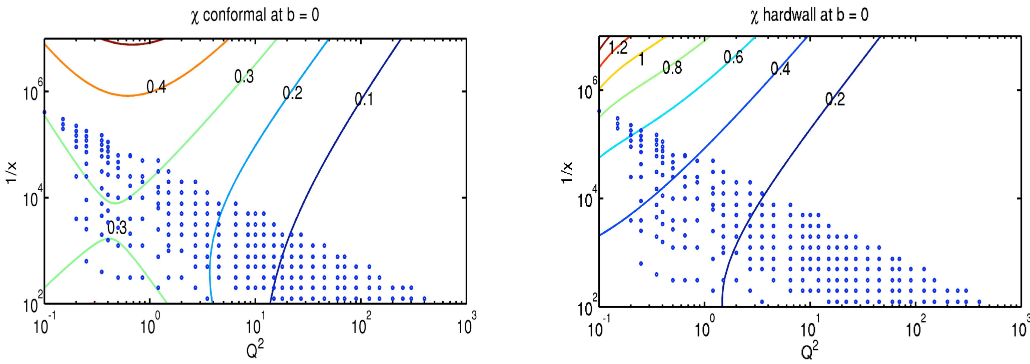

Figure 8.6: Contour for $Im\ \chi(s,b,z,z')$ for conformal and hard-wall respectively, with $z' \simeq z_0$ fixed, as a function of x and z, $(z = Q^{-1})$, at zero impact parameter, $\vec{b} = 0$.

The eikonal for the hard-wall model, $\chi_{hw}(s,b,z,z')$, can be obtained via a spectral representation [1, 3]. However, it is difficult to cast $\chi_{hw}(s,b,z,z')$ in a form amenable for direct manipulation, except for its integrated form, $\int d^2b\ Im\ \chi_{hw}(s,b,z,z')$, given by (8.3.8). Fortunately, the effect of eikonalization at HERA is likely to be weak except for Q^2 small. We will therefore provide an approximate treatment which incorporates the more important new features due to confinement.

Let us begin by first working in a momentum representation, (8.3.7) and focus on $Im\ \chi_{hw}(\tau,t,z,z')$. For $t \neq 0$, $Im\ \chi_{hw}(\tau,t,z,z')$ can be formally obtained by solving an integral equation

$$\begin{aligned} Im\ \chi_{hw}(\tau,t,z,z') &= Im\ \chi_{hw}(\tau,0,z,z') \\ &+ \frac{\alpha_0 t}{2}\int_0^{\tau} d\tau' \int_0^{z_0} d\tilde{z}\ \tilde{z}^2\ Im\ \chi_{hw}(\tau',0,z,\tilde{z}) Im\ \chi_{hw}(\tau-\tau',t,\tilde{z},z') \end{aligned} \tag{8.5.2}$$

with $Im\ \chi_{hw}(\tau,0,z,z')$ given by Eq. (8.3.8). Solution to this integral equation can be investigated numerically, which is currently under way and will be reported separately. Here an approximate treatment will be provided.

The single-most important consequence of confinement is the existence of a mass gap. In the conformal limit, $\chi_c(\tau, t, z, z')$ has a branch point at $t = 0$, which is responsible for a power-like fall off at large impact separation. For instance, in the supergravity limit where $j \to 2$, this leads to the well-known cutoff for b large,

$$\chi_c(\tau, b, z, z') \sim e^{\tau} b^{-6} \, . \tag{8.5.3}$$

Incidentally, the eikonal becomes real in this limit. More generally, a power decrease signals the presence of a $t = 0$ singularity in the momentum representation. In contrast, for hard-wall, because of confinement, $\chi_c(\tau, t, z, z')$ is regular at $t = 0$, with its nearest singularity at $t = m_0^2$, m_0 the mass of the lightest tensor. Because of the mass gap, confinement leads to an exponential damping, i.e., in the supergravity limit, it again leads to a real eikonal, but with an exponential cutoff

$$\chi_{hw}(\tau, b, z, z') \sim e^{\tau} e^{-m_0 b} \tag{8.5.4}$$

To illustrate the effect of confinement, we show in Fig, 8.7 the ratio of the hard-wall eikonal to the conformal eikonal calculated numerically, as a function of b/z_0 and z/z_0, with $z' \simeq z_0$ fixed. Note the rapid drop when $b > z_0$ and, in comparison, a relative slow variation in z.

To fully explore the consequence of confinement at finite 't Hooft coupling, it is useful to work with the Pomeron kernel in the J-plane. It can be shown that the eikonal for the hard-wall model has a cutoff at large b of the form

$$Im\ \chi_{hw}(\tau, b, z, z') \sim \exp[-m_1 b - (m_0 - m_1)^2\ b^2/4\rho\tau] \tag{8.5.5}$$

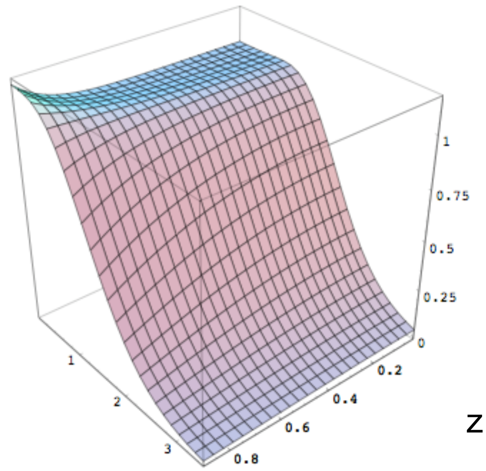

Figure 8.7: Ratio of hard-wall to conformal eikonal Contour in the super-gravity limit, $\chi_{hw}(\hat{s}, b, z, z')/\chi_c(\hat{s}, b, z, z')$. The ratio is independent of $\hat{s}$ and is plotted against z/z_0 and b/z_0, with $0 < z/z_0 < 1$ and $z' = z_0$ fixed.

where m_1 and m_0 are solutions of $\partial_z(z^2 J_0(mz)) \mid_{z=z_0} = 0$ and $\partial_z(z^2 J_2(mz)) \mid_{z=z_0} = 0$ respectively. (We have $m_1 \simeq 1.6\ z_0^{-1}$ and $m_0 \simeq 3.8\ z_0^{-1}$. [7]). Although the J-plane is difficult to carry out analytically, it can be treated, for instance, numerically. For our current analysis, we shall modify our earlier the conformal hard-wall eikonal, by taking the large-b cutoff, (8.5.5), into account. For b-small, as well as to take into account the proper boundary condition near the IR hard-wall, we shall take $Im\ \chi_{hw}(\tau, b, z, z')$ to be of the form $Im\ \chi_{hw}^{(0)}(\tau, b, z, z') \sim Im\ \chi_c(\tau, b, z, z') + \mathcal{F}(\tau, z, z') Im\ \chi_c(\tau, b, z, z_0^2/z')$. We therefore adopt the following simple ansatz[4] where $Im\ \chi_{hw}(\tau, b, z, z') \sim D(\tau, b) Im\ \chi_{hw}^{(0)}(\tau, b, z, z')$, where

$$D(\tau, b) = \begin{cases} 1\ , & b < z_0 \\ \frac{\exp[-m_1 b - (m_0 - m_1)^2\ b^2/4\rho\tau]}{\exp[-m_1 z_0 - (m_0 - m_1)^2\ z_0^2/4\rho\tau]}\ , & b > z_0 \end{cases} \tag{8.5.6}$$

[4]This ansatz should be further improved as one moves to smaller x-value beyond the HERA range. This will be addressed in a future publication where we also treat elastic and total cross sections, as well as diffractive Higgs production at LHC.

Lastly, we provide an overall factor $C(\tau, z, z')$ which can be fixed by the normalization condition (8.3.8).

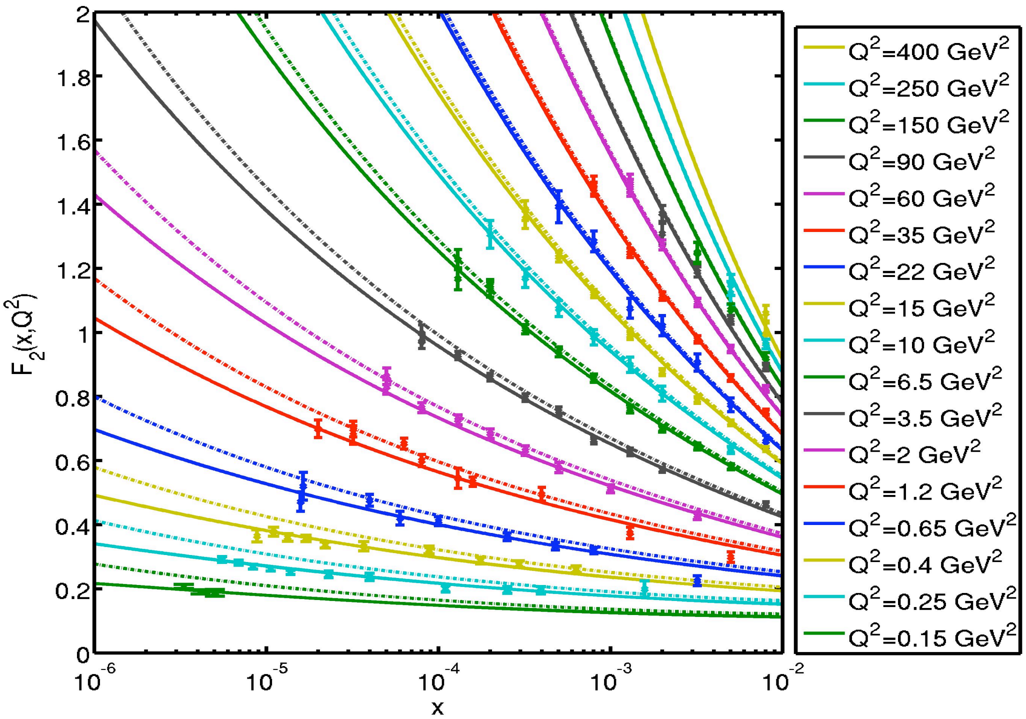

Figure 8.8: Fit to the combined H1-ZEUS small-x data for $F_2(x, Q^2)$ by a hard-wall eikonal treatment. We have exhibited both the hard-wall single Pomeron fits, (in dashed lines), and the hard-wall eikonal, (in solid lines), together for a better visual comparison. The fit include 249 data points, with $x < 10^{-2}$, and 34 Q^2 values, ranging from 0.1 GeV^2 to 400 GeV^2. Only data set for 17 Q^2 values are shown.

In Fig. 8.8, we have collected both the BPST hard-wall Pomeron fits, (dashed lines), and the hard-wall eikonal, (solid lines), in one place for a better visual effect. For the latter fit, real part of the eikonal is included dispersively. For clarity, we only show data for 17 Q^2 sets, out of 34. We find that the confinement-improved eikonal treatment allows a surprisingly good fit to all HERA small-x data, with Q^2 ranging from $0.1\,GeV^2$ to $400\,GeV^2$ and for $x < 10^{-2}$, with a $\chi^2 = 1.04$, after performing a similar sieve-procedure as done earlier. The parameters for the best fits remain basically the same, with

$$\rho = 0.7833\pm0.0035,\ g_0^2 = 104.81\pm1.41,\ z_0 = 6.04\pm0.15\, GeV^{-1},\ Q' = 0.4439\pm0.0177\, GeV. \tag{8.5.7}$$

Whereas these two fits are indistinguishable for most HERA data, they do begin to diverge as one moves to smaller x values, e.g., to the LHC range.

Our analysis confirms that saturation effects is minimal for $Q^2 \geq O(1)\ GeV^2$ at HERA energy range. For $Q \leq O(1)\ GeV^2$, eikonal treatment can achieve a better fit than that by a single hard-wall Pomeron where saturation effects can begin to be felt. In Fig. 8.2, we show by the dotted blue curve the eikonal improved effective Pomeron intercept based on hard-wall eikonal. Note that this further lowers the effective intercept as one moves to smaller Q^2. As mentioned earlier, this is consistent with the view of "soft Pomeron" dominance for hadronic cross sections in the near forward region, with an effective intercept $\alpha_P \simeq 1.08$. In Fig. 8.6b, we provide a contour plots for this confinement-improved eikonal, $Im\ \chi_{hw}(\hat{s}, b, z, z')$ at $b = 0$. By focussing on the eikonal at $b = 0$, we also see that it is increasing important to include non-linear effects, particularly for $Q^2 = O(1) GeV^2$. This of course indicates the onset of saturation, (8.5.1), and this is schematically represented in Fig. 8.1 by a saturation line. In fact, for any Q^2, for $1/x$ sufficiently small, eikonalization will always be necessary.

Chapter 9

Conclusions

We are at the end of our journey. But before looking forward, let us look back and try to distill the main ideas we have encountered. As physicists, we ultimately want to understand how nature works. Therefore no matter what we calculate, eventually it has to agree with observations. If we want to claim we understand how particles interact with each other, eventually we have to link our understanding to quantities that can be measured in experiments. This work has tried to explain some aspects of one of the means that particles can interact, which is via the strong interaction.

The strong interaction is unique among the currently known interactions in nature, in that it gets weaker when the interacting states get closer to each other. This leads to many interesting effects, some of which we encountered in chapter 4, but it can make it difficult to study in some regimes. We have encountered ideas from many different areas of physics, but it is satisfying to see that in recent years they have been moving together to provide results at strong coupling. In particular, it has turned out that string theory, among its many other possible uses not addressed here, is a great tool for studying non-perturbative aspects of QCD.

We saw how string theory can give a non-perturbative formulation of the Pomeron, and then generalized this procedure to desribe a non-perturbative Odderon as well. However, as summarized in [56], the strongest evidence for Odderon, at this point, is more theoretical than experimental. Our current analysis has provided further support for its existence from a non-perturbative perspective. Nevertheless, puzzles remain on why it is so difficult to observe the Odderon experimentally. It has been suggested that direct exclusive production holds the best chance for observing the Odderon. One would expect that at $t = 0$ the Odderon would dominate over the quark anti-quark (meson) Regge trajectories and that for large $t < 0$, there would be a distinguishing hard components similar to that expected for the BFKL Pomeron. If so, better understanding and control of the Odderon intercept and its on-shell string vertex-coupling would be useful.

DIS then gets the string theoretic treatment. We use the gauge/string duality to derive expressions for the structure function $F_2(x, Q^2)$, and then fit the results to small-x data. We consider two models, one where the string theory is on AdS space, which corresponds to the dual theory being $\mathcal{N} = 4SYM$, a conformal theory, and the other where the string theory is on AdS space with a hard-wall cutoff, which is a toy model for confinement. We find that if we first look at just the ZEUS data [5, 101], for values of Q^2 ranging from $0.65\, GeV^2$ to $650\, GeV^2$ and for $x < 10^{-2}$ both the conformal and the hard-wall model fit well. However, including the more recent combined H1-ZEUS small-x data, [6], with more small Q^2 data, going down to $Q^2 = 0.15 GeV^2$, we find that the hard-wall model fits very well, while the conformal model cannot fit the data any more. The conformal model does not improve through eikonalization either. More generally, contrary to other current expectations we find that, the importance of confinement sets in before the importance of saturation, defined as $\chi \simeq O(1)$, figure 8.1. However, we are not completely sure right now if this is just a consequence of the model we use, or a more general property of confining theories. One of the future projects is to give this question a definite answer.

We see that there are two very important features of the strong interaction that we must be able to reproduce: confinement and the unitarity bound. Therefore an eikonalized confining theory, which would satisfy both those features, would be a very useful theory to have, and could lead to interesting developments. In [10] we only give an approximate treatment to eikonalizing the hard-wall Pomeron exchange, and we find that although at HERA energies it improves the overall fit, it does so only very slightly. The best fit for the single hard-wall Pomeron exchange model had a renormalized $\chi^2 = 1.07$, versus a $\chi^2 = 1.04$ for the eikonal version of the same. However, we expect this difference to be more significant as we achieve LHC energies. Work is already in progress to numerically find the hard-wall eikonal, and compare it to total cross section measurements. Results will be reported in future publications.

Equally important is the application of gauge/string duality to the production of the Higgs boson (also known as the SX boson). One of the possible discovery channels for the Higgs could be double diffractive proton-proton scattering. Hence a thorough theoretical understanding would be very interesting. BPST Pomeron exchange could be applied to this process, but the important new feature now would be the coupling of the Higgs, described by a non-normalizable current, to two Pomerons. Work on this is already underway, and we expect to report the results soon.

These are just a few of the many yet to be explored research areas. Although important progress has been made in physics in the past ten years, there is still a lot that remains to be done.

Appendix A

Kinematics

A.1 Scattering

First we look at $2 \to 2$ scattering, in the all incoming convention. The Mandelstam variables are (2.1.9)

$$s = -(p_1 + p_2)^2 \quad t = -(p_1 + p_3)^2 \quad u = -(p_1 + p_4)^2 \, .$$

Let us look at a s channel process $1 + 2 \to 3 + 4$. The momenta are

$$\begin{aligned} p_1 &= \begin{pmatrix} E_1 \\ \mathbf{p_1} \end{pmatrix}, \qquad p_2 = \begin{pmatrix} E_2 \\ -\mathbf{p_1} \end{pmatrix} \\ p_3 &= \begin{pmatrix} -E_3 \\ -\mathbf{p_3} \end{pmatrix}, \qquad p_4 = \begin{pmatrix} -E_4 \\ \mathbf{p_3} \end{pmatrix} \end{aligned} \tag{A.1.1}$$

with

$$s = (E_1 + E_2)^2 = (E_3 + E_4)^2 \tag{A.1.2}$$

$$E_1 = \tfrac{1}{2\sqrt{s}}(s + m_1^2 - m_2^2)\,,\ E_2 = \tfrac{1}{2\sqrt{s}}(s + m_2^2 - m_1^2) \tag{A.1.3}$$

$$E_3 = \tfrac{1}{2\sqrt{s}}(s + m_3^2 - m_4^2)\,,\ E_4 = \tfrac{1}{2\sqrt{s}}(s + m_4^2 - m_3^2) \tag{A.1.4}$$

$$\mathbf{p_1}^2 = \tfrac{1}{4s}\,[s - (m_1 + m_2)^2]\,[s - (m_1 - m_2)^2] \tag{A.1.5}$$

$$\mathbf{p_3}^2 = \tfrac{1}{4s}\,[s - (m_3 + m_4)^2]\,[s - (m_3 - m_4)^2] \tag{A.1.6}$$

$$t = m_1^2 + m_3^2 - 2(E_1 E_3 - |\mathbf{p_1}||\mathbf{p_3}|\cos\theta_s) \tag{A.1.7}$$

$$u = m_1^2 + m_4^2 - 2(E_1 E_4 + |\mathbf{p_1}||\mathbf{p_3}|\cos\theta_s)\,. \tag{A.1.8}$$

θ_s is the scattering angle, i.e. the angle between $\mathbf{p_1}$ and $\mathbf{p_3}$.

In terms of the Lorentz invariants, the factor $|\mathbf{p_1}|\sqrt{s}$ that appears in the cross section (2.1.24) is

$$|\mathbf{p_1}|^2 s = \frac{1}{4}\,\left[s - (m_1 + m_2)^2\right]\left[s - (m_1 - m_2)^2\right]\,. \tag{A.1.9}$$

The physical region for this process is given by

$$s \geq (m_1 + m_2)^2 \qquad -1 \leq \cos\theta_s \leq 1\,. \tag{A.1.10}$$

In the special case when all the $m_i = m$, the equations simplify

$$E_1 = E_2 = E_3 = E_4 = \frac{\sqrt{s}}{2} \tag{A.1.11}$$

$$\mathbf{p_1}^2 = \mathbf{p_3}^2 = \frac{1}{4}\left[s - 4m^2\right] \tag{A.1.12}$$

$$t = -2\mathbf{p}^2(1 - \cos\theta_s) = (2m^2 - \frac{s}{2})(1 - \cos\theta_s) \tag{A.1.13}$$

$$u = (2m^2 - \frac{s}{2})(1 + \cos\theta_s) \tag{A.1.14}$$

We can express the scattering angle in terms of t and s

$$\cos\theta_s = 1 + \frac{2t}{s - 4m^2}\,. \tag{A.1.15}$$

From here we can see that the physical region is

$$s \geq 4m^2, \quad t \leq 0, \quad u \leq 0\,. \tag{A.1.16}$$

In the high energy limit $s \gg m^2$ and (A.1.15) simplifies

$$\cos\theta_s \approx 1 + \frac{2t}{s}\,. \tag{A.1.17}$$

A.2 Light-cone Coordinates

Take particle 1 to be traveling along the z axis and particle 2 along $-z$. Then define

$$p^{\pm} = E \pm p^3 \tag{A.2.1}$$

We can then split the coordinates into p^+, p_- and $\mathbf{p}_\perp = (p_1, p_2)$.

For simplicity, let us work in the case where all the masses are equal, and in the Regge limit $s \gg m^2$, ${}^{t}\!/\!{}_{s} \to 0$ Then

$$\mathbf{p}^2 = \frac{1}{2}(s - 4m^2) \approx \frac{s}{2} \tag{A.2.2}$$

$$\cos\theta_s \approx 1 + \frac{2t}{s} \tag{A.2.3}$$

$$\sin\theta_s \approx \frac{2}{\sqrt{s}}\sqrt{-t} \tag{A.2.4}$$

$$p_1^+ \approx \sqrt{s} \tag{A.2.5}$$

$$p_1^- \approx 0 \tag{A.2.6}$$

$$p_2^+ \approx 0 \tag{A.2.7}$$

$$p_2^- \approx \sqrt{s} \tag{A.2.8}$$

$$p_3 = \begin{pmatrix} -\sqrt{s} \\ 0 \\ -\sqrt{-t} \\ 0 \end{pmatrix} \tag{A.2.9}$$

$$p_4 = \begin{pmatrix} 0 \\ -\sqrt{s} \\ \sqrt{-t} \\ 0 \end{pmatrix} \tag{A.2.10}$$

We see that one set of momenta has a large + component (i.e. p_1 and p_3) and the other a large − component (i.e. p_2 and p_4). The momentum transfer is

$$p_1 + p_3 = q = \begin{pmatrix} 0 \\ 0 \\ -\sqrt{-t} \\ 0 \end{pmatrix}, \tag{A.2.11}$$

and therefore $q = \mathbf{q}_\perp$ and

$$\mathbf{q}_\perp{}^2 = -t\,. \tag{A.2.12}$$

A.3 DIS Kinematics

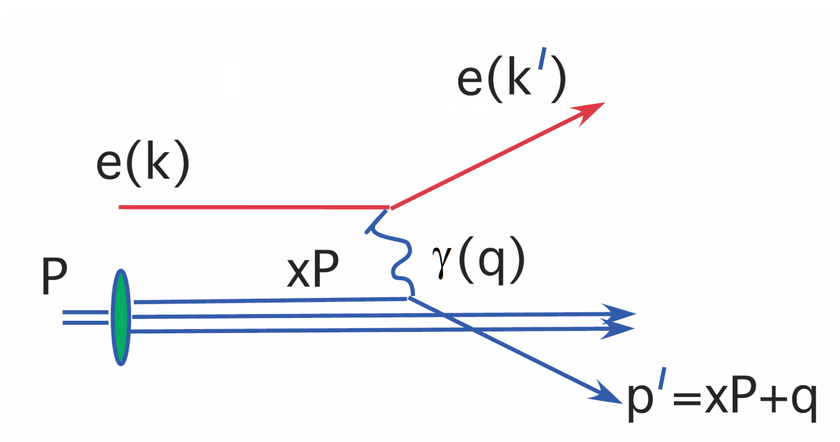

Figure A.1: Kinematics for DIS.

The momentum transfer is give by:

$$Q^2 = -(k - k')^2\,. \tag{A.3.1}$$

x is the fraction of the proton's momentum carried by the hadron. In the limit where the masses of the partons and the proton are negligible, we can derive

$$\begin{aligned} p'^2 &= (q + xp)^2 = 0 \\ \implies x &= \frac{Q^2}{2p \cdot q}\,. \end{aligned} \tag{A.3.2}$$

The mass of the hadronic final state is given by

$$W^2 = (p + q)^2 = \frac{Q^2}{x}(1 - x)\,. \tag{A.3.3}$$

Appendix B

Wave Equations

We outline the derivation of the wave equations that were used to find the energy levels in the supergravity theory. The discussion here is similar to that in [4], except we now work with the AdS_5 metric, (6.1.1), with $R = 1$ for simplicity, and a hard-wall cutoff.

The simplest equation is the scalar wave equation for the dilaton and the axion. For the transverse traceless metric fluctuations, one can simply work with the linearized Einstein equation. Both of these can be found in [4]. Let us focus here on the case of the two-form fields, $B_{\mu\nu}$ and $C_{\mu\nu}$, which at the linear level are conveniently combined into a single complex field, $\tilde{B}_{\mu\nu} = B_{\mu\nu} + iC_{\mu\nu}$. (We drop the subscript 2 of $C_{2,\mu\nu}$ in what follows to simplify the writing.) Let us introduce a Maxwell operator for two-forms

$$(\Box_{Maxwell}\, \tilde{B})_{\alpha\beta} = \frac{3}{\sqrt{-g}} g_{\alpha\mu} g_{\beta\nu} \partial_\lambda (\sqrt{-g} g^{\lambda\lambda'} g^{\mu\mu'} g^{\nu\nu'} \partial_{[\lambda'} \tilde{B}_{\mu'\nu']}) \,, \tag{B.0.1}$$

or, equivalently,

$$(\Box_{Maxwell}\ \tilde{B})_{\alpha\beta} \quad = \quad g_{\alpha\mu}g_{\beta\nu}(g^{\mu\mu'}g^{\nu\nu'}\tilde{H}_{\mu'\nu'\lambda})^{;\lambda}\ , \tag{B.0.2}$$

where

$$\tilde{H}_{\mu\nu\lambda} = \partial_\mu \tilde{B}_{\nu\lambda} + \partial_\nu \tilde{B}_{\lambda\mu} + \partial_\lambda \tilde{B}_{\mu\nu}\ , \tag{B.0.3}$$

is the associated field strength. For ease of writing, we adopt the standard shorthand: $\Box_{Maxwell}\ \tilde{B}_{\alpha\beta}$ for $(\Box_{Maxwell}\ \tilde{B})_{\alpha\beta}$.

It was shown in [60] that this field satisfies the equation

$$(\Box_{Maxwell} - k(k+4))\tilde{B}_{\mu\nu} + 2i\epsilon_{\mu\nu}{}^{\rho\lambda\sigma}\partial_\rho \tilde{B}_{\lambda\sigma} = 0\ , \tag{B.0.4}$$

for $k = 0, 1, \cdots$ harmonics on S^5. Since the second order differential operator factorizes into two first order operators, solutions fall into two classes,

$$\begin{aligned} i(*D\tilde{B}^{(1)})_{\mu\nu} \quad &= \quad 2(k+4)\tilde{B}^{(1)}_{\mu\nu}, \\ -i(*D\tilde{B}^{(2)})_{\mu\nu} \quad &= \quad 2k\tilde{B}^{(2)}_{\mu\nu}\ , \end{aligned} \tag{B.0.5}$$

where $(*D\tilde{B})_{\mu\nu} = \epsilon_{\mu\nu}{}^{\rho\lambda\sigma}\partial_\rho \tilde{B}_{\lambda\sigma}$ and I is the identity matrix. It is convenient to iterate these first order equations to get the second order equations,

$$\begin{aligned} (\Box_{Maxwell} - (k+4)^2)\tilde{B}^{(1)}_{\mu\nu} \quad &= \quad 0\ , \\ (\Box_{Maxwell} - k^2)\tilde{B}^{(2)}_{\mu\nu} \quad &= \quad 0\ . \end{aligned} \tag{B.0.6}$$

B.1 Counting Modes

To count the number of independent fluctuations for a supergravity field, we imagine harmonic plane waves propagating in the AdS radial direction, r, with Euclidean time, x_4. For example, the metric fluctuations in AdS_5

$$G_{\mu\nu} = \bar{G}_{\mu\nu} + h_{\mu\nu}(x) \tag{B.1.1}$$

in the fixed background $\bar{G}_{\mu\nu}$ are taken to be of the form $h_{\mu\nu}(r, x_4)$. There is no dependence on the other spatial coordinates, $\vec{x} = (x_1, x_2, x_3)$.

Metric Fluctuations

A graviton has two polarization indices. If we were in flat space-time, we could go to a gauge where these indices took on values among (x_1, x_2, x_3) and not from the set (x_4, r). The polarization tensor should also be traceless. This leaves $(3 \times 4)/2 - 1 = 5$ independent components. In the AdS space-time, we can count the number of graviton modes the same way, though the actual modes that we construct will have this form of polarization only at $r \to \infty$; for finite r, other components of polarization will be constrained to acquire nonzero values [61, 4]. Therefore, a set of *five independent* polarizations can be characterized by the following non-vanishing components at $r \to \infty$,

$$h_{ij} : \quad h_{ij} = h_{ji} \ , \quad \text{and} \quad Tr\ h = 0 \ , \quad i = 1, 2, 3 \ . \tag{B.1.2}$$

These five states form a spin-2 representation under $SO(3)$ as indicated in Table 7.2. Let us consider perturbations of the following form:

$$h_{ij}(r, x_4) = h_{ij}\ t(r)\ e^{-mx_4} \tag{B.1.3}$$

where $i, j = 1, 2, 3$, with h_{ij} an arbitrary constant traceless-symmetric 3×3 tensor. From linearized Einstein's equations about the AdS_5 background, one finds

$$[-r\frac{d}{dr}r\frac{d}{dr} + 4]t(r) = \frac{m^2}{r^2}t(r)\ . \tag{B.1.4}$$

leading to Eq. (7.4.7).

Scalar Fields

There are fluctuations for the dilaton ϕ and the axion C_0. These can be combined to form a complex field $\tilde{\Phi} = e^{-\bar{\phi}-\phi} + iC_0 \simeq e^{-\bar{\phi}}(1-\phi) + iC_0$. There is also a scalar G_α^α associated with the volume fluctuations in S^5, (with $m^2_{AdS} = 32$). However, we will not consider this mode here.

Let us consider perturbations of the following form:

$$\begin{aligned} \phi(r, x_4) &= S_1(r)\ e^{ik_4 x_4} \\ C(r, x_4) &= S_2(r)\ e^{ik_4 x_4}\ . \end{aligned} \tag{B.1.5}$$

and re-write $k_4 = im$. From the scalar Laplacian, one finds, for $i = 1, 2$,

$$-\frac{d}{dr}r^5\frac{d}{dr}S_i(r) = m^2\ r\ S_i(r), \tag{B.1.6}$$

leading to Eq. (7.4.11).

Kalb-Ramond Two-Form Fields

As explained earlier, the field equation for $\tilde{B}$ can be factorized into two first order equations, and each can be iterated leading to a second order equation of the form

$$\Box_{Maxwell}\, \tilde{B}_{\mu\nu} + m^2_{AdS,i} \tilde{B}_{\mu\nu} = 0\ . \tag{B.1.7}$$

where $m^2_{AdS,1} = (k+4)^2$ and $m^2_{AdS,2} = k^2$, $k = 0, 1, \cdots$. For the purpose of counting modes, polarizations for massless 2-form in AdS_5 can also be restricted to be transverse, with fields depending only on (x_4, r). Therefore, the polarization tensor is an antisymmetric 2-tensor in the direction x_1, x_2, x_3, leading to 3 independent components. On the other hand, since we in general need to work with massive 2-form, longitudinal modes are allowed and it would appear that the polarization tensor is an antisymmetric tensor in coordinates x_1, x_2, x_3, r, with 6 independent components. This assertion turns out not to be the case, and, the number of independent (complex) components for our massive 2-form, $\tilde{B}_{\mu\nu}$ is also 3, as if we are dealing with a massless case. This less than intuitive fact follows from the first order relation, relating real and imaginary parts and leading to further constraints.

One must check that solutions to the second order equation for $\tilde{B}_{\mu\nu}$, actually are valid solutions to the original wave equation. For example, consider the ansatz

$$B_{12} = -B_{21} = b_{12} Q_1(r) r^2 e^{ik_4 x_4} \quad \text{and} \quad C_{12} = -C_{21} = 0\ . \tag{B.1.8}$$

Once we have a solution for B_{12}, the first order equations will determine $C_{34} = -C_{43} \neq 0$ and $C_{r3} = -C_{3r} \neq 0$, while allowing all other components of B and C to be zero. This does not place any constraints on B_{12} itself. From Eq. (B.0.6), Q_1 now satisfies Eq. (7.4.11). A similar ansatz

$$C_{12} = -C_{21} = c_{12} Q_2(r) r^2 e^{ik_4 x_4} \quad \text{and} \quad B_{12} = -B_{21} = 0 \; . \tag{B.1.9}$$

would lead to Eq. (7.4.11) for Q_2, and $B_{34} = -B_{43} \neq 0$ and $B_{r3} = -B_{3r} \neq 0$, while allowing all other components of B and C to be zero.

From these examples, one finds that the number of independent complex tensor fields, $\tilde{B}_{\mu\nu}$, is reduced from 6 to 3. Independent components can be chosen at $r \to \infty$,

$$\begin{aligned} B_{ij} \quad &: \quad B_{ij} = -B_{ji} \; , \quad i,j = 1,2,3, \\ C_{ij} \quad &: \quad C_{ij} = -C_{ji} \; , \quad i,j = 1,2,3, \end{aligned} \tag{B.1.10}$$

each corresponds to spin-1 under $SO(3)$, as indicated in Table 7.2.

There still remain two cases to consider, (1) $m^2_{AdS} = (4+k)^2$, and $m^2_{AdS} = k^2$. Since we do not consider fluctuations in S^5, we can restrict to $k = 0$, i.e., we can restrict to $m^2_{AdS,1} = 16$ and $m^2_{AdS,2} = 0$. As pointed in [4], the case of $m^2_{AdS,2} = 0$ can be gauged away. Therefore, the state with $j = 1$ associated with this mode decouples. However, at finite but large λ, Regge recurrences will be developed. As one moves away from $j = 1$, Regge trajectory associated with this mode should survive [1].

Dimension	State J^{PC}	Operator	Supergravity
$\Delta = 4$	0^{++}	$Tr(FF) = \vec{E}^a \cdot \vec{E}^a - \vec{B}^a \cdot \vec{B}^a$	ϕ
$\Delta = 4$	2^{++}	$T_{ij} = E^a_i \cdot E^a_j + B^a_i \cdot B^a_j - \text{trace}$	G_{ij}
$\Delta = 4$	0^{-+}	$Tr(F\tilde{F}) = \vec{E}^a \cdot \vec{B}^a$	C_0
$\Delta = 6$	1^{+-}	$Tr(F_{\mu\nu}\{F_{\rho\sigma}, F_{\lambda\eta}\}) \sim d^{abc}F^aF^bF^c$	B_{ij}
$\Delta = 6$	1^{--}	$Tr(\tilde{F}_{\mu\nu}\{F_{\rho\sigma}, F_{\lambda\eta}\}) \sim d^{abc}\tilde{F}^aF^bF^c$	$C_{2,ij}$

Table B.1: Gauge invariant local gluonic operators for QCD_4 with $\Delta \leq 6$, and their supergravity duals.

B.2 Low Dimensional Gauge Invariant Operators

We note that the basic idea behind the AdS/CFT correspondence in the context of glueballs is similar to an observation made much earlier by Fritzsch and Minkowski [109], by Bjorken [110] and by Jaffe, Johnson and Ryzak [111]. Namely that the low mass glueball spectrum can be qualitatively understood in terms of local gluon interpolating operators of minimal dimension. For example, Ref. [111] lists all gauge invariant operators for dimension $\Delta = 4, 5$ and 6. Eliminating operators that are zero by the classical equation of motion and states that decouple because of the conservation of the energy momentum tensor, the operators are in rough correspondence with all the low mass glueballs states, as computed in a constituent gluon [112, 113] or bag model. Indeed more recently Kuti [114] has pointed out that a more careful use of the spherical cavity approximation even gives a rather good quantitative match to the lowest 11 states in the lattice spectrum. Consequently it is interesting to compare this set of operators with the supergravity model.

We list in table B.1 all the operators for $\Delta \leq 6$, based on our cutoff AdS_5, except the

[1] A related issue in flat-space was first discussed in the original work by Kalb and Ramond, [107] and also in [108]. By invoking coupling to open strings, this would be spin-1 state acquires a mass through a Higgs-like mechanism.

operators with explicit derivatives, e.g., $Tr[FDF]$ and $Tr[FDDF]$. In this table we have used a Minkowski metric. The column on the right lists the supergravity mode that couples to each operator. It is comforting to point out that our solutions for Kalb-Ramond modes, B and C_2, at $m^2_{AdS} = 16$, precisely lead to $\Delta = 6$ at $j = 1$.

Appendix C

Simplification of Scattering Amplitudes in the Regge Limit of Flat Space String Theory

We show explicit calculations for some string scattering amplitudes, omitting the overall normalization constants. We would like to show that, in the Regge limit, six particle amplitudes factorize into products of two four particle amplitudes, that include a Pomeron or Odderon vertex operator. This provides the physical picture of scattering happening via Pomeron or Odderon exchange. Instead of using the expressions for these vertex operators we found in chapters 6 and 7 directly, we instead explicitly show how these vertex operators can be extracted. That is why this section might seem more complex than necessary, but in fact looking at the final result we see that using the said vertex operators has the computational advantage of requiring one less integral to be performed.

C.0.1 4 tachyons

$$z_1 \to 0, \quad z_2 \to z, \quad z_3 \to 1, \quad z_4 \to \infty$$

$$A_4 = \int d^2z \left\langle e^{ik_1X(0)} e^{ik_2X(z,\bar{z})} e^{ik_3X(1)} e^{ik_4X(\infty)} \right\rangle$$

$$= \int d^2z \, |z|^{\alpha' k_1 k_2} \left\langle 0, k_1 \left| \exp(-k_2 \sum \frac{1}{m} \alpha_m z^{-m} - c.c) \exp(k_2 \sum \frac{1}{m} \alpha_{-m} z^m + c.c) \right.\right.$$

$$\left.\left. \exp(-k_3 \sum \frac{1}{n} \alpha_n - c.c) \exp(k_3 \sum \frac{1}{n} \alpha_{-n} + c.c) \right| 0, k_4 \right\rangle$$

$$= \int d^2z \, |z|^{\alpha' k_1 k_2} \, |1-z|^{\alpha' k_2 k_3} \tag{C.0.1}$$

C.0.2 3 tachyons + 1 massless tensor

First let us calculate

$$\langle V_T V_T V_T V_G \rangle$$

$$A_4 = \int d^2z \left\langle e^{ik_1X(0)} e^{ik_2X(z,\bar{z})} e^{ik_3X(1)} : g_{\mu\nu} \partial X^\mu \bar{\partial} X^\nu e^{ik_4X(\infty)} : \right\rangle$$

$$= \int d^2z \, |z|^{\alpha' k_1 k_2} \left\langle 0, k_1 \left| \exp(k_2 \sum \frac{1}{m} \alpha_{-m} z^m + c.c) \exp(-k_3 \sum \frac{1}{n} \alpha_n - c.c) \right.\right.$$

$$\left.\left. \exp(k_3 \sum \frac{1}{n} \alpha_{-n} + c.c) g_{\mu\nu} \alpha_1^\mu \tilde{\alpha}_1^\nu \right| 0, k4 \right\rangle$$

$$= \int d^2z \, |z|^{\alpha' k_1 k_2} \, |1-z|^{\alpha' k_2 k_3} \left\langle \exp(k_2 \sum \frac{1}{m} \alpha_{-m} z^m + c.c) \exp(k_3 \sum \frac{1}{n} \alpha_{-n} + c.c) g_{\mu\nu} \alpha_1^\mu \tilde{\alpha}_1^\nu \right\rangle$$

$$= \int d^2z \, |z|^{\alpha' k_1 k_2} \, |1-z|^{\alpha' k_2 k_3} \, g_{\mu\nu} \left\langle (1 + k_2 \alpha_{-1} z)(1 + k_3 \alpha_{-1}) \alpha_1^\mu \right\rangle \left\langle (1 + k_2 \tilde{\alpha}_{-1} \bar{z})(1 + k_3 \tilde{\alpha}_{-1}) \tilde{\alpha}_1^\nu \right\rangle$$

$$= \int d^2z \, |z|^{\alpha' k_1 k_2} \, |1-z|^{\alpha' k_2 k_3} \, g_{\mu\nu} (k_3^\mu + k_2^\mu z)(k_3^\nu + k_2^\nu \bar{z}) \tag{C.0.2}$$

Similarly if V_G is at first position

$$\langle V_G V_T V_T V_T \rangle = \int d^2z\, |z|^{\alpha' k_1 k_2}\, |1-z|^{\alpha' k_2 k_3}\, g_{\mu\nu}(k_3^\mu + k_2^\mu \frac{1}{z})(k_3^\nu + k_2^\nu \frac{1}{\bar{z}}).$$

Note that the results apply equally well if our massless tensor is Kalb-Ramond field instead of a graviton - $g_{\mu\nu}$ would just be replaced by the anti-symmetric $\varepsilon_{\mu\nu}$ in that case.

C.0.3 2 tachyons + 2 massless tensors

$$\langle V_G V_T V_T V_G \rangle$$

$$A_4 = \int d^2z\, |z|^{\alpha' k_1 k_2}\, |1-z|^{\alpha' k_2 k_3}$$

$$\Big\langle g_{1\mu\nu} \alpha_{-1}^\mu \tilde{\alpha}_{-1}^\nu \exp(k_2 \sum \frac{1}{m} \alpha_{-m} z^m + c.c) \exp(-k_2 \alpha_1 \frac{1}{z} - c.c.)$$

$$\exp(-k_3 \sum \frac{1}{n} \alpha_n - c.c) \exp(k_3 \alpha_{-1} + c.c.) g_{4\rho\sigma} \alpha_1^\rho \tilde{\alpha}_1^\sigma \Big\rangle$$

$$= \int d^2z\, |z|^{\alpha' k_1 k_2}\, |1-z|^{\alpha' k_2 k_3}\, g_{1\mu\nu} g_{4\rho\sigma} \Big\langle \alpha_{-1}^\mu \tilde{\alpha}_{-1}^\nu \exp(-k_3 \alpha_1 - c.c.) \exp(-k_2 \alpha_1 \frac{1}{z} - c.c.)$$

$$\exp(k_2 \alpha_{-1} z + c.c.) \exp(k_3 \alpha_{-1} + c.c.) \alpha_1^\rho \tilde{\alpha}_1^\sigma \rangle$$

$$= \int d^2z\, |z|^{\alpha' k_1 k_2}\, |1-z|^{\alpha' k_2 k_3}\, g_{1\mu\nu} g_{4\rho\sigma} \Big\langle \alpha_{-1}^\mu (1 - k_3 \alpha_1)(1 - k_2 \alpha_1 \frac{1}{z})(1 + k_2 \alpha_{-1} z)(1 + k_3 \alpha_{-1}) \alpha_1^\rho \Big\rangle$$

$$\Big\langle \tilde{\alpha}_{-1}^\nu (1 - k_3 \tilde{\alpha}_1)(1 - k_2 \tilde{\alpha}_1 \frac{1}{\bar{z}})(1 + k_2 \tilde{\alpha}_{-1} \bar{z})(1 + k_3 \tilde{\alpha}_{-1}) \tilde{\alpha}_1^\sigma \Big\rangle$$

$$= \int d^2z\, |z|^{\alpha' k_1 k_2}\, |1-z|^{\alpha' k_2 k_3}\, g_{1\mu\nu} g_{4\rho\sigma} \Big\langle (\alpha_{-1}^\mu - k_3^\mu - k_2^\mu \frac{1}{z})(\alpha_1^\rho + k_3^\rho + k_2^\rho z) \Big\rangle$$

$$\Big\langle \tilde{\alpha}_{-1}^\nu - k_3^\nu - k_2^\nu \frac{1}{\bar{z}})(\tilde{\alpha}_1^\sigma + k_3^\sigma + k_2^\sigma \bar{z}) \Big\rangle$$

$$= \int d^2z\, |z|^{\alpha' k_1 k_2}\, |1-z|^{\alpha' k_2 k_3}\, g_{1\mu\nu} g_{4\rho\sigma} [\eta^{\mu\rho} - (k_3^\mu + k_2^\mu \frac{1}{z})(k_3^\rho + k_2^\rho z)][\eta^{\nu\sigma} - (k_3^\nu + k_2^\nu \frac{1}{\bar{z}})(k_3^\sigma + k_2^\sigma \bar{z})].$$

Similarly for $\langle V_B V_T V_T V_B \rangle$

$$\int d^2z\, |z|^{\alpha' k_1 k_2}\, |1-z|^{\alpha' k_2 k_3}\, \varepsilon_{1\mu\nu} \varepsilon_{4\rho\sigma} [\eta^{\mu\rho} - (k_3^\mu + k_2^\mu \frac{1}{z})(k_3^\rho + k_2^\rho z)][\eta^{\nu\sigma} - (k_3^\nu + k_2^\nu \frac{1}{\bar{z}})(k_3^\sigma + k_2^\sigma \bar{z})].$$

C.0.4 2 tachyons +1 graviton + 1 Kalb-Ramond

This amplitude should be zero, due to charge conservation. Let us check if that is indeed the case.

By the previous method

$$\int d^2z\, |z|^{\alpha' k_1 k_2}\, |1-z|^{\alpha' k_2 k_3}\, \varepsilon_{1\mu\nu} g_{4\rho\sigma} [\eta^{\mu\rho} - (k_3^\mu + k_2^\mu \frac{1}{z})(k_3^\rho + k_2^\rho z)][\eta^{\nu\sigma} - (k_3^\nu + k_2^\nu \frac{1}{\bar{z}})(k_3^\sigma + k_2^\sigma \bar{z})].$$

The term involving

$$\varepsilon_{1\mu\nu} g_{4\rho\sigma} \eta^{\mu\rho} \eta^{\nu\sigma} = \varepsilon_1 \cdot g_4 = 0$$

since it is a product of an anti-symmetric with a symmetric tensor.

Hence we are left with

$$\int d^2z\, |z|^{\alpha' k_1 k_2}\, |1-z|^{\alpha' k_2 k_3}\, \varepsilon_{1\mu\nu} g_{4\rho\sigma} [-\eta^{\mu\rho} (k_3^\nu + k_2^\nu \frac{1}{\bar{z}})(k_3^\sigma + k_2^\sigma \bar{z}) - \eta^{\nu\sigma} (k_3^\mu + k_2^\mu \frac{1}{z})(k_3^\rho + k_2^\rho z) +$$

$$+ (k_3^\mu + k_2^\mu \frac{1}{z})(k_3^\rho + k_2^\rho z)(k_3^\nu + k_2^\nu \frac{1}{\bar{z}})(k_3^\sigma + k_2^\sigma \bar{z})].$$

Let us look at the last term. If we transform

$$\mu \to \nu, \quad \rho \to \sigma, \qquad z \to \bar{z}$$

we have

$$\int d^2z\, |z|^{\alpha' k_1 k_2}\, |1-z|^{\alpha' k_2 k_3}\, \varepsilon_{1\mu\nu} g_{4\rho\sigma} (k_3^\mu + k_2^\mu \frac{1}{z})(k_3^\rho + k_2^\rho z)(k_3^\nu + k_2^\nu \frac{1}{\bar{z}})(k_3^\sigma + k_2^\sigma \bar{z})$$

$$= - \int d^2z\, |z|^{\alpha' k_1 k_2}\, |1-z|^{\alpha' k_2 k_3}\, \varepsilon_{1\mu\nu} g_{4\rho\sigma} (k_3^\nu + k_2^\nu \frac{1}{\bar{z}})(k_3^\mu + k_2^\mu \frac{1}{z})(k_3^\sigma + k_2^\sigma \bar{z})(k_3^\rho + k_2^\rho z)$$

$$= 0.$$

The minus sign comes because

$$\varepsilon_{1\mu\nu} \to \varepsilon_{1\nu\mu} = -\varepsilon_{1\mu\nu}.$$

Now let's look at the two remaining terms. In the second term we will again transform

$$\mu \to \nu, \quad \rho \to \sigma, \qquad z \to \bar{z}$$

to get

$$\int d^2z\, |z|^{\alpha' k_1 k_2}\, |1-z|^{\alpha' k_2 k_3}\, \varepsilon_{1\mu\nu} g_{4\rho\sigma} \eta^{\nu\sigma} (k_3^\mu + k_2^\mu \frac{1}{z})(k_3^\rho + k_2^\rho z)$$

$$= - \int d^2z\, |z|^{\alpha' k_1 k_2}\, |1-z|^{\alpha' k_2 k_3}\, \varepsilon_{1\mu\nu} g_{4\rho\sigma} \eta^{\mu\rho} (k_3^\nu + k_2^\nu \frac{1}{\bar{z}})(k_3^\sigma + k_2^\sigma \bar{z})$$

which is the negative of the first term. Hence their sum will give zero.

Therefore

$$\langle V_B V_T V_T V_G \rangle = 0.$$

This concludes the summary of the 4-particle amplitudes that are interesting for our discussion. All these amplitudes should be exact (at tree level), we did not use the high energy limit yet.

C.1 6-particle amplitudes

In this section we will calculate the amplitudes for a few interesting 6-particle cases. Here the final answer will still be exact but we will write it in a form that will make it convenient to extract the Regge limit.

C.1.1 6-tachyons

The result of 4-particles can be quickly generalized to 6 particles. Taking

$$z_1 \to 0, \quad z_5 \to 1, \quad z_6 \to \infty$$

we get

$$\begin{aligned} A_6 = & \int d^2z_2 d^2z_3 d^2z_4 \, |z_2|^{\alpha' k_1 k_2} |z_3|^{\alpha' k_1 k_3} |z_4|^{\alpha' k_1 k_4} \\ & \Big\langle \exp(k_2 \sum \frac{1}{m}\alpha_{-m} z_2^m + c.c) \exp(-k_3 \sum \frac{1}{n}\alpha_n z_3^{-n} - c.c) \exp(k_3 \sum \frac{1}{m}\alpha_{-m} z_3^m + c.c) \\ & \exp(-k_4 \sum \frac{1}{n}\alpha_n z_4^{-n} - c.c) \exp(k_4 \sum \frac{1}{m}\alpha_{-m} z_4^m + c.c) \exp(-k_5 \sum \frac{1}{n}\alpha_n - c.c) \Big\rangle \\ = & \int d^2z_2 d^2z_3 d^2z_4 \, |z_2|^{\alpha' k_1 k_2} |z_3|^{\alpha' k_1 k_3} |z_4|^{\alpha' k_1 k_4} |z_2 - z_3|^{\alpha' k_2 k_3} |z_3 - z_4|^{\alpha' k_3 k_4} |z_2 - z_4|^{\alpha' k_2 k_4} \\ & |1 - z_4|^{\alpha' k_4 k_5} |1 - z_3|^{\alpha' k_3 k_5} |1 - z_2|^{\alpha' k_2 k_5} . \end{aligned} \tag{C.1.1}$$

This part will actually be the same even when we add particles with spin, it will just be multiplied by a tensorial term.

Let us now transform the result and rewrite it as:

$$A_6 = \int d^2z_4 \, |1-z_4|^{\alpha' k_4 k_5} \, |z_4|^{\alpha' k k_4} \int d^2z_3 \, |1-z_3|^{\alpha' k_2 k_3} \, |z_3|^{-\alpha' k k_3}$$

$$\int d^2w \, |w|^{-\alpha(t)-2} \, |1-w|^{\alpha' k_2 k_5} \left|1-\frac{w}{z_4}\right|^{\alpha' k_2 k_4} \left|1-\frac{w}{z_4 z_3}\right|^{\alpha' k_3 k_4} \left|1-\frac{w}{z_3}\right|^{\alpha' k_3 k_5}. \qquad \text{(C.1.2)}$$

To get to this form, important things to note are:

- convention used is all incoming momenta;
- $k^2 = -m^2$;
- $k^\mu = k_1^\mu + k_2^\mu + k_3^\mu$;
- to derive this result we had to transform

  $$z_3 \to w_3 = \frac{1}{z_3}$$

  followed by

  $$w_3 \to z_3' = z_3 w_3$$

  and then rewrite z_2 as w. Therefore the relationship between the $z_3$that appears in equation (C.1.1) and in equation (C.1.2) is

  $$z_3 \to \frac{w}{z_3}. \qquad \text{(C.1.3)}$$

This will be important later.

- $\alpha(t) = 2 - \frac{\alpha' k^2}{2}$;
- for tachyon $\alpha' k^2 = 4$;

C.1.2 5 tachyon + 1 massless tensor

We will take the massless particle at position 6:

$$\langle V_T V_T V_T V_T V_T V_G \rangle \,.$$

$$A_6 = \int d^2 z_2 d^2 z_3 d^2 z_4 \, |z_2|^{\alpha' k_1 k_2} \, |z_3|^{\alpha' k_1 k_3} \, |z_4|^{\alpha' k_1 k_4} \, |z_2 - z_3|^{\alpha' k_2 k_3} \, |z_3 - z_4|^{\alpha' k_3 k_4} \, |z_2 - z_4|^{\alpha' k_2 k_4}$$

$$|1 - z_4|^{\alpha' k_4 k_5} \, |1 - z_3|^{\alpha' k_3 k_5} \, |1 - z_2|^{\alpha' k_2 k_5} \, g_{6\mu\nu}$$

$$\Big\langle \exp(k_2 \sum \frac{1}{m} \alpha_{-m} z_2^m + c.c) \exp(k_3 \sum \frac{1}{m} \alpha_{-m} z_3^m + c.c)$$

$$\exp(k_4 \sum \frac{1}{m} \alpha_{-m} z_4^m + c.c) \exp(k_5 \alpha_{-1} + c.c) \alpha_1^\mu \tilde{\alpha}_1^\nu \Big\rangle$$

$$= \int d^2 z_2 d^2 z_3 d^2 z_4 \, |z_2|^{\alpha' k_1 k_2} \, |z_3|^{\alpha' k_1 k_3} \, |z_4|^{\alpha' k_1 k_4} \, |z_2 - z_3|^{\alpha' k_2 k_3} \, |z_3 - z_4|^{\alpha' k_3 k_4} \, |z_2 - z_4|^{\alpha' k_2 k_4}$$

$$|1 - z_4|^{\alpha' k_4 k_5} \, |1 - z_3|^{\alpha' k_3 k_5} \, |1 - z_2|^{\alpha' k_2 k_5} \, g_{6\mu\nu}$$

$$\langle (1 + k_2 \alpha_{-1} z_2)(1 + k_3 \alpha_{-1} z_3)(1 + k_4 \alpha_{-1} z_4)(1 + k_5 \alpha_{-1}) \alpha_1^\mu \rangle$$

$$\langle (1 + k_2 \tilde{\alpha}_{-1} \bar{z}_2)(1 + k_3 \tilde{\alpha}_{-1} \bar{z}_3)(1 + k_4 \tilde{\alpha}_{-1} \bar{z}_4)(1 + k_5 \tilde{\alpha}_{-1}) \tilde{\alpha}_1^\nu \rangle$$

$$= \int d^2 z_2 d^2 z_3 d^2 z_4 \, |z_2|^{\alpha' k_1 k_2} \, |z_3|^{\alpha' k_1 k_3} \, |z_4|^{\alpha' k_1 k_4} \, |z_2 - z_3|^{\alpha' k_2 k_3} \, |z_3 - z_4|^{\alpha' k_3 k_4} \, |z_2 - z_4|^{\alpha' k_2 k_4}$$

$$|1 - z_4|^{\alpha' k_4 k_5} \, |1 - z_3|^{\alpha' k_3 k_5} \, |1 - z_2|^{\alpha' k_2 k_5}$$

$$g_{6\mu\nu}(k_5^\mu + k_4^\mu z_4 + k_3^\mu z_3 + k_2^\mu z_2)(k_5^\nu + k_4^\nu \bar{z}_4 + k_3^\nu \bar{z}_3 + k_2^\nu \bar{z}_2).$$

Similarly to the 6 tachyon case this can be rewritten

$$A_6 = \int d^2 z_4 \left|1 - z_4\right|^{\alpha' k_4 k_5} \left|z_4\right|^{\alpha' k k_4} \int d^2 z_3 \left|1 - z_3\right|^{\alpha' k_2 k_3} \left|z_3\right|^{-\alpha' k k_3}$$

$$\int d^2 w \left|w\right|^{-\alpha(t)-2} \left|1 - w\right|^{\alpha' k_2 k_5} \left|1 - \frac{w}{z_4}\right|^{\alpha' k_2 k_4} \left|1 - \frac{w}{z_4 z_3}\right|^{\alpha' k_3 k_4} \left|1 - \frac{w}{z_3}\right|^{\alpha' k_3 k_5}$$

$$g_{6\mu\nu}(k_5^\mu + k_4^\mu z_4 + k_3^\mu \frac{w}{z_3} + k_2^\mu w)(k_5^\nu + k_4^\nu \bar{z}_4 + k_3^\nu \frac{\bar{w}}{\bar{z}_3} + k_2^\nu \bar{w}),$$

where we have used the transformation (C.1.3). This result is the same for Kalb-Ramond if we replace $g_{6\mu\nu}$ by $\varepsilon_{6\mu\nu}$.

C.1.3 4-tachyons + 2 massless tensors

Similarly to the last part we get

$$A_6 = \int d^2 z_2 d^2 z_3 d^2 z_4 \left|z_2\right|^{\alpha' k_1 k_2} \left|z_3\right|^{\alpha' k_1 k_3} \left|z_4\right|^{\alpha' k_1 k_4} \left|z_2 - z_3\right|^{\alpha' k_2 k_3} \left|z_3 - z_4\right|^{\alpha' k_3 k_4} \left|z_2 - z_4\right|^{\alpha' k_2 k_4}$$

$$\left|1 - z_4\right|^{\alpha' k_4 k_5} \left|1 - z_3\right|^{\alpha' k_3 k_5} \left|1 - z_2\right|^{\alpha' k_2 k_5} g_{1\alpha\beta} g_{6\mu\nu}$$

$$\Big\langle \alpha_{-1}^\alpha (1 - k_5 \alpha_1)(1 - k_4 \alpha_1 \frac{1}{z_4})(1 - k_3 \alpha_1 \frac{1}{z_3})(1 - k_2 \alpha_1 \frac{1}{z_2})$$

$$(1 + k_2 \alpha_{-1} z_2)(1 + k_3 \alpha_{-1} z_3)(1 + k_4 \alpha_{-1} z_4)(1 + k_5 \alpha_{-1}) \alpha_1^\mu \rangle$$

$$\Big\langle \tilde{\alpha}_{-1}^\beta (1 - k_5 \tilde{\alpha}_1)(1 - k_4 \tilde{\alpha}_1 \frac{1}{\bar{z}_4})(1 - k_3 \tilde{\alpha}_1 \frac{1}{\bar{z}_3})(1 - k_2 \tilde{\alpha}_1 \frac{1}{\bar{z}_2})$$

$$(1 + k_2 \tilde{\alpha}_{-1} \bar{z}_2)(1 + k_3 \tilde{\alpha}_{-1} \bar{z}_3)(1 + k_4 \tilde{\alpha}_{-1} \bar{z}_4)(1 + k_5 \tilde{\alpha}_{-1}) \tilde{\alpha}_1^\nu \rangle$$

$$= \int d^2z_2 d^2z_3 d^2z_4 \, |z_2|^{\alpha' k_1 k_2} \, |z_3|^{\alpha' k_1 k_3} \, |z_4|^{\alpha' k_1 k_4} \, |z_2 - z_3|^{\alpha' k_2 k_3} \, |z_3 - z_4|^{\alpha' k_3 k_4} \, |z_2 - z_4|^{\alpha' k_2 k_4}$$

$$|1 - z_4|^{\alpha' k_4 k_5} \, |1 - z_3|^{\alpha' k_3 k_5} \, |1 - z_2|^{\alpha' k_2 k_5} \, g_{1\alpha\beta} g_{6\mu\nu}$$

$$\left\langle (\alpha^\alpha_{-1} - k^\alpha_5 - k^\alpha_4 \frac{1}{z_4} - k^\alpha_3 \frac{1}{z_3} - k^\alpha_2 \frac{1}{z_2})(\alpha^\mu_1 + k^\mu_5 + k^\mu_2 z_2 + k^\mu_3 z_3 + k^\mu_4 z_4) \right\rangle$$

$$\left\langle (\tilde{\alpha}^\beta_{-1} - k^\beta_5 - k^\beta_4 \frac{1}{\bar{z}_4} - k^\beta_3 \frac{1}{\bar{z}_3} - k^\beta_2 \frac{1}{\bar{z}_2})(\tilde{\alpha}^\nu_1 + k^\nu_5 + k^\nu_2 \bar{z}_2 + k^\nu_3 \bar{z}_3 + k^\nu_4 \bar{z}_4) \right\rangle$$

$$= \int d^2z_2 d^2z_3 d^2z_4 \, |z_2|^{\alpha' k_1 k_2} \, |z_3|^{\alpha' k_1 k_3} \, |z_4|^{\alpha' k_1 k_4} \, |z_2 - z_3|^{\alpha' k_2 k_3} \, |z_3 - z_4|^{\alpha' k_3 k_4} \, |z_2 - z_4|^{\alpha' k_2 k_4}$$

$$|1 - z_4|^{\alpha' k_4 k_5} \, |1 - z_3|^{\alpha' k_3 k_5} \, |1 - z_2|^{\alpha' k_2 k_5} \, g_{1\alpha\beta} g_{6\mu\nu}$$

$$[\eta^{\alpha\mu} - (k^\alpha_5 + k^\alpha_4 \frac{1}{z_4} + k^\alpha_3 \frac{1}{z_3} + k^\alpha_2 \frac{1}{z_2})(k^\mu_5 + k^\mu_2 z_2 + k^\mu_3 z_3 + k^\mu_4 z_4)]$$

$$[\eta^{\beta\nu} - (k^\beta_5 + k^\beta_4 \frac{1}{\bar{z}_4} + k^\beta_3 \frac{1}{\bar{z}_3} + k^\beta_2 \frac{1}{\bar{z}_2})(k^\nu_5 + k^\nu_2 \bar{z}_2 + k^\nu_3 \bar{z}_3 + k^\nu_4 \bar{z}_4)]. \tag{C.1.4}$$

This can be rewritten as

$$A_6 = \int d^2z_4 \, |1 - z_4|^{\alpha' k_4 k_5} \, |z_4|^{\alpha' k k_4} \int d^2z_3 \, |1 - z_3|^{\alpha' k_2 k_3} \, |z_3|^{-\alpha' k k_3}$$

$$\int d^2w \, |w|^{-\alpha(t)} \, |1 - w|^{\alpha' k_2 k_5} \left|1 - \frac{w}{z_4}\right|^{\alpha' k_2 k_4} \left|1 - \frac{w}{z_4 z_3}\right|^{\alpha' k_3 k_4} \left|1 - \frac{w}{z_3}\right|^{\alpha' k_3 k_5}$$

$$g_{1\alpha\beta} g_{6\mu\nu} [\eta^{\alpha\mu} - (k^\alpha_5 + k^\alpha_4 \frac{1}{z_4} + k^\alpha_3 \frac{z_3}{w} + k^\alpha_2 \frac{1}{w})(k^\mu_5 + k^\mu_2 w + k^\mu_3 \frac{w}{z_3} + k^\mu_4 z_4)]$$

$$[\eta^{\beta\nu} - (k^\beta_5 + k^\beta_4 \frac{1}{\bar{z}_4} + k^\beta_3 \frac{\bar{z}_3}{\bar{w}_3} + k^\beta_2 \frac{1}{\bar{w}_2})(k^\nu_5 + k^\nu_2 \bar{w}_2 + k^\nu_3 \frac{\bar{w}_3}{\bar{z}_3} + k^\nu_4 \bar{z}_4)]. \tag{C.1.5}$$

The important thing to notice in this result is that the power of $|w|$ is $-\alpha(t)$ instead of the usual $-\alpha(t) - 2$. This is because for a graviton $\alpha' k^2 = 0$.

It is clear that for Kalb-Ramond we just replace $g_{1\alpha\beta} g_{6\mu\nu}$ with $\varepsilon_{1\alpha\beta} \varepsilon_{6\mu\nu}$.

C.1.4 4 tachyon + 1 graviton + 1 Kalb-Ramond

Similarly to the case considered in C.0.4, this amplitude should be zero. Let us see if this is indeed the case.

Again starting from (C.1.4) we can multiply out the tensorial part into a sum of 4 terms.

The first term is

$$\varepsilon_1 \cdot g_6 = 0.$$

In the last term we switch

$$\alpha \to \beta \quad \mu \to \nu \quad z_2 \to \tilde{z}_2 \quad z_3 \to \tilde{z}_3 \quad z_4 \to \tilde{z}_4$$

to get

$$\varepsilon_{1\alpha\beta} g_{6\mu\nu}[\eta^{\alpha\mu} - (k_5^\alpha + k_4^\alpha \frac{1}{z_4} + k_3^\alpha \frac{1}{z_3} + k_2^\alpha \frac{1}{z_2})(k_5^\mu + k_2^\mu z_2 + k_3^\mu z_3 + k_4^\mu z_4)]$$

$$[\eta^{\beta\nu} - (k_5^\beta + k_4^\beta \frac{1}{\bar{z}_4} + k_3^\beta \frac{1}{\bar{z}_3} + k_2^\beta \frac{1}{\bar{z}_2})(k_5^\nu + k_2^\nu \bar{z}_2 + k_3^\nu \bar{z}_3 + k_4^\nu \bar{z}_4)]$$

$$= -\varepsilon_{1\alpha\beta} g_{6\mu\nu}[\eta^{\alpha\mu} - (k_5^\alpha + k_4^\alpha \frac{1}{z_4} + k_3^\alpha \frac{1}{z_3} + k_2^\alpha \frac{1}{z_2})(k_5^\mu + k_2^\mu z_2 + k_3^\mu z_3 + k_4^\mu z_4)]$$

$$[\eta^{\beta\nu} - (k_5^\beta + k_4^\beta \frac{1}{\bar{z}_4} + k_3^\beta \frac{1}{\bar{z}_3} + k_2^\beta \frac{1}{\bar{z}_2})(k_5^\nu + k_2^\nu \bar{z}_2 + k_3^\nu \bar{z}_3 + k_4^\nu \bar{z}_4)] = 0.$$

Similarly we can show that the remaining two terms sum to zero.

Hence if we have one Kalb-Ramond one graviton and 4 tachyons the amplitude is zero.

This concludes the cases we will look at in the Regge limit.

C.2 Single Regge limit

We look at scattering $1 + 6 \to 2 + 3 + 4 + 5$. In this section we finally look at the Regge limit. We will consider momenta k_1, k_2, k_3 to have a large $-$ component, of order $\sim \sqrt{s}$, and similarly for the $+$ component of momenta k_4, k_5, k_6. The $+$ component of k_1, k_2, k_3 and the $-$ component of k_4, k_5, k_5 will be of order $\sim 1/\sqrt{s}$. See Appendix A.2 to see how this comes about in the simpler case of 4 particle scattering.

C.2.1 6 tachyons

In the Regge limit small w will give the important contribution. Hence we can exponentiate

$$\int d^2w\, |w|^{-\alpha(t)-2}\, |1-w|^{\alpha' k_2 k_5} \left|1-\frac{w}{z_4}\right|^{\alpha' k_2 k_4} \left|1-\frac{w}{z_4 z_3}\right|^{\alpha' k_3 k_4} \left|1-\frac{w}{z_3}\right|^{\alpha' k_3 k_5}$$

$$= \int d^2w\, |w|^{-\alpha(t)-2} \exp[-w\alpha'(k_2k_5 + \frac{k_2k_4}{z_4} + \frac{k_3k_4}{z_3z_4} + \frac{k_3k_5}{z_3}) + c.c.]$$

$$= \int d^2w\, |w|^{-\alpha(t)-2} \exp[-w\alpha'(k_2 + \frac{k_3}{z_3}) \cdot (k_5 + \frac{k_4}{z_4}) - c.c.].$$

This can be integrated to give

$$A_6 = \int d^2z_4\, |1-z_4|^{\alpha' k_4 k_5}\, |z_4|^{\alpha' k k_4}\, \eta_{\mu\rho}\eta_{\nu\sigma}[(k_5^\rho + \frac{k_4^\rho}{z_4})(k_5^\sigma + \frac{k_4^\sigma}{\bar{z}_4})]^{\frac{\alpha(t)}{2}}$$

$$\int d^2z_3\, |1-z_3|^{\alpha' k_2 k_3}\, |z_3|^{-\alpha' k k_3}\, [(k_2^\mu + \frac{k_3^\mu}{z_3})(k_2^\nu + \frac{k_3^\nu}{\bar{z}_3})]^{\frac{\alpha(t)}{2}}.$$

This factorized into a product of an integral that depends just on z_3 and an integral that depends just on z_4. But the momenta in one of the integrals are contracted with the momenta in the other.

In the center of mass frame in light cone coordinates, one of the momenta has the + component $\sim \sqrt{s}$ and $-$ component $\sim \frac{1}{\sqrt{s}}$ and the opposite for the momenta on the other side. In the high energy limit $\sqrt{s} \to \infty$ and only the components $\sim \sqrt{s}$ are relevant.

In this limit the amplitude becomes

$$A_6 = \int d^2 z_4 \, |1 - z_4|^{\alpha' k_4 k_5} \, |z_4|^{\alpha' k k_4} \left| k_5 + \frac{k_4}{z_4} \right|_+^{\alpha(t)} \int d^2 z_3 \, |1 - z_3|^{\alpha' k_2 k_3} \, |z_3|^{-\alpha' k k_3} \left| k_2 + \frac{k_3}{z_3} \right|_-^{\alpha(t)} .$$

Here the amplitude is fully factorized.

Looking at the expression we can see that the integrals have the form of 3 tachyon + 1 graviton scattering amplitude eq. (C.0.2)

We want to interpret this result as happening via exchange of a Pomeron.

Hence we want to get the same result by computing the amplitudes

$$\langle V_T(k_1, 0) V_T(k_2, z_2) V_T(k_3, 1) V_{PL}(-k, \infty) \rangle \, \langle V_{PR}(k, 0) V_T(k_4, z_4) V_T(k_5, 1) V_T(k_6, \infty) \rangle \, .$$

But we also had to do a transformation eq (C.1.3). Therefore the first part should actually be

$$\langle V_{PL}(-k, 0) V_T(k_3, z_3) V_T(k_2, 1) V_T(k_1, \infty) \rangle \, .$$

Looking back at eq (C.0.2) we see that V_{PL} should have the form

$$V_{PL} = (\partial X^- \tilde{\partial} X^-)^{\frac{\alpha(t)}{2}} e^{-ikX}$$

and V_{PR} should have the form

$$V_{PR} = (\partial X^+ \tilde{\partial} X^+)^{\frac{\alpha(t)}{2}} e^{ikX}.$$

Let us calculate

$$\langle V_{PL}(-k,0) V_T(k_3,z_3) V_T(k_2,1) V_T(k_1,\infty) \rangle$$
$$= \int d^2 z_3 \, |z_3|^{-\alpha' k k_3} \left\langle (g_{\mu\nu} \alpha^\mu_{-1} \alpha^\nu_{-1})^{\frac{\alpha(t)}{2}} \exp(-k_3 \sum \frac{1}{m} \alpha_m z_3^m + c.c.) \exp(-k_3 \sum \frac{1}{n} \alpha_n + c.c.) \right\rangle$$

where $g_{--} = 1$ and $g_{\mu\nu} = 0$ for $(\mu, \nu) \neq (-,-)$.

If $t = 0$ this reduces to eq. (C.0.2) and gives

$$\int d^2 z_3 \, |1 - z_3|^{\alpha' k_2 k_3} \, |z_3|^{-\alpha' k k_3} \left| k_2 + \frac{k_3}{z_3} \right|_- .$$

To calculate the case $\alpha(t) \neq 0$, notice that in the final result the total power that $g_{\mu\nu}$ is raised to must be $\frac{\alpha(t)}{2}$. Hence the leading order term will be proportional to

$$[g_{\mu\nu}(k_2^\mu + \frac{k_3^\mu}{z_3})(k_2^\nu + \frac{k_3^\nu}{\bar{z}_3})]^{\frac{\alpha(t)}{2}},$$

which upon substituting $g_{\mu\nu}$ becomes

$$\left| k_2 + \frac{k_3}{z_3} \right|_-^{\alpha(t)} .$$

Hence the amplitude is

$$\int d^2 z_3 \, |1 - z_3|^{\alpha' k_2 k_3} \, |z_3|^{-\alpha' k k_3} \left| k_2 + \frac{k_3}{z_3} \right|_-^{\alpha(t)} .$$

Similarly for

$$\langle V_{PR}(k,0) V_T(k_4, z_4) V_T(k_5, 1) V_T(k_6, \infty)\rangle$$

we obtain

$$\int d^2 z_4 \, |1-z_4|^{\alpha' k_4 k_5} \, |z_4|^{\alpha' k k_4} \left| k_5 + \frac{k_4}{z_4} \right|_+^{\alpha(t)} .$$

Hence the insertion of the Pomeron vertex operator gives us the correct answer.

Notice also that for $t = 0$ $\alpha(t) = 1$ and the Pomeron becomes the graviton while for $t = -\frac{4}{\alpha'}$ $\alpha(t) = 0$ and the Pomeron is the tachyon.

C.2.2 5 tachyon + 1 graviton

Recall that the amplitude for this was

$$A_6 = \int d^2 z_4 \, |1-z_4|^{\alpha' k_4 k_5} \, |z_4|^{\alpha' k k_4} \int d^2 z_3 \, |1-z_3|^{\alpha' k_2 k_3} \, |z_3|^{-\alpha' k k_3}$$

$$\int d^2 w \, |w|^{-\alpha(t)-2} \, |1-w|^{\alpha' k_2 k_5} \left| 1 - \frac{w}{z_4} \right|^{\alpha' k_2 k_4} \left| 1 - \frac{w}{z_4 z_3} \right|^{\alpha' k_3 k_4} \left| 1 - \frac{w}{z_3} \right|^{\alpha' k_3 k_5}$$

$$g_{6\mu\nu}(k_5^\mu + k_4^\mu z_4 + k_3^\mu \frac{w}{z_3} + k_2^\mu w)(k_5^\nu + k_4^\nu \bar{z}_4 + k_3^\nu \frac{\bar{w}}{\bar{z}_3} + k_2^\nu \bar{w}),$$

Again in the Regge limit the small w will dominate. This means that we can again exponentiate and keep the terms that do not depend on w in the tensorial part. This gives us

$$\int d^2 w \, |w|^{-\alpha(t)-2} \exp[-w\alpha'(k_2 + \frac{k_3}{z_3}) \cdot (k_5 + \frac{k_4}{z_4}) - c.c.] g_{6\mu\nu}(k_5^\mu + k_4^\mu z_4)(k_5^\nu + k_4^\nu \bar{z}_4)$$

which keeping the large component gives

$$\int d^2 z_4 \, |1-z_4|^{\alpha' k_4 k_5} \, |z_4|^{\alpha' k k_4} \left| k_5 + \frac{k_4}{z_4} \right|_{+}^{\alpha(t)} g_{6\mu\nu} (k_5^\mu + k_4^\mu z_4)(k_5^\nu + k_4^\nu \bar{z}_4)$$

$$\int d^2 z_3 \, |1-z_3|^{\alpha' k_2 k_3} \, |z_3|^{-\alpha' k k_3} \left| k_2 + \frac{k_3}{z_3} \right|_{-}^{\alpha(t)} .$$

The integral over $d^2 z_3$ is the same as in the previous section.

Let's see if inserting the Pomeron vertex operator on the right gives us the correct answer.

We need to calculate:

$$\langle V_{PR}(k,0) V_T(k_4, z_4) V_T(k_5, 1) V_G(k_6, \infty) \rangle$$

$$= \int d^2 z_4 \, |z_4|^{\alpha' k k_4} \left\langle (g_{R\mu\nu} \partial X^\mu \bar{\partial} \bar{X}^\nu)^{\frac{\alpha(t)}{2}} V_T V_T g_{6\rho\sigma} \partial X^\rho \bar{\partial} \bar{X}^\sigma \right\rangle$$

where $g_{R++} = 1$ and $g_{R\mu\nu} = 0$ for $(\mu, \nu) \neq (+,+)$.

Again for $t = 0$ this gives the 4 particle amplitude with 2 gravitons which is to leading order

$$\int d^2 z_4 \, |z_4|^{\alpha' k k_4} \, |1-z_4|^{\alpha' k_4 k_5} \, g_{R\mu\nu} g_{6\rho\sigma} (k_5^\mu + k_4^\mu \frac{1}{z_4})(k_5^\nu + k_4^\nu \frac{1}{\bar{z}_4})(k_5^\rho + k_4^\rho z_4)(k_5^\rho + k_4^\rho \bar{z}_4)$$

which upon substituting $g_{R\mu\nu}$ becomes

$$\int d^2 z_4 \, |z_4|^{\alpha' k k_4} \, |1-z_4|^{\alpha' k_4 k_5} \left| k_5 + \frac{k_4}{z_4} \right|_{+} g_{6\rho\sigma} (k_5^\rho + k_4^\rho z_4)(k_5^\rho + k_4^\rho \bar{z}_4).$$

We see that in this case the answer is correct. When $t \neq 0$ again all the terms in the amplitude must have $g_{R\mu\nu}$ raised to the power of $\frac{\alpha(t)}{2}$. The leading order terms will be proportional to

$$[g_{R\mu\nu}(k_5^\mu + k_4^\mu \frac{1}{z_4})(k_5^\nu + k_4^\nu \frac{1}{\bar{z}_4})]^{\frac{\alpha(t)}{2}} g_{6\rho\sigma}(k_5^\rho + k_4^\rho z_4)(k_5^\rho + k_4^\rho \bar{z}_4)$$

which is just

$$\left| k_5 + \frac{k_4}{z_4} \right|_+^{\alpha(t)} g_{6\rho\sigma}(k_5^\rho + k_4^\rho z_4)(k_5^\rho + k_4^\rho \bar{z}_4).$$

So again inserting the Pomeron vertex operator gives the correct answer.

C.2.3 4 tachyons + 2 gravitons

We have for this process

$$A_6 = \int d^2 z_4 \, |1 - z_4|^{\alpha' k_4 k_5} \, |z_4|^{\alpha' k k_4} \int d^2 z_3 \, |1 - z_3|^{\alpha' k_2 k_3} \, |z_3|^{-\alpha' k k_3}$$

$$\int d^2 w \, |w|^{-\alpha(t)} \, |1 - w|^{\alpha' k_2 k_5} \left| 1 - \frac{w}{z_4} \right|^{\alpha' k_2 k_4} \left| 1 - \frac{w}{z_4 z_3} \right|^{\alpha' k_3 k_4} \left| 1 - \frac{w}{z_3} \right|^{\alpha' k_3 k_5}$$

$$g_{1\alpha\beta} g_{6\mu\nu} [\eta^{\alpha\mu} - (k_5^\alpha + k_4^\alpha \frac{1}{z_4} + k_3^\alpha \frac{z_3}{w} + k_2^\alpha \frac{1}{w})(k_5^\mu + k_2^\mu w + k_3^\mu \frac{w}{z_3} + k_4^\mu z_4)]$$

$$[\eta^{\beta\nu} - (k_5^\beta + k_4^\beta \frac{1}{\bar{z}_4} + k_3^\beta \frac{\bar{z}_3}{\bar{w}} + k_2^\beta \frac{1}{\bar{w}})(k_5^\nu + k_2^\nu \bar{w}_2 + k_3^\nu \frac{\bar{w}}{\bar{z}_3} + k_4^\nu \bar{z}_4)].$$

which in the Regge limit becomes

$$\int d^2 w \, |w|^{-\alpha(t)} \exp[-w\alpha'(k_2 + \frac{k_3}{z_3}) \cdot (k_5 + \frac{k_4}{z_4}) - c.c.]$$

$$g_{1\alpha\beta} g_{6\mu\nu} (k_3^\alpha \frac{z_3}{w} + k_2^\alpha \frac{1}{w})(k_5^\mu + k_4^\mu z_4)(k_3^\beta \frac{\bar{z}_3}{\bar{w}} + k_2^\beta \frac{1}{\bar{w}})(k_5^\nu + k_4^\nu \bar{z}_4)$$

$$= \int d^2 w \, |w|^{-\alpha(t)-2} \exp[-w\alpha'(k_2 + \frac{k_3}{z_3}) \cdot (k_5 + \frac{k_4}{z_4}) - c.c.]$$

$$g_{1\alpha\beta}g_{6\mu\nu}(k_3^\alpha z_3 + k_2^\alpha)(k_5^\mu + k_4^\mu z_4)(k_3^\beta \bar{z}_3 + k_2^\beta)(k_5^\nu + k_4^\nu \bar{z}_4).$$

After integrating over w we get similar to the previous sections

$$A_6 = \int d^2 z_4 \, |1 - z_4|^{\alpha' k_4 k_5} \, |z_4|^{\alpha' k k_4} \left| k_5 + \frac{k_4}{z_4} \right|_+^{\alpha(t)} g_{6\mu\nu}(k_5^\mu + k_4^\mu z_4)(k_5^\nu + k_4^\nu \bar{z}_4)$$

$$\int d^2 z_3 \, |1 - z_3|^{\alpha' k_2 k_3} \, |z_3|^{-\alpha' k k_3} \left| k_2 + \frac{k_3}{z_3} \right|_-^{\alpha(t)} g_{1\alpha\beta}(k_3^\alpha z_3 + k_2^\alpha)(k_3^\beta \bar{z}_3 + k_2^\beta).$$

Again we see that this factorized nicely.

We want to reproduce this by inserting a Pomeron vertex operator and calculating

$$\langle V_{PL}(-k,0)V_T(k_3,z_3)V_T(k_2,1)V_T(k_1,\infty)\rangle \, \langle V_{PR}(k,0)V_T(k_4,z_4)V_T(k_5,1)V_T(k_6,\infty)\rangle \, .$$

We already calculated the second of these integrals in the last section to get

$$\langle V_{PR}(k,0)V_T(k_4,z_4)V_T(k_5,1)V_T(k_6,\infty)\rangle =$$

$$\int d^2 z_4 \, |z_4|^{\alpha' k k_4} \, |1 - z_4|^{\alpha' k_4 k_5} \left| k_5 + \frac{k_4}{z_4} \right|_+^{\alpha(t)} g_{6\rho\sigma}(k_5^\rho + k_4^\rho z_4)(k_5^\rho + k_4^\rho \bar{z}_4).$$

The second amplitude can be calculated analogously to get

$$\langle V_{PL}(-k,0)V_T(k_3,z_3)V_T(k_2,1)V_T(k_1,\infty)\rangle =$$

$$\int d^2 z_3 \, |1 - z_3|^{\alpha' k_2 k_3} \, |z_3|^{-\alpha' k k_3} \left| k_2 + \frac{k_3}{z_3} \right|_-^{\alpha(t)} g_{1\alpha\beta}(k_3^\alpha z_3 + k_2^\alpha)(k_3^\beta \bar{z}_3 + k_2^\beta).$$

We see that inserting the Pomeron vertex operator gives the correct answer in this case as well.

C.2.4 4 tachyons + 2 Kalb-Ramond

The first part of solving this problem is similar to solving the 2 graviton case, but needs to be done more carefully. We take the Regge limit and write the amplitude

$$A_6 = \int d^2 z_4 \, |1 - z_4|^{\alpha' k_4 k_5} \, |z_4|^{\alpha' k k_4} \int d^2 z_3 \, |1 - z_3|^{\alpha' k_2 k_3} \, |z_3|^{-\alpha' k k_3}$$

$$\int d^2 w \, |w|^{-\alpha(t)} \exp[-w\alpha'(k_2 + \frac{k_3}{z_3}) \cdot (k_5 + \frac{k_4}{z_4}) - c.c.]$$

$$\varepsilon_{1\alpha\beta}\varepsilon_{6\mu\nu}[\eta^{\alpha\mu} - \frac{1}{w}(k_3^\alpha z_3 + k_2^\alpha)(k_5^\mu + k_4^\mu z_4)][\eta^{\beta\nu} - \frac{1}{\bar{w}}(k_3^\beta \bar{z}_3 + k_2^\beta)(k_5^\nu + k_4^\nu \bar{z}_4)].$$

Let us focus on calculating the w integral

$$\int dw w^{\frac{-\alpha(t)}{2}} \, |w|^{-\alpha(t)} \exp[-w\alpha'(k_2 + \frac{k_3}{z_3}) \cdot (k_5 + \frac{k_4}{z_4})][\eta^{\alpha\mu} - \frac{1}{w}(k_3^\alpha z_3 + k_2^\alpha)(k_5^\mu + k_4^\mu z_4)]$$

$$= [(k_2 + \frac{k_3}{z_3}) \cdot (k_5 + \frac{k_4}{z_4})]^{\frac{\alpha(t)}{2} - 1}$$

$$[\eta^{\alpha\mu} - (k_2 + \frac{k_3}{z_3}) \cdot (k_5 + \frac{k_4}{z_4})(k_3^\alpha z_3 + k_2^\alpha)(k_5^\mu + k_4^\mu z_4)].$$

Hence the integral over $d^2 w$ will give

$$[(k_2 + \frac{k_3}{z_3}) \cdot (k_5 + \frac{k_4}{z_4})]^{\frac{\alpha(t)}{2} - 1}[(k_2 + \frac{k_3}{\bar{z}_3}) \cdot (k_5 + \frac{k_4}{\bar{z}_4})]^{\frac{\alpha(t)}{2} - 1}$$

$$[\eta^{\alpha\mu} - (k_2 + \frac{k_3}{z_3}) \cdot (k_5 + \frac{k_4}{z_4})(k_3^\alpha z_3 + k_2^\alpha)(k_5^\mu + k_4^\mu z_4)]$$

$$[\eta^{\beta\nu} - (k_2 + \frac{k_3}{\bar{z}_3}) \cdot (k_5 + \frac{k_4}{\bar{z}_4})(k_3^\beta \bar{z}_3 + k_2^\beta)(k_5^\nu + k_4^\nu \bar{z}_4)].$$

We now try to factorize this. Again we will take k_5 and k_4 to have large $+$ components and k_2 and k_3 large $-$ components. The outside factor is:

$$\left|k_5 + \frac{k_4}{z_4}\right|_+^{\alpha(t)-2} \left|k_2 + \frac{k_3}{z_3}\right|_-^{\alpha(t)-2} .$$

Now on the inside we expect the largest term to be coming from

$$\eta_{\rho\gamma}\eta_{\sigma\delta}(k_5 + \frac{k_4}{z_4})^\rho (k_2 + \frac{k_3}{z_3})^\gamma (k_3^\alpha z_3 + k_2^\alpha)(k_5^\mu + k_4^\mu z_4) \tag{C.2.1}$$

$$(k_5 + \frac{k_4}{\bar{z}_4})^\sigma (k_2 + \frac{k_3}{\bar{z}_3})^\delta (k_3^\beta \bar{z}_3 + k_2^\beta)(k_5^\nu + k_4^\nu \bar{z}_4).$$

Now if here we take

$$\left|k_5 + \frac{k_4}{z_4}\right|_+$$

because of anti-symmetry of $\varepsilon_{1\mu\nu}$ we can change $\mu \to \nu$ followed by $z_4 \to \bar{z_4}$ which will give zero. Similarly with $\left|k_2 + \frac{k_3}{z_3}\right|_-$. Terms of next order will contain

$$(k_5 + \frac{k_4}{z_4})_+ (k_5 + \frac{k_4}{\bar{z}_4})_\perp, \qquad (k_5 + \frac{k_4}{z_4})_\perp (k_5 + \frac{k_4}{\bar{z}_4})_+$$

from one side and

$$(k_2 + \frac{k_3}{z_3})_- (k_2 + \frac{k_3}{\bar{z}_3})_\perp, \qquad (k_2 + \frac{k_3}{z_3})_\perp (k_2 + \frac{k_3}{\bar{z}_3})_-$$

from the other.

So in equation (C.2.1) (ρ, σ) can be $(+, \perp)$ and $(\perp, +)$ and (γ, δ) can be $(-, \perp)$ and $(\perp, -)$. Since we have a sum over all $\rho, \sigma, \gamma, \delta$ there will be four terms in total of this order.

However, since

$$\eta_{+\perp} = \eta_{-\perp} = 0,$$

only two of these terms will survive:

$$(k_5 + \frac{k_4}{z_4})_+ (k_2 + \frac{k_3}{z_3})_- (k_5 + \frac{k_4}{\bar{z}_4})_\perp (k_2 + \frac{k_3}{\bar{z}_3})_\perp \times$$

$$\times (k_3^\alpha z_3 + k_2^\alpha)(k_5^\mu + k_4^\mu z_4)(k_3^\beta \bar{z}_3 + k_2^\beta)(k_5^\nu + k_4^\nu \bar{z}_4)$$

and

$$(k_5 + \frac{k_4}{z_4})_\perp (k_2 + \frac{k_3}{z_3})_\perp (k_5 + \frac{k_4}{\bar{z}_4})_+ (k_2 + \frac{k_3}{\bar{z}_3})_- \times$$

$$\times (k_3^\alpha z_3 + k_2^\alpha)(k_5^\mu + k_4^\mu z_4)(k_3^\beta \bar{z}_3 + k_2^\beta)(k_5^\nu + k_4^\nu \bar{z}_4).$$

If we change in the second term $\alpha \to \beta$, $\mu \to \nu$ followed by $z_3 \to \bar{z}_3$ and $z_4 \to \bar{z}_4$ we see that these two terms are equal.

This gives, putting back the integrals over z_3 and z_4

$$A_6 = \int d^2 z_4 \, |1 - z_4|^{\alpha' k_4 k_5} \, |z_4|^{\alpha' k k_4} \left| k_5 + \frac{k_4}{z_4} \right|_+^{\alpha(t)-2} (k_5 + \frac{k_4}{z_4})_+ (k_5 + \frac{k_4}{\bar{z}_4})_\perp$$

$$\varepsilon_{6\mu\nu} (k_5^\mu + k_4^\mu z_4)(k_5^\nu + k_4^\nu \bar{z}_4)$$

$$\int d^2 z_3 \, |1 - z_3|^{\alpha' k_2 k_3} \, |z_3|^{-\alpha' k k_3} \left| k_2 + \frac{k_3}{z_3} \right|_-^{\alpha(t)-2} (k_2 + \frac{k_3}{z_3})_- (k_2 + \frac{k_3}{\bar{z}_3})_\perp$$

$$\varepsilon_{1\alpha\beta} (k_3^\alpha z_3 + k_2^\alpha)(k_3^\beta \bar{z}_3 + k_2^\beta).$$

We see that it factorized! Note that there should be a factor of two, but we have not been keeping track of the overall normalization.

Now we will try to see what vertex operator gives this answer.

So we want to split into something like

$$\langle V_{OL} V_T V_T V_{K-R} \rangle \langle V_{OR} V_T V_T V_{K-R} \rangle$$

with V_O something like

$$(\xi_{\mu\nu} \partial X^\mu \bar{\partial} X^\nu)(g_{\rho\sigma} \partial X^\rho \bar{\partial} X^\sigma)^{\frac{\alpha(t)}{2}-1}.$$

The part $(g_{\rho\sigma} \partial X^\rho \partial X^\sigma)^{\frac{\alpha(t)}{2}-1}$ will produce the part that we have in other amplitudes as well with $g_{\rho\sigma}$ just g_{++} on one side and g_{--} on the other.

What to take for ξ?

We calculate

$$A_{\alpha\beta\gamma\delta} \left\langle \partial X^\alpha \bar{\partial} X^\beta V_T V_T V_{K-R} \right\rangle \left\langle \partial X^\gamma \bar{\partial} X^\delta V_T V_T V_{K-R} \right\rangle .$$

Using results from the first section this will give

$$A_6 = \int d^2 z_4 \, |1 - z_4|^{\alpha' k_4 k_5} \, |z_4|^{\alpha' k k_4} \int d^2 z_3 \, |1 - z_3|^{\alpha' k_2 k_3} \, |z_3|^{-\alpha' k k_3} \, \varepsilon_{1\rho\sigma} \varepsilon_{1\alpha\beta} A_{\alpha\beta\gamma\delta}$$

$$[\eta^{\alpha\mu} - (k_5^\alpha + \frac{k_4^\alpha}{z_4})(k_5^\mu + k_4^\mu z_4)][\eta^{\beta\nu} - (k_5^\beta + \frac{k_4^\beta}{\bar{z}_4})(k_5^\nu + k_4^\nu \bar{z}_4)]$$

$$[\eta^{\gamma\rho} - (k_2^\gamma + \frac{k_3^\gamma}{z_3})(k_3^\rho z_3 + k_2^\rho)][\eta^{\delta\sigma} - (k_2^\delta + \frac{k_3^\delta}{\bar{z}_3})(k_3^\sigma \bar{z}_3 + k_2^\sigma)].$$

Again from here we want the leading order term to come from

$$\varepsilon_{1\rho\sigma} \varepsilon_{6\mu\nu} A_{\alpha\beta\gamma\delta} (k_5^\alpha + \frac{k_4^\alpha}{z_4})(k_5^\mu + k_4^\mu z_4)(k_5^\beta + \frac{k_4^\beta}{\bar{z}_4})(k_5^\nu + k_4^\nu \bar{z}_4)$$

$$(k_2^\gamma + \frac{k_3^\gamma}{z_3})(k_3^\rho z_3 + k_2^\rho)(k_2^\delta + \frac{k_3^\delta}{\bar{z}_3})(k_3^\sigma \bar{z}_3 + k_2^\sigma).$$

But if we change $\rho \to \sigma$ we get that this is

$$-\varepsilon_{1\rho\sigma}\varepsilon_{6\mu\nu}A_{\alpha\beta\gamma\delta}(k_5^\alpha + \frac{k_4^\alpha}{z_4})(k_5^\mu + k_4^\mu z_4)(k_5^\beta + \frac{k_4^\beta}{\bar{z}_4})(k_5^\nu + k_4^\nu \bar{z}_4)$$

$$(k_2^\gamma + \frac{k_3^\gamma}{z_3})(k_3^\sigma z_3 + k_2^\sigma)(k_2^\delta + \frac{k_3^\delta}{\bar{z}_3})(k_3^\rho \bar{z}_3 + k_2^\rho)$$

If we now change $z_3 \to \bar{z}_3$ we get for the second line

$$(k_2^\gamma + \frac{k_3^\gamma}{\bar{z}_3})(k_3^\sigma \bar{z}_3 + k_2^\sigma)(k_2^\delta + \frac{k_3^\delta}{z_3})(k_3^\rho z_3 + k_2^\rho).$$

If $A_{\alpha\beta\gamma\delta}$ was symmetric under the change $\gamma \to \delta$ this would give zero due to symmetry. Therefore the symmetric part of $A_{\alpha\beta\gamma\delta}$ under the change $\gamma \to \delta$ is zero and $A_{\alpha\beta\gamma\delta}$ is antisymmetric under this change, and similarly under $\alpha \to \beta$.

Therefore we cannot take $--$ for k_2! So we will take the next order terms (i.e. keep on each side a momentum term of $O(\sqrt{s})$ and a momentum term of $O(1)$). This will mean that for $A_{\alpha\beta\gamma\delta}$ the components which we keep are

$$A_{+\perp-\perp}, \quad A_{+\perp\perp-}, \quad A_{\perp+-\perp} \quad and \quad A_{\perp+\perp-}.$$

The first of these terms gives

$$A_{+\perp-\perp}\varepsilon_{1\rho\sigma}\varepsilon_{6\mu\nu}(k_5^\mu + k_4^\mu z_4)(k_5^\nu + k_4^\nu \bar{z}_4)(k_3^\rho z_3 + k_2^\rho)(k_3^\sigma \bar{z}_3 + k_2^\sigma)$$

$$(k_5 + \frac{k_4}{z_4})_+(k_5 + \frac{k_4}{\bar{z}_4})_\perp(k_2 + \frac{k_3}{z_3})_-(k_2 + \frac{k_3}{\bar{z}_3})_\perp,$$

the second gives

$$A_{+\perp\perp-}\varepsilon_{1\rho\sigma}\varepsilon_{6\mu\nu}(k_5^\mu + k_4^\mu z_4)(k_5^\nu + k_4^\nu \bar{z}_4)(k_3^\rho z_3 + k_2^\rho)(k_3^\sigma \bar{z}_3 + k_2^\sigma)$$

$$(k_5 + \frac{k_4}{z_4})_+(k_5 + \frac{k_4}{\bar{z}_4})_\perp(k_2 + \frac{k_3}{z_3})_\perp(k_2 + \frac{k_3}{\bar{z}_3})_-,$$

the third is

$$A_{\perp+-\perp}\varepsilon_{1\rho\sigma}\varepsilon_{6\mu\nu}(k_5^\mu + k_4^\mu z_4)(k_5^\nu + k_4^\nu \bar{z}_4)(k_3^\rho z_3 + k_2^\rho)(k_3^\sigma \bar{z}_3 + k_2^\sigma)$$

$$(k_5 + \frac{k_4}{z_4})_\perp(k_5 + \frac{k_4}{\bar{z}_4})_+(k_2 + \frac{k_3}{z_3})_-(k_2 + \frac{k_3}{\bar{z}_3})_\perp,$$

and the last is

$$A_{\perp+\perp-}\varepsilon_{1\rho\sigma}\varepsilon_{6\mu\nu}(k_5^\mu + k_4^\mu z_4)(k_5^\nu + k_4^\nu \bar{z}_4)(k_3^\rho z_3 + k_2^\rho)(k_3^\sigma \bar{z}_3 + k_2^\sigma)$$

$$(k_5 + \frac{k_4}{z_4})_\perp(k_5 + \frac{k_4}{\bar{z}_4})_+(k_2 + \frac{k_3}{z_3})_\perp(k_2 + \frac{k_3}{\bar{z}_3})_-.$$

Let us now look at the second term. By using the antisymmetry of $A_{\alpha\beta\gamma\delta}$ under $\gamma \to \delta$ we can rewrite $A_{+\perp\perp-}$ as $-A_{+\perp-\perp}$, and this will make the second term

$$-A_{+\perp-\perp}\varepsilon_{1\rho\sigma}\varepsilon_{6\mu\nu}(k_5^\mu + k_4^\mu z_4)(k_5^\nu + k_4^\nu \bar{z}_4)(k_3^\rho z_3 + k_2^\rho)(k_3^\sigma \bar{z}_3 + k_2^\sigma)$$

$$(k_5 + \frac{k_4}{z_4})_+(k_5 + \frac{k_4}{\bar{z}_4})_\perp(k_2 + \frac{k_3}{z_3})_\perp(k_2 + \frac{k_3}{\bar{z}_3})_-.$$

If we now change $z_3 \to \bar{z}_3$ and $\rho \to \sigma$ we get that this becomes

$$A_{+\perp-\perp}\varepsilon_{1\rho\sigma}\varepsilon_{6\mu\nu}(k_5^\mu + k_4^\mu z_4)(k_5^\nu + k_4^\nu \bar{z}_4)(k_3^\rho z_3 + k_2^\rho)(k_3^\sigma \bar{z}_3 + k_2^\sigma)$$

$$(k_5+\frac{k_4}{z_4})_+(k_5+\frac{k_4}{\bar{z}_4})_\perp(k_2+\frac{k_3}{z_3})_-(k_2+\frac{k_3}{\bar{z}_3})_\perp,$$

which is exactly the first term. Similarly we can show that the third and fourth terms are also equal to the first term, and they are all added together. Therefore after proper normalization we can just keep

$$\varepsilon_{1\rho\sigma}\varepsilon_{6\mu\nu}(k_5^\mu+k_4^\mu z_4)(k_5^\nu+k_4^\nu\bar{z}_4)(k_3^\rho z_3+k_2^\rho)(k_3^\sigma\bar{z}_3+k_2^\sigma)$$

$$(k_5+\frac{k_4}{z_4})_+(k_5+\frac{k_4}{\bar{z}_4})_\perp(k_2+\frac{k_3}{z_3})_-(k_2+\frac{k_3}{\bar{z}_3})_\perp$$

which gives for the amplitude

$$A_6=\int d^2z_4\,|1-z_4|^{\alpha' k_4k_5}\,|z_4|^{\alpha' kk_4}\left|k_5+\frac{k_4}{z_4}\right|_+^{\alpha(t)-2}(k_5+\frac{k_4}{z_4})_+(k_5+\frac{k_4}{\bar{z}_4})_\perp$$

$$\varepsilon_{6\mu\nu}(k_5^\mu+k_4^\mu z_4)(k_5^\nu+k_4^\nu\bar{z}_4)$$

$$\int d^2z_3\,|1-z_3|^{\alpha' k_2k_3}\,|z_3|^{-\alpha' kk_3}\left|k_2+\frac{k_3}{z_3}\right|_-^{\alpha(t)-2}(k_2+\frac{k_3}{z_3})_-(k_2+\frac{k_3}{\bar{z}_3})_\perp$$

$$\varepsilon_{1\rho\sigma}(k_3^\rho z_3+k_2^\rho)(k_3^\sigma\bar{z}_3+k_2^\sigma)$$

which agrees exactly with the result already obtained.

C.3 Summary

The moral of the story:

We look at processes where one set of momenta has a large + component, and the other a large − component. We split the vertex operators into the two sets, and insert a Pomeron or Odderon vertex operator at an end of each set. Then we can write our $2n$ particle amplitudes as a product of two $n+1$ particle amplitudes. Note we considered the cases where $2n$ is even but this is not necessary. The $n+1$ particle amplitudes are generally easier to calculate, as they involve doing fewer integrals. The extra vertex operators we must add, are either the Pomeron or the Odderon vertex operator. In the case that the n particle amplitudes on each side are symmetric under charge conjugation (which corresponds to $z \to \bar{z}$ on the world sheet), we must include the Pomeron vertex operator, as due to symmetry, Odderon exchange would vanish in this process. On the other hand, if the n particle amplitudes are antisymmetric under charge conjugation, now Pomeron exchange would vanish and we must go to the next order term, give by the Odderon which is itself antisymmetric and would thus restore symmetry when inserted in the scattering amplitude.

For Pomeron vertex operator we need to insert

$$:(\partial X^+ \bar{\partial} X^+)^{\frac{\alpha(t)}{2}} e^{ikX}:$$

on one side and

$$:(\partial X^- \bar{\partial} X^-)^{\frac{\alpha(t)}{2}} e^{-ikX}:$$

on the other.

For Odderon vertex operator we need to insert

$$:(\partial X^+ \bar{\partial} X^\perp)(\partial X^+ \bar{\partial} X^+)^{\frac{\alpha(t)}{2}-1} e^{ikX}:$$

on one side and

$$: (\partial X^- \bar{\partial} X^\perp)(\partial X^- \bar{\partial} X^-)^{\frac{\alpha(t)}{2}-1} e^{-ikX} :$$

on the other.

Bibliography

[1] R. C. Brower, J. Polchinski, M. J. Strassler, and C.-I. Tan, "The Pomeron and Gauge/String Duality," *JHEP* **12** (2007) 005, hep-th/0603115.

[2] R. C. Brower, M. J. Strassler, and C.-I. Tan, "On the Eikonal Approximation in AdS Space," *JHEP* **03** (2009) 050, 0707.2408.

[3] R. C. Brower, M. J. Strassler, and C.-I. Tan, "On The Pomeron at Large 't Hooft Coupling," *JHEP* **03** (2009) 092, 0710.4378.

[4] R. C. Brower, S. D. Mathur, and C.-I. Tan, "Glueball Spectrum for QCD from AdS Supergravity Duality," *Nucl. Phys.* **B587** (2000) 249–276, hep-th/0003115.

[5] **ZEUS** Collaboration, J. Breitweg *et al.*, "ZEUS results on the measurement and phenomenology of F2 at low x and low Q**2," *Eur. Phys. J.* **C7** (1999) 609–630, hep-ex/9809005.

[6] **H1** Collaboration, F. D. Aaron *et al.*, "Combined Measurement and QCD Analysis of the Inclusive ep Scattering Cross Sections at HERA," *JHEP* **01** (2010) 109, 0911.0884.

[7] R. C. Brower, M. Djuric, and C.-I. Tan, "Odderon in gauge/string duality," *JHEP* **0907** (2009) 063, 0812.0354.

[8] R. C. Brower, M. Djuric, and C.-I. Tan, "Saturation and Confinement: Analyticity, Unitarity and AdS/CFT Correspondence," 0812.1299.

[9] R. Brower, M. Djuric, and C.-I. Tan, "Elastic and Diffractive Scattering after AdS / CFT," 0911.3463.

[10] R. C. Brower, M. Djuric, I. Sarcevic, and C.-I. Tan, "String-Gauge Dual Description of Deep Inelastic Scattering at Small-x," 1007.2259.

[11] D. H. Politzer, "Asymptotic freedom: An approach to strong interactions," *Physics Reports* **14** (November, 1974) 129–180.

[12] D. J. Gross and F. Wilczek, "Asymptotically Free Gauge Theories. I," *Physical Review D* **8** (November, 1973) 3633+.

[13] D. H. Politzer, "Reliable Perturbative Results for Strong Interactions?," *Physical Review Letters* **30** (June, 1973) 1346+.

[14] D. J. Gross and F. Wilczek, "Ultraviolet Behavior of Non-Abelian Gauge Theories," *Physical Review Letters* **30** (June, 1973) 1343+.

[15] M. Peskin and D. Schroeder, *An introduction to quantum field theory.* Westview Pr, 1995.

[16] S. Donnachie, *Pomeron physics and QCD.* Cambridge Univ Pr, 2002.

[17] M. Froissart, "Asymptotic behavior and subtractions in the mandelstam representation," *Phys. Rev.* **123** (Aug, 1961) 1053–1057.

[18] H. Fried, *Basics of functional methods and eikonal models.* Basics of. Editions Frontières, 1990.

[19] A. Donnachie and P. V. Landshoff, "Elastic scattering and diffraction dissociation," *Nuclear Physics B* **244** (1984), no. 2, 322 – 336.

[20] C. Ewerz, "The odderon in quantum chromodynamics,".

[21] W. Greiner, S. Schramm, and E. Stein, *Quantum chromodynamics.* Springer Verlag, 2007.

[22] B. Ioffe, V. Fadin, and L. Lipatov, "Quantum chromodynamics: perturbative and nonperturbative aspects,".

[23] G. Sterman, J. Smith, J. Collins, J. Whitmore, R. Brock, J. Huston, J. Pumplin, W. Tung, H. Weerts, C. Yuan, *et al.*, "Handbook of perturbative QCD," *Reviews of Modern Physics* **67** (1995), no. 1, 157–248.

[24] K. Nakamura and P. D. Group, "Review of particle physics," *Journal of Physics G: Nuclear and Particle Physics* **37** (2010), no. 7A, 075021.

[25] J.-P. Françoise, G. L. Naber, and T. S. Tsun, eds., *Encyclopedia of Mathematical Physics, Volumes I-V.* Academic Press, 1 ed., June, 2006.

[26] T. Banks, *Modern quantum field theory: a concise introduction.* Cambridge University Press, 2008.

[27] A. Zee, *Quantum Field Theory in a Nutshell.* In a Nutshell. Princeton University Press, 2010.

[28] R. Ellis, W. Stirling, and B. Webber, *QCD and collider physics.* Cambridge monographs on particle physics, nuclear physics, and cosmology. Cambridge University Press, 2003.

[29] F. Halzen and A. Martin, *Quarks and leptons: an introductory course in modern particle physics*. Wiley, 1984.

[30] M. Green, J. Schwarz, and E. Witten, *Superstring theory: Introduction*. Cambridge monographs on mathematical physics. Cambridge University Press, 1988.

[31] J. Polchinski, *String theory: An introduction to the bosonic string*. No. v. 1 in Cambridge monographs on mathematical physics. Cambridge University Press, 1998.

[32] J. Polchinski, "Introduction to Gauge/Gravity Duality," 1010.6134.

[33] O. Aharony, S. S. Gubser, J. Maldacena, H. Ooguri, and Y. Oz, "Large n field theories, string theory and gravity," *Physics Reports* **323** (2000), no. 3-4, 183 – 386.

[34] J. Polchinski and M. J. Strassler, "Hard scattering and gauge / string duality," *Phys. Rev. Lett.* **88** (2002) 031601, hep-th/0109174.

[35] L. Cornalba, M. S. Costa, and J. Penedones, "Eikonal Approximation in AdS/CFT: Resumming the Gravitational Loop Expansion," arXiv:0707.0120 [hep-th].

[36] L. Cornalba, M. S. Costa, J. Penedones, and R. Schiappa, "Eikonal approximation in AdS/CFT: From shock waves to four- point functions," hep-th/0611122.

[37] L. Cornalba, M. S. Costa, J. Penedones, and R. Schiappa, "Eikonal approximation in AdS/CFT: Conformal partial waves and finite N four-point functions," *Nucl. Phys.* **B767** (2007) 327–351, hep-th/0611123.

[38] L. Cornalba, "Eikonal Methods in AdS/CFT: Regge Theory and Multi-Reggeon Exchange," 0710.5480.

[39] L. Lukaszuk and B. Nicolescu, "A Possible Interpretation of p p Rising Total Cross-Sections," *Nuovo Cim. Lett.* **8** (1973) 405–413.

[40] G. Bialkowski, K. Kang, and B. Nicolescu, "High-Energy Data and the Structure of the Odd Signature Amplitude of Pion-Nucleon Scattering," *Nuovo Cim. Lett.* **13** (1975) 401.

[41] J. Finkelstein, H. M. Fried, K. Kang, and C. I. Tan, "Forward Scattering at Collider Energies and Eikonal Unitarization of Odderon," *Phys. Lett.* **B232** (1989) 257.

[42] R. Avila, P. Gauron, and B. Nicolescu, "How can the Odderon be detected at RHIC and LHC," *Eur. Phys. J.* **C49** (2007) 581–592, hep-ph/0607089.

[43] B. Nicolescu, "The Odderon at RHIC and LHC," 0707.2923.

[44] L. N. Lipatov, "Reggeization of the Vector Meson and the Vacuum Singularity in Nonabelian Gauge Theories," *Sov. J. Nucl. Phys.* **23** (1976) 338–345.

[45] E. A. Kuraev, L. N. Lipatov, and V. S. Fadin, "The Pomeranchuk Singularity in Nonabelian Gauge Theories," *Sov. Phys. JETP* **45** (1977) 199–204.

[46] I. I. Balitsky and L. N. Lipatov, "The Pomeranchuk Singularity in Quantum Chromodynamics," *Sov. J. Nucl. Phys.* **28** (1978) 822–829.

[47] L. N. Lipatov, "The Bare Pomeron in Quantum Chromodynamics," *Sov. Phys. JETP* **63** (1986) 904–912.

[48] R. Kirschner and L. N. Lipatov, "Bare Reggeons in Asymptotically Free Theories," *Z. Phys.* **C45** (1990) 477.

[49] J. Kwiecinski and M. Praszalowicz, "Three Gluon Integral Equation and Odd c Singlet Regge Singularities in QCD," *Phys. Lett.* **B94** (1980) 413.

[50] J. Bartels, "High-Energy Behavior in a Nonabelian Gauge Theory. 2. First Corrections to T(n—>m) Beyond the Leading LNS Approximation," *Nucl. Phys.* **B175** (1980) 365.

[51] R. A. Janik and J. Wosiek, "Solution of the odderon problem," *Phys. Rev. Lett.* **82** (1999) 1092–1095, hep-th/9802100.

[52] M. A. Braun, "Odderon and QCD," hep-ph/9805394.

[53] J. Bartels, L. N. Lipatov, and G. P. Vacca, "A New Odderon Solution in Perturbative QCD," *Phys. Lett.* **B477** (2000) 178–186, hep-ph/9912423.

[54] L. N. Lipatov, "Asymptotic behavior of multicolor QCD at high energies in connection with exactly solvable spin models," *JETP Lett.* **59** (1994) 596–599.

[55] L. D. Faddeev and G. P. Korchemsky, "High-energy QCD as a completely integrable model," *Phys. Lett.* **B342** (1995) 311–322, hep-th/9404173.

[56] C. Ewerz, "The odderon: Theoretical status and experimental tests," hep-ph/0511196.

[57] Y. Hatta, E. Iancu, K. Itakura, and L. McLerran, "Odderon in the color glass condensate," *Nucl. Phys.* **A760** (2005) 172–207, hep-ph/0501171.

[58] Y. V. Kovchegov, L. Szymanowski, and S. Wallon, "Perturbative odderon in the dipole model," *Phys. Lett.* **B586** (2004) 267–281, hep-ph/0309281.

[59] A. Kovner and M. Lublinsky, "Odderon and seven Pomerons: QCD Reggeon field theory from JIMWLK evolution," *JHEP* **02** (2007) 058, hep-ph/0512316.

[60] H. J. Kim, L. J. Romans, and P. van Nieuwenhuizen, "The Mass Spectrum of Chiral N=2 D=10 Supergravity on S**5," *Phys. Rev.* **D32** (1985) 389.

[61] R. C. Brower, S. D. Mathur, and C.-I. Tan, "Discrete Spectrum of the Graviton in the AdS(5) Black Hole Background," *Nucl. Phys.* **B574** (2000) 219–244, hep-th/9908196.

[62] N. R. Constable and R. C. Myers, "Spin-two Glueballs, Positive Energy Theorems and the AdS/CFT Correspondence," *JHEP* **10** (1999) 037, hep-th/9908175.

[63] H. Boschi-Filho and N. R. F. Braga, "QCD / string holographic mapping and glueball mass spectrum," *Eur. Phys. J.* **C32** (2004) 529–533, hep-th/0209080.

[64] H. Boschi-Filho, N. R. F. Braga, and H. L. Carrion, "Glueball Regge Trajectories from Gauge/String Duality and the Pomeron," hep-th/0507063.

[65] S. J. Brodsky and G. F. de Teramond, "Light-Front Hadron Dynamics and AdS/CFT Correspondence," *Phys. Lett.* **B582** (2004) 211–221, hep-th/0310227.

[66] A. Karch and E. Katz, "Adding Flavor to AdS/CFT," *JHEP* **06** (2002) 043, hep-th/0205236.

[67] C. A. Ballon Bayona, H. Boschi-Filho, and N. R. F. Braga, "Deep inelastic scattering from gauge string duality in the soft wall model," *JHEP* **03** (2008) 064, 0711.0221.

[68] C. A. Ballon Bayona, H. Boschi-Filho, and N. R. F. Braga, "Deep inelastic structure functions from supergravity at small x," *JHEP* **10** (2008) 088, 0712.3530.

[69] L. Cornalba and M. S. Costa, "Saturation in Deep Inelastic Scattering from AdS/CFT," *Phys. Rev.* **D78** (2008) 096010, 0804.1562.

[70] L. Cornalba, M. S. Costa, and J. Penedones, "Deep Inelastic Scattering in Conformal QCD," *JHEP* **03** (2010) 133, 0911.0043.

[71] L. Cornalba, M. S. Costa, and J. Penedones, "AdS black disk model for small-x DIS," *Phys. Rev. Lett.* **105** (2010) 072003, 1001.1157.

[72] Y. Hatta, E. Iancu, and A. H. Mueller, "Deep inelastic scattering off a N=4 SYM plasma at strong coupling," *JHEP* **01** (2008) 063, 0710.5297.

[73] Y. Hatta, E. Iancu, and A. H. Mueller, "Deep inelastic scattering at strong coupling from gauge/string duality : the saturation line," *JHEP* **01** (2008) 026, 0710.2148.

[74] Y. Hatta, "Small-x physics in QCD and in gauge/string duality," *Prog. Theor. Phys. Suppl.* **174** (2008) 298–305.

[75] J. L. Albacete, Y. V. Kovchegov, and A. Taliotis, "Heavy Quark Potential at Finite Temperature in AdS/CFT Revisited," *Phys. Rev.* **D78** (2008) 115007, 0807.4747.

[76] J. L. Albacete, Y. V. Kovchegov, and A. Taliotis, "DIS on a Large Nucleus in AdS/CFT," *JHEP* **07** (2008) 074, 0806.1484.

[77] Y. V. Kovchegov, Z. Lu, and A. H. Rezaeian, "Comparing AdS/CFT Calculations to HERA F_2 Data," *Phys. Rev.* **D80** (2009) 074023, 0906.4197.

[78] Y. V. Kovchegov, "R-Current DIS on a Shock Wave: Beyond the Eikonal Approximation," 1005.0374.

[79] A. Taliotis, "DIS from the AdS/CFT correspondence," *Nucl. Phys.* **A830** (2009) 299c–302c, 0907.4204.

[80] B. Pire, C. Roiesnel, L. Szymanowski, and S. Wallon, "On AdS/QCD correspondence and the partonic picture of deep inelastic scattering," *Phys. Lett.* **B670** (2008) 84–90, 0805.4346.

[81] Y. Yoshida, "The Virtual Photon Structure Functions and AdS/QCD Correspondence," *Prog. Theor. Phys.* **123** (2010) 79–87, 0902.1015.

[82] J.-H. Gao and B.-W. Xiao, "Polarized Deep Inelastic and Elastic Scattering From Gauge/String Duality," *Phys. Rev.* **D80** (2009) 015025, 0904.2870.

[83] Y. Hatta, T. Ueda, and B.-W. Xiao, "Polarized DIS in N=4 SYM: Where is spin at strong coupling?," *JHEP* **08** (2009) 007, 0905.2493.

[84] J. Bartels, J. Kotanski, A. M. Mischler, and V. Schomerus, "Regge limit of R-current correlators in AdS Supergravity," *Nucl. Phys.* **B830** (2010) 153–178, 0908.2301.

[85] J. Bartels, J. Kotanski, A. M. Mischler, and V. Schomerus, "R-current six-point correlators in AdS_5 Supergravity," 0912.3072.

[86] J.-H. Gao and B.-W. Xiao, "Nonforward Compton scattering in AdS/CFT correspondence," *Phys. Rev.* **D81** (2010) 035008, 0912.4333.

[87] C. Marquet, C. Roiesnel, and S. Wallon, "Virtual Compton Scattering off a Spinless Target in AdS/QCD," *JHEP* **04** (2010) 051, 1002.0566.

[88] E. Iancu, "Parton saturation at strong coupling from AdS/CFT," 1009.1278.

[89] J. Polchinski and M. J. Strassler, "Deep inelastic scattering and gauge/string duality," *JHEP* **05** (2003) 012, hep-th/0209211.

[90] L. N. Lipatov, "Small-x Physics in Perturbative QCD," *Phys. Rept.* **286** (1997) 131–198, hep-ph/9610276.

[91] A. Donnachie and P. V. Landshoff, "Small x: Two pomerons!," *Phys. Lett.* **B437** (1998) 408–416, hep-ph/9806344.

[92] A. Capella, U. Sukhatme, C.-I. Tan, and J. Tran Thanh Van, "Dual parton model," *Phys. Rept.* **236** (1994) 225–329.

[93] E. Levin and C.-I. Tan, "Heterotic Pomeron: A Unified Treatment of High-Energy Hadronic Collisions in QCD," *Proc. for International Symposium on Multiparticle Dynamics," Santiago, Spain, July 1992, and Workshop on Small-x and Diffractive Physics at Tevatron", FNAL, Sept. 1992* (1992) hep-ph/9302308.

[94] S. Bondarenko, E. Levin, and C. I. Tan, "High Energy Amplitude as an Admixture of Soft and Hard Pomerons," *Nucl. Phys.* **A732** (2004) 73, hep-ph/0306231.

[95] I. Balitsky, "Operator expansion for high-energy scattering," *Nucl. Phys.* **B463** (1996) 99–160, hep-ph/9509348.

[96] Y. V. Kovchegov, "Unitarization of the BFKL pomeron on a nucleus," *Phys. Rev.* **D61** (2000) 074018, hep-ph/9905214.

[97] Y. V. Kovchegov, "Small-x F2 structure function of a nucleus including multiple pomeron exchanges," *Phys. Rev.* **D60** (1999) 034008, hep-ph/9901281.

[98] B. Z. Kopeliovich, E. Levin, A. H. Rezaeian, and I. Schmidt, “Direct photons at forward rapidities in high-energy pp collisions,” *Phys. Lett.* **B675** (2009) 190–195, 0902.4287.

[99] E. Levin and I. Potashnikova, “Soft interaction at high energy and N=4 SYM,” *JHEP* **06** (2009) 031, 0902.3122.

[100] S. K. Domokos, J. A. Harvey, and N. Mann, “The Pomeron contribution to p p and p bar p scattering in AdS/QCD,” *Phys. Rev.* **D80** (2009) 126015, 0907.1084.

[101] **ZEUS** Collaboration, S. Chekanov *et al.*, “Measurement of the neutral current cross section and F2 structure function for deep inelastic e+ p scattering at HERA,” *Eur. Phys. J.* **C21** (2001) 443–471, hep-ex/0105090.

[102] G. Soyez, “Global QCD fit from $Q^2 = 0$ to $Q^2 = 30000\ GeV^2$ with Regge-compatible initial condition,” *Phys. Rev.* **D71** (2005) 076001, hep-ph/0407098.

[103] M. M. Block, E. L. Berger, and C.-I. Tan, “Small x behavior of parton distributions from the observed Froissart energy dependence of the deep inelastic scattering cross section,” *Phys. Rev. Lett.* **97** (2006) 252003, hep-ph/0610296.

[104] E. L. Berger, M. M. Block, and C.-I. Tan, “Analytic expression for the joint x and Q^2 dependences of the structure functions of deep inelastic scattering,” *Phys. Rev. Lett.* **98** (2007) 242001, hep-ph/0703003.

[105] M. M. Block, “Sifting data in the real world,” *Nucl. Instrum. Meth.* **A556** (2006) 308–324, physics/0506010.

[106] L. V. Gribov, E. M. Levin, and M. G. Ryskin, “Semihard Processes in QCD,” *Phys. Report.* **100** (1983) 1–50.

[107] M. Kalb and P. Ramond, "Classical direct interstring action," *Phys. Rev.* **D9** (1974) 2273.

[108] E. Cremmer and J. Scherk, "Spontaneous dynamical breaking of gauge symmetry in dual models," *Nucl. Phys.* **B72** (1974) 117–124.

[109] H. Fritzsch and P. Minkowski, "Psi Resonances, Gluons and the Zweig Rule," *Nuovo Cim.* **A30** (1975) 393.

[110] J. D. Bjorken, "ELEMENTS OF QUANTUM CHROMODYNAMICS,". Presented at the SLAC Summer Institute on Particle Physics, Stanford, Calif., Jul 9-20, 1979.

[111] R. L. Jaffe, K. Johnson, and Z. Ryzak, "QUALITATIVE FEATURES OF THE GLUEBALL SPECTRUM," *Ann. Phys.* **168** (1986) 344.

[112] A. B. Kaidalov and Y. A. Simonov, "Glueball masses and pomeron trajectory in nonperturbative QCD approach," *Phys. Lett.* **B477** (2000) 163–170, hep-ph/9912434.

[113] A. B. Kaidalov and Y. A. Simonov, "Odderon and pomeron from the vacuum correlator method," *Phys. Lett.* **B636** (2006) 101–106, hep-ph/0512151.

[114] C. J. Morningstar, K. J. Juge, and J. Kuti, "Where is the string limit in QCD?," *Nucl. Phys. Proc. Suppl.* **73** (1999) 590–595, hep-lat/9809098.